2020-08

Insights Into the Link Between Mitochondrial Dynamics and Peripheral Neuropath

Almutawaa, Walaa Saeed

UNIVERSITY OF CALGARY

Insights into the Link Between Mitochondrial Dynamics and Peripheral Neuropathies

by

Walaa Saeed Almutawaa

A THESIS

SUBMITTED TO THE FACULTY OF GRADUATE STUDIES

IN PARTIAL FULFILMENT OF THE REQUIREMENTS FOR THE

DEGREE OF DOCTOR OF PHILOSOPHY

GRADUATE PROGRAM IN BIOCHEMISTRY AND MOLECULAR BIOLOGY

CALGARY, ALBERTA

AUGUST, 2020

Abstract

Mitochondrial dynamics, which include fusion and fission events, determine mitochondrial morphology and reflect mitochondrial health within the cell. Mitochondrial dynamics are important for mitochondrial functions, including but not limited to, cellular respiration, energy production, and mitochondrial DNA (mtDNA) maintenance. Defects in mitochondrial fission and fusion proteins are associated with a number of neurological disorders including the peripheral neuropathy Charcot-Marie-Tooth Type II disease (CMT2). The research presented in this thesis centers around a novel fission protein, NMIIC (encoded by the MYH14 gene), and a well-characterized fusion protein, Mfn2, and how defects in these proteins affects mitochondrial dynamics and contribute to disease.

In my first study, examining a CMT2 pathogenic variant in MYH14 that is associated with a peripheral neuropathy phenotype, I reported for the first time the role of *NMIIC* as a key player in mitochondrial fission. Characterization of this R941L variant in overexpression studies, and in patient fibroblasts indicated impairment of mitochondrial fission in these cells. Intriguingly, the distribution of mtDNA was also affected in fibroblast harbouring the R941L mutation. Collectively, these observations revealed a novel role for NMIIC in mitochondrial fission with defects linked to the pathogenicity of CMT2.

In my second project, I examined the novel Q367H variant of MFN2, a regulator of mitochondrial fusion, which also has other important cellular roles. While pathogenic mutations in MFN2 are typically associated with CMT2, the Q367H variant I characterized was associated with myopathy phenotype rather than a peripheral neuropathy. Although commonly assumed that the peripheral neuropathy phenotype associated with *MFN2* mutations is due to impaired mitochondrial fusion, accumulating evidence supported by our new data characterizing the

Q367H mutation, suggests that this may not be the case. Here, I examined the effects of the Mfn2 H367Q mutation on mitochondrial morphology, endoplasmic reticulum (ER) morphology, bioenergetics function, and lipid droplet morphology. These parameters were altered in MFN2 Q367H patient fibroblasts, suggesting that this mutation is pathogenic, and thus expanding the phenotypic presentation of phenotypes in patients with MFN2 mutations. Overall, my studies provided novel insight into the link between mitochondrial dynamics and peripheral neuropathy by expanding the list of mitochondrial dynamics genes associated with peripheral neuropathy, and by characterizing mitochondrial dysfunction caused by a novel mutation in MFN2 that is not associated with CMT2.

Preface

Chapter 3 of this thesis has been published as Walaa Almutawaa[b,1], Christopher Smith[a1], Rasha Sabouny[a,b], Ryan B. Smit[a,b],TianZhao[a,b], Rachel Wong[a,b],Laurie Lee-Glover[a,b], Justine Desrochers-Goyette[c,d], Hema Saranya Ilamathi[c,d], Care4Rare Canada Consortium, Oksana Suchowersky[e],MarcGermain[c,d], Paul E. Mains[a,b], Jillian S. Parboosingh[a], Gerald Pfeffer[a,b]. Micheil Innes[a,f], Timothy E. Shutt[a,b,f,]

"The R941L mutation in *MYH14* disrupts mitochondrial fission and associates with peripheral neuropath"

Biomedicine, vol 45, Page 379-392

---

1 First authors contributed equally.

a Alberta Children's Hospital Research Institute, Department of Medical Genetics, Cumming School of Medicine, University of Calgary, Calgary, AB, Canada

b Department of Biochemistry & Molecular Biology, Cumming School of Medicine, University of Calgary, Calgary, AB, Canada

c Groupe de Recherche en Signalisation Cellulaire and Département de Biologie Médicale, Université du Québec à Trois-Rivières, Trois-Rivières, QC,CanadadCentre de Recherche Biomed, Université du Québec à Trois-Rivières, Trois-Rivières, QC, Canada

e Departments of Medicine (Neurology), Medical Genetics and Pediatrics, University of Alberta, Edmonton, AB, Canada

f Hotchkiss Brain Institute, Department of Clinical Neurosciences, Cumming School of Medicine, University of Calgary, Calgary, AB, Canada

Chapter 4 of this Thesis is original, unpublished, independent work by the author, Walaa Almutawaa. Experiments reported in Chapters 4 were covered by Ethics Certificate number REB15-2763 and REB16-2196 issued by the University of Calgary Conjoint Health Ethics Board for the project “Cellular models”, approved at July 12, 2017 and for the project Genetics of neuromuscular approved at 3-May-2016

Acknowledgements

First and foremost, I would like to thank my self for my perseverance to make it to the end for this degree. I would like to thank my supervisor Dr. Timothy Shutt. It has been an honor to be associated with him during the most critical phase of my degree. I appreciate all his contributions of time, ideas, and funding to make my research experience productive and stimulating. I would like to thank members of Dr. Shutt's lab for their immense contributions to my personal and professional time. I am especially grateful to, Eman Alkahteeb, Erik Fraunberger, Rasha Sabouny, and Tian Zhao. I appreciate their presence, friendship, and sharing ideas and (sciency) feedback. I would like to thank Dr. Childs and Dr. Kurash for granting access to their microscope to do all imaging studies. I would also like to acknowledge the ACHRI facility at the Foothills Campus, where I performed all experiments of the current thesis. I want to thank my family; my mother, my brothers; Anas, and Abdulrahman for taking care of me and my home shores at my down times during my studies. I also want to thank my partner Waleed Hafiz for his valuable teachings on accepting and loving "who I am" and for his continuous emotional and spiritual guidance through my tough times. I want to thank my friends, Hayat Baba and Summer Helmi, for their ongoing motivation and support. I also want to thank the Saudi government for granting me scholarships through the King Abdullah scholarship program and Tiba University scholarships. I want to thank Lisa Milsuk for taking care of the administrative tasks during my studies. I appreciate my committee members, Dr. Paul Mains and Dr. Gerald Pfeffer, for their help, availability, and for coordinating my defense. Finally, my time at the University of Calgary (UofC) was expanding my horizon on personal growth. So, thank you UofC.

Dedication

To Afaf Telmesani, my mother, who has always invested her efforts towards teaching me the lesson of independence.

I would like to thank you for this valued lesson.

This Thesis is dedicated to you.

I love you.

Table of Contents

List of Tables

Chapter Three

Chapter Four

Appendix -A-

List of Figures and Illustrations

Chapter One

Chapter Three

Chapter Four

Chapter Five

Appendix-A-

Appendix-B-

List of Symbols, Abbreviations and Nomenclature

Abbreviation	Abbreviated for
AKAP1	A-kinase-anchoring protein 1
AKAP12	A-kinase-anchoring protein 12
B-Actin	Human gene and protein abbreviation ACTB/ACTB
CMT	Charcot Marie-Tooth Diseases
Drp1	Dynamin-Related Protein 1
DNM2	Dynamin-2
Fis-1	Mitochondrial Fission-1 Protein
INF2	Inverted Formin 2
GDAP1	Ganglioside-induced differentiation-associated protein 1
GOF	Gain of Function

GTPase	GTPase-activating proteins
HR	Heptad repeat (HR*)* coiled-coil regions 1 and
GED	GTPase Effector Domain
LOF	Loss of Function
ER	Endoplasmic Reticulum
M17	Human Neuroblastoma BE(2)-*M17 cell line*
MRLC	Myosin regulatory light chain
MAMs	Mitochondrial Associated Membranes
MIMs	Mitochondrial Inner membranes
MiD 49	Mitochondrial Division (MiD) Proteins 49
MiD 51	Mitochondrial Division (MiD) Proteins 51

Mito-ER	Mitochondrial-Er contact sites
MOMs	Mitochondrial Outer Membranes
MFF/Mff	Mitochondrial Fission Factor
MFN1 / Mfn2	Mitofusion 1
MFN2/ Mfn2	Mitofusion 2
NMIIA	Non muscle Myosin heavy Chain A
NMIIB	Non Muscle Myosin Heavy Chain B
NMMIC	Non Muscle Myosin Heavy Chain C protein
MYH14	Non Muscle Myosin gene
mtDNA	Mitochondrial DNA
NPs	Neuropathies

OPA1/Opa1	Mitochondrial Dynamin like GTPase
OSCC	Oral Squamous Cell Carcinoma
PE	Phosphatidylethanolamine
PC	Phosphatidylcholine
PH	Pleckstrin homology domain
PRD	Proline/arginine Rich Domain
PKA	Protein Kinase A
PKC	Protein Kinase C
RhoA	RhoA activates ROCK (***RhoA kinase***)/ Ras homolog family member A (RhoA)
ROCK	Rho associated Kinase

SSeCKS	Src-suppressed C kinase substrate
TPRs	tandem tetratricopeptide repeats
U2OS	Human Bone Osteosarcoma Epithelial Cells

Epigraph

“The world breaks every one

And afterward

Many are strong at the broken places “

-Ernest Hemingway-

Chapter One

Introduction and Literature Review

Introduction

Mitochondria have long been recognized as the cellular powerhouse for energy production. In contrast to the early traditional model of mitochondria being static and bean-shaped organelles, mitochondria are now perceived as highly dynamic organelles. Recent live-cell imaging studies illuminated the dynamic nature of mitochondria in various cell types (Kuznetsov, Hermann, Saks, Hengster, & Margreiter, 2009; Mitra & Lippincott-Schwartz, 2010). Interestingly, live-cell studies demonstrated the ability of mitochondria to distribute throughout the cell and to acquire various shapes. Such studies also showed that mitochondria do not operate as isolated organelles; instead, they function as a collective in which its activity is governed by 'mitochondrial dynamics'. Each mitochondrion's morphology is altered continuously by fusion and fission events. The term "mitochondrial dynamics" has come to encompass additional behaviors of mitochondria, such as transport along the cytoskeleton or axons, selective degradation by the mitophagy, and interactions with other organelles like the endoplasmic reticulum (ER). Numerous vital proteins involved in the regulation of mitochondrial dynamics came to light during the last decade. Currently, it is widely becoming accepted that mitochondrial dynamics are reflective of mitochondrial health within the cells. Also, recent genetic studies highlighted a significant correlation between mitochondrial dynamics and human diseases. Mitochondrial dynamics defects are reported in numerous disorders ranging from cancer to neurodegeneration.

Mitochondria have many biochemical functions, each of which can be potentially influenced by alteration in their dynamics. The connection between mitochondrial dynamics and specifics disorders seems to be context-dependent (L. Chen, Winger, & Knowlton, 2014). Intriguingly, genetic defects in mitochondrial dynamics are directly linked to a subset of peripheral neuropathies (PNs). For instance, the Charcot-Marie-Tooth syndrome (CMT), central to my studies in this thesis, is linked to mutations in many mitochondria fusion and fission genes. However, how disturbances in mitochondrial dynamics contribute to CMT diseases pathogenesis or its progression is still an active research area. This introduction presents a general overview of the current understanding of mitochondrial dynamics, and reviews emerging studies that correlate mitochondrial fission/fusion events with peripheral neuropathies.

1.2 Mitochondrial Dynamics Overview

Mitochondrial dynamics play a significant role in shaping mitochondrial network morphology. Mitochondrial morphology is organized mainly by a balanced interplay of fusion and fission events. This interplay maintains mitochondrial population health and facilitates mitochondrial response to the continuous physiological and biochemical changes (Nakada, Ono, & Hayashi, 2002). Mitochondrial dynamics are crucial in maintaining mitochondrial functions quality and cellular hemostasis. Cells with a fragmented network are more prone to cellular death. Generally, fused network enhances oxidative phosphorylation (OXPHOS) and increases ATP biogenesis (Westermann, 2012). On the other hand, fission events facilitate the proper fragmentation of mitochondria during cell division, and distribution of mitochondria along cytoskeletal tracks (Mishra & Chan, 2014). While some regulatory pathways are recognized for mediating fission and fusion, several players are still unrevealed. A group of dynamin-related GTPases mediates fusion and fission events (Hales & Fuller, 1997). These GTPases are highly

conserved enzymes from yeast to humans, sharing a homologous GTPase domain and transmembrane regions, illustrated in [Figure 1.1]. These proteins form complexes to alter curvature of mitochondrial membranes to mediate fusion or fission events. Thus, disturbance of mitochondrial dynamics can impact many cellular functions (Ferree & Shirihai, 2012).

1.2.1 Mitochondrial Fission in Mammals

Mitochondrial fission is characterized by the division of one mitochondrion into two daughter mitochondria. Mitochondrial fission is involved in several cellular pathways including mitochondrial inheritance, mitophagy, and apoptosis (Flis & Daum, 2013; Frank et al., 2001; Ishihara et al., 2009; Kane & Youle, 2010; Y. J. Lee, Jeong, Karbowski, Smith, & Youle, 2004; Yu, Fox, Burwell, & Yoon, 2005). A lack of fission leads to highly interconnected mitochondrial networks, deficits in mitochondrial bioenergetics, loss or depletion of mitochondrial DNA (mtDNA), and alterations in apoptotic signaling (Landes & Martinou, 2011; Parone et al., 2008; Sheridan & Martin, 2010; Westermann, 2010). Elements of the fission machinery were first identified in yeast and worm genetic studies. In mammals, studies of mitochondrial dynamics identified several proteins. Most of the fission proteins belong to the GTPase protein family. Mitochondrial fission occurs in three main steps; 1) endoplasmic reticulum (ER)-mediated mitochondrial constriction, 2) Drp1 assembly and oligomerization, 3) mitochondrial scission and fission complex disassembly- these steps are discussed in section 1.2.1.2-.

1.2.1.1 Mitochondrial Fission Proteins

Dynamin Related Protein (Drp1). Drp1 plays a significant role in mitochondrial fission in mammalian cells. Overexpression of Drp1 in mammalian cells causes an excessive mitochondrial fragmentation (Hu, Huang, & Li, 2017). In contrast, cells lacking Drp1 shows large and abnormal mitochondria (Favaro et al., 2019).

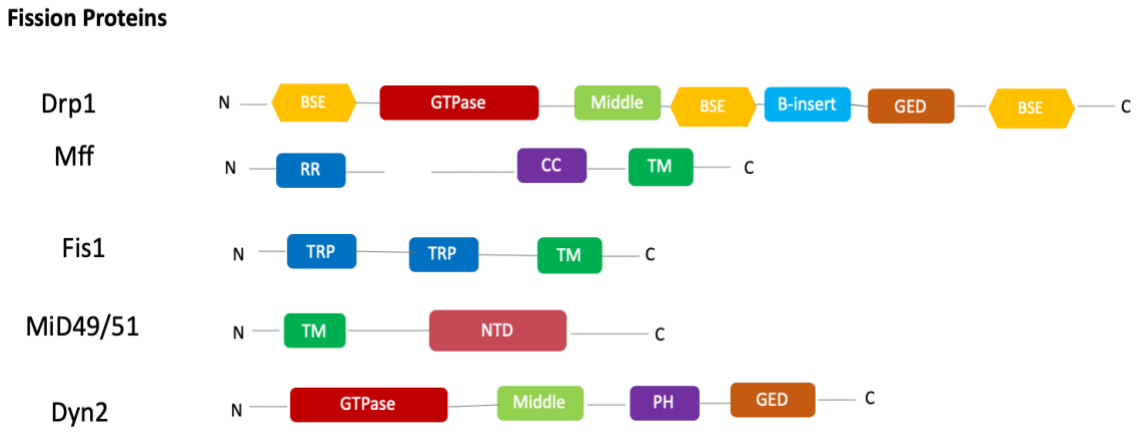

Figure.1.1 Schematic representation of structural domains of Fission proteins. Illustration of the core machinery proteins involved in mitochondrial fission and fusion. In regards to Mfns; The classical model proposes that Mfn2 contains two transmembrane (TM) domains in between HR1 and HR2 domains. Alternatively, Mfns have been recently demonstrated to only have one TM that lies between the two HR domains. Domains are depicted in different colors. BSE, bundle signalling elements; CC, coil-coi; GED, GTPase effector domain; HR, heptad repeats; NTD, nucleotidyl transferase; PH, Pleckstrin homology; PR , Proline rich; RR, Repeat region; TRP, tetratricopeptide repeat; TM, transmembrane.

Drp1 comprises a GTPase domain followed by a middle domain, a variable domain, and a GTPase effector domain (GED) [Figure 1.1]. The large middle domain and an assembly domain at the C-terminal participate in regulating the GTPase activity and oligomerization of the Drp1 protein. Drp1 is located mainly in the cytosol. However, a small pool of Drp1 molecules localizes to future fission sites at the mitochondrial outer membrane (MOMs) during fission events (Smirnova, Shurland, Ryazantsev, & van der Bliek, 1998). Drp1 monomers gather into oligomers at the MOMs to form constricting filaments around the mitochondrial tubules (Bui and Shaw, 2013). These filaments generate constriction force against mitochondria tubules via GTP hydrolysis.

Mitochondrial Adaptor Proteins. Several mitochondrial adaptors mediate the recruitment of Drp1 from the cytoplasm to the mitochondria (e.g., Mff, MiD49 and MiD51 and Fis1). These adaptors facilitate Drp1 localization and oligomerization at the MOMs (Olson et al., 2013). The exact role of each adaptor and the functional overlap between these various adaptors remain to be explored.

Mitochondrial Fission Protein (Mff). Mff, located at the MOMs and thought to be the primary receptor for Drp1 (Gandre-Babbe and van der Bliek, 2008; Losón et al., 2013; Otera et al., 2010) [Figure 1.1]. Mff is suggested to allow Drp1 anchoring to the MOMs to facilitate constriction during fission event (Osellame et al., 2016; Otera et al., 2010; Palmer et al., 2011). Loss of Mff causes a significant decrease in mitochondrial fission and shows highly elongated mitochondria

Mitochondria Division Protein 49 (MiD 49) and Mitochondria Division Protein 51 (MiD 51). MiD49 and MiD51 are also adaptors for Drp1. Both MiDs are anchored to the MOMs and organize the assembly of Drp1 oligomers as rings at mitochondrial constriction sites

(Gandre-Babbe and van der Bliek, 2008; Losón et al., 2013; Otera et al., 2010; Palmer et al., 2013, 2011). MiD49 and MiD51 comprise an inactive nucleotidyltransferase domain that can recruit Drp1 to mitochondrial fission sites independent of other adaptors (Losón et al., 2014, 2015, 2013; Osellame et al., 2016; Otera et al., 2016; Richter et al., 2014). Both MiDs are proposed to be part of the mitochondrial fission machinery. However, the role of MiDs in fission is still under debate. In an earlier study, a double knockdown of MiDs caused mitochondrial tubules elongation and a reduction in Drp1 recruitment, supporting their role in mitochondrial fission (Palmer et al., 2011). In contrast, overexpressing either MiD49 or MiD51 also caused mitochondrial tubules lengthening in a couple of reports (Palmer et al., 2011; Zhao et al., 2011). However, those observations were not reproduced in later studies (Palmer et al., 2013). *In-vitro* studies showed that MiD49 increased the ability of Drp1 to constrict the mitochondrial tubules (Koirala et al., 2013). In later studies, the overexpression of MiD49 and MiD51 proteins were found to promote mitochondrial fission independent of other adaptor proteins (Loson, Song, Chen, & Chan, 2013; Palmer et al., 2013). Hence, the exact role of each MiD and its functional overlap during fission events are not fully understood. Last but not least, MiDs are suggested to be involved in regulating cristae during apoptotic signaling. Drp1-mediated fission through MiD49 or MiD51, but not Mff, is required for cristae opening and cytochrome C release following apoptotic induction (Otera, Miyata, Kuge, & Mihara, 2016).

Mitochondrial Fission-1 Protein (Fis1). Fis1 is another adaptor protein for fission machinery. Fis1 is a small protein embedded in the MOMs via its C-terminal transmembrane domain. The majority of Fis1 protein faces the cytosol. Several studies showed that an increased levels of Fis1 promote mitochondrial fragmentation in Drp1-dependent fission (James et al., 2003; Yoon et al., 2003; Stojanovski et al., 2004). However, these observations were not

replicated in later studies (Osellame et al., 2016; Palmer et al., 2011). Also, Fis1 knockout cells demonstrated very mild fission defects, raising a question about the precise role of Fis1 in Drp1 recruitment or its direct involvement in fission machinery. Recent studies suggest that Fis1 is involved in regulating mitochondrial fission in conditions restricted to stress, apoptosis, or mitophagy (Iwasawa, Mahul-Mellier, Datler, Pazarentzos, & Grimm, 2011; Shen et al., 2014).

Non-muscle Myosins (NMIIs). Prior to constriction of mitochondrial tubules, a pre-constriction step occurs via the endoplasmic reticulum. The constriction of mitochondrial tubules is mediated by the actin-myosin cytoskeleton formed at the ER-mitochondria contact sites. In this context, NMIIs proteins are crucial players mediating mitochondrial fission. NMIIs proteins are motor proteins that are involved in a wide range of cellular processes, including but are not limited to, cell migration, cell adhesion, and cytokinesis (Betapudi, Licate, & Egelhoff, 2006; Lo et al., 2004; Vicente-Manzanares, Zareno, Whitmore, Choi, & Horwitz, 2007; Conti, Even-Ram, Liu, Yamada, & Adelstein, 2004; Shewan et al., 2005; Ma et al., 2012; Pollard, 2010). NMII is a hexamer formed by dimerization of two heavy chains. Each heavy chain binds two light chains (Billington, Wang, Mao, Adelstein, & Sellers, 2013). NMII is composed of three significant domains; head, neck, and tail [figure 1.2]. The head contains the motor myosin heavy chain (MHC), which makes up the N-terminus and generates force via ATP hydrolysis. The neck is characterized by a lever arm region that binds the essential light chain (ELC) and the regulatory light chain (RLC). The ELC stabilizes the lever arm, and the RLC regulates the myosin's enzymatic activity in a phosphorylation-dependent manner (Heissler & Manstein, 2013; Vicente-Manzanares, Ma, Adelstein, & Horwitz, 2009). The tail comprises an α-helical region to facilitate the heavy chains' dimerization forming the distinct coiled-coil domain at the C-terminus of myosin II molecules.

In mammals, there are three genes (*MYH9*, *MYH10*, and *MYH14*) encoding the NMII heavy chains; Myosin IIA, myosin IIB, and myosin IIC paralogs sharing 60–80% amino acid sequence similarity (Jung et al., 2008). *In vivo*, alternative splicing of these NMIIs genes leads to a wide range of expressed variants (Golomb et al., 2004; Takahashi, Kawamoto, & Adelstein, 1992). Alternatively spliced variants of the MHC, ELC, and RLC are known to be expressed in specific tissues, but our understanding of their functional specificities is still limited (Golomb et al., 2004). The expression of all three NMIIs is necessary for embryo growth and development (Conti & Adelstein, 2008). Not all NMIIs are expressed in one tissue, but tissues often express at least one or two of the NMIIs. Hence, the preferential expression of the NMIIs in different cell types may suggest a distinct non-redundant role of each NMII paralog. Recent evidence demonstrated the involvement of the NMIIs in mitochondrial fission events via ER-action-myosin mediated constriction (Korobova, Gauvin, & Higgs, 2014; Korobova, Ramabhadran, & Higgs, 2013). Drp1 tends to co-precipitate with actin filaments, and the NMIIs are suggested to enhance this interaction (Hatch et al., 2014; Ji, Hatch, Merrill, Strack, & Higgs, 2015). In support of this observation, overexpression of myosin mutants reduced the co-precipitation of Drp1 to actin filaments (DuBoff, Gotz, & Feany, 2012). Suppression of NMIIA or NMIIB, via siRNA or chemical inhibition, caused mitochondrial elongation and decreased the amount of mitochondrially bound Drp1 (Korobova, Gauvin, & Higgs, 2014). Also, the suppression of the myosin regulatory light chain (MRLC) caused mitochondrial lengthening. Intriguingly, NMII inhibition reversed the effect of the constitutively active INF2, which is a protein required for actin polymerization filaments (Hatch, Gurel, & Higgs, 2014). Interestingly, the NMIIC protein, in which a specific mutation is linked to CMT peripheral neuropathy, is expressed abundantly in the nervous system (Betapudi, 2014; Donaudy et al., 2004).

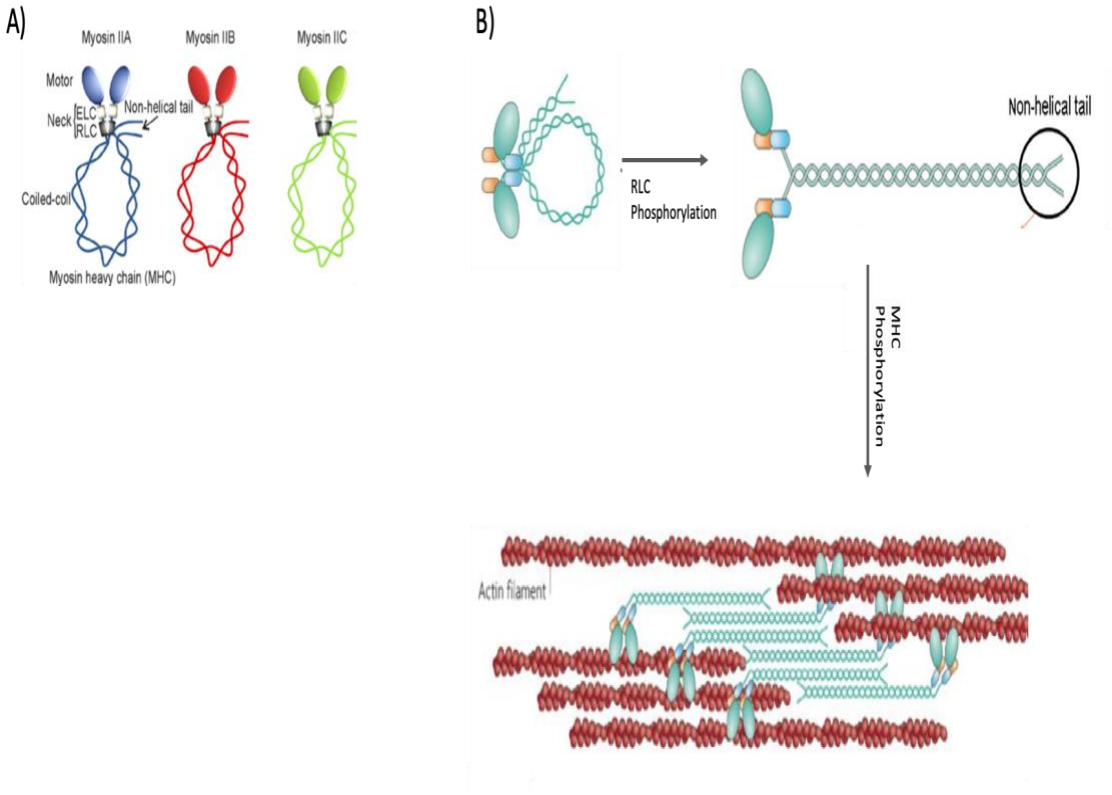

Figure 1.2 Non-Muscle Myosins (NMIIs).
A) A schematic representation for the subunits and domains of the NMIIs. NMII form a dimer through interactions between the α-helical coiled-coil domains. The globular head domain contains the actin-binding regions and the enzymatic Mg^{2+}-ATPase motor domains. The essential light chains (ELCs) and the regulatory light chains (RLCs) bind to the heavy chains at the lever arms that link the head and rod domains. B) In the absence of RLC phosphorylation, NM II molecules assemble into filaments through interactions between their domains. These filaments bind to actin through their head domains and the ATPase activity of the head, enabling a conformational change that moves actin filaments in an anti-parallel manner. Bipolar myosin filaments link actin filaments together in thick bundles that form cellular structures such as stress fibres. Adapted and modified from (Betapudi, 2014; Vicente-Manzanares, Ma, Adelstein, & Horwitz, 2009).

Dynamin 2 (DNM2). *In vitro*, biochemical studies suggested that Drp1 alone may not be sufficient to constrict mitochondrial tubules to elicit fission, and other factors might be required (Bui & Shaw, 2013). Recent live-cell imaging experiments showed that DNM2 acts downstream of Drp1 to facilitate final scission of mitochondrial tubules in fission event (J. E. Lee, Westrate, Wu, Page, & Voeltz, 2016). In this work, knockdown of DNM2 caused an elongation of mitochondria tubules and demonstrated a highly constricted tubule between two populations of preassembled Drp1 polymers (J. E. Lee, Westrate, Wu, Page, & Voeltz, 2016). In contrast to Drp1, which can be found at most constricted mitochondrial sites, DNM*2* only localizes transiently to facilitate mitochondrial membrane scission. In these experiments, the fluorescently labeled DNM2 and Drp1 were observed differentially segregated in daughter organelles (J. E. Lee et al., 2016). While Drp1 remains present on both daughter mitochondria following scission, DNM2 appears to be present only on one of the two opposing mitochondria (Lee et al., 2016), implicating that DNM2 might function as a facilitator to execute constriction but not necessarily severing mitochondrial tubules. Overexpression of DNM2 mutants lacking the GTPase, pleckstrin homology domain (PH), or the (PRD) domain did not rescue the elongated phenotype in mitochondria lacking DNM2, suggesting the significance of these domains in mitochondrial fission.

The role of DNM2 in mitochondrial dynamics is intriguing with respect to its links to several disease pathogenesis (Durieux et al., 2010). Mutations in DNM2 gene are causatives for CMT disease (Tinelli, Pereira, & Suter, 2013; Zuchner et al., 2005), and centronuclear myopathy (Bitoun et al., 2005; Cowling et al., 2011; Durieux et al., 2010; Kierdaszuk et al., 2013), and patients phenotypes are often associated with mitochondrial dysfunction. In addition, multiple mtDNA deletions (a phenotype found in some cells lacking mitochondrial fusion) were reported

in patients carrying DNM2 gene mutations associated with centronuclear myopathy and cardiomyopathy (Gal et al., 2015).

1.2.1.2 Steps in Mitochondrial Fission

Our understanding of how fission occurs has evolved during the last few years. We now appreciate that fission occurs in three distinct steps [figure 1.3]:

Step 1- ER-Mediated Mitochondrial Constriction. It is now recognized that the ER extends tubules around mitochondria to provide an initial constriction event, which allow Drp1to be recruited and assembled. This phenomenon is observed even in cells lacking DRP1; ER still wraps around and constricts mitochondria. The actin-myosin cytoskeleton modulates the ER-mediated mitochondrial constriction step (Higgs, 2005; Korobova, Ramabhadran, & Higgs, 2013). The actin filaments are recruited to the ER-mitochondrial contact sites, where polymerization and nucleation of actin filaments occur via the ER–formin (INF-2) and other proteins (Higgs, 2005). The NMIIA and NMIIB work with the actin filaments to provide the mechanical force required for this ER-mediated construction (Billington, Wang, Mao, Adelstein, & Sellers, 2013; DuBoff, Gotz, & Feany, 2012; Korobova, Gauvin, & Higgs, 2014). However, the role of the previously recognized NMIIC, which is a member of the NMIIs family, in mitochondrial fission has not been identified in the literature. NMIIC role in mitochondrial fission was studied for the first time in this study (Chapter 3).

Step 2- Drp1 Assembly and Oligomerization. Following the ER-mediated mitochondrial constriction, Drp1 monomers translocate to the MOMs and assemble into a homo-oligomeric complex. This process is mediated by Drp1 interacting with actin filaments as well as other anchored MOMs receptors (Fis-1, Mff, MiD49, and MiD51), forming a ring-like structure (Tilokani et al., 2018). As discussed earlier, the exact role of these adaptor proteins in

mitochondrial fission is not clear yet. However, these adaptors are suggested to be involved in the oligomerization and stabilization of Drp1 at the MOMs. Next, Drp1 oligomerizes by GTP hydrolysis, which also facilitates the constriction of the oligomeric Drp1 ring.

Step 3- Mitochondrial Fission and Fission Complex Disassembly.

Currently, mitochondrial fission encompassing the division of the MIMs is still under extensive research. Based on observations from apoptosis-mediated mitochondrial fission studies, it is suggested that MIMs fission might occur before MOMs constriction (Suen, Norris, & Youle, 2008). Researchers are trying to answer the question of how the Drp1 rings mediate the final constriction to mitochondrial tubules. An earlier report documented that mammalian Drp1 can constrict mitochondrial tubules forming a ring that can reach to 15 nM in size (Koirala et al., 2013). This diameter of the constricted Drp1 ring was found not to be enough for full scission to occur to mitochondrial tubules (Hatch, Gurel, & Higgs, 2014). This finding suggests that the final cleavage of mitochondrial tubules may require an additional player.

Recently, DNM2, which has intrinsic membrane fission properties, was found to induce membrane constriction or "pinching off" effect to mitochondrial tubules (Lee, Westrate, Wu, Page, & Voeltz, 2016). However, two recent reports showed that fission events can still occur in DNM2 knockout cells (Fonseca, Sanchez-Guerrero, Milosevic, & Raimundo, 2019; Kamerkar, Kraus, Sharpe, Pucadyil, & Ryan, 2018). These latter observations strongly suggest that fission is Drp1-dependent, and Drp1 alone can sever mitochondrial tubules. In final steps to fission, the Drp1 ring is thought to dissemble along with fission complex by an unknown mechanism (Hatch et al., 2014).

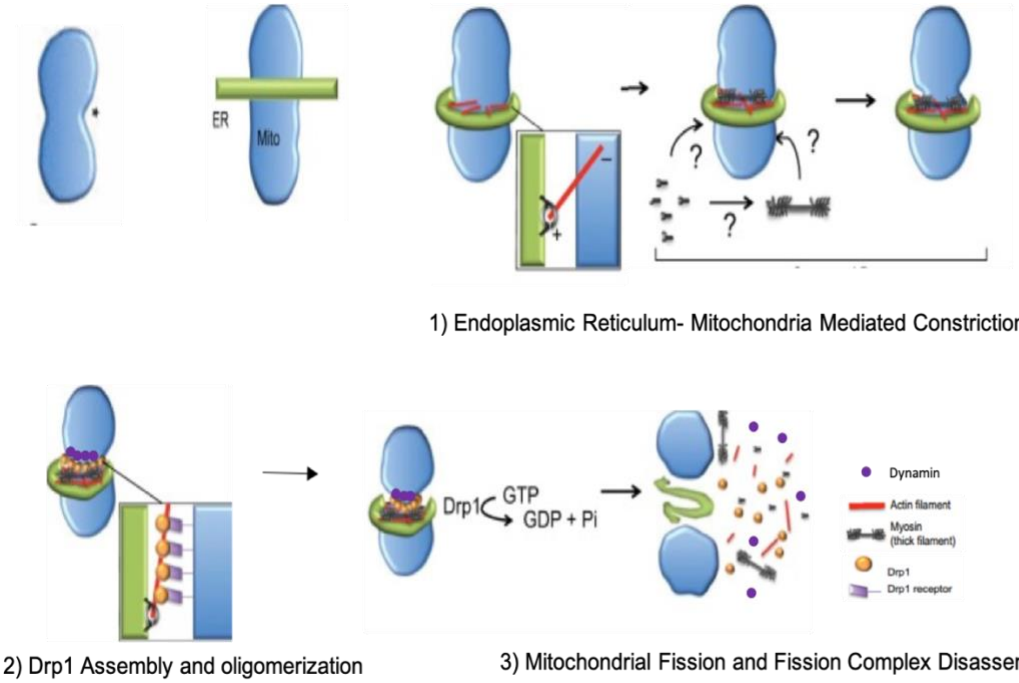

Figure 1.3 Steps in Mitochondrial Fission.
1) The ER-mediated mitochondrial constriction. At first, the MOM (blue) is marked by an unknown mechanism followed by ER (green) wrapping around mitochondria to establish actin-cytoskeleton network at contact sites with mitochondria. The NMIIA, NMIIB and/or NMIIC are recruited to facilitate the actin-myosin cytoskeleton for subsequent force generation. 2) Drp-1 monomers are recruited to bind to the MOM's receptors (Fis-1, Mff, and MiD49/MiD51) and oligomerize to form a ring-like structure at fission sites. This step is catalyzed by GTP hydrolysis to facilitate constriction of fission sites.3) Mitochondrial fragmentation and fission complex disassembly. Adapted from Hatch et al., 2014

Although recent progress in mitochondrial fission highlighted various proteins linked to fission regulation, our library of factors regulating fission is not yet complete. More studies are required to explore proteins and factors involved in mitochondrial dynamics.

1.2.2 Mitochondrial Fusion in Mammals

Mitochondrial fusion is defined as the merging of two mitochondria resulting in one mitochondrion. Upon fusion, interconnected mitochondrial networks are formed, and the mitochondrial metabolic machinery is activated (Skulachev, 2001). Fusion often occurs in three significant steps and is promoted by three mitochondrial localized GTPases that facilitate complete fusion events. While the partial fusion of the MOMs can occur, complete fusion event requires the fusion of MIMs as well. The next few sections discuss fusion proteins and the sequential steps in fusion events.

1.2.2.1 Mitochondrial Fusion Proteins

Mitofusins (Mfns). Mitofusin1 (Mfn1) and Mitofusin 2 (Mfn2) are homologous proteins localizing at the MOMs (Chen et al. 2003, Rojo et al. 2002, Santel & Fuller 2001). Mfns are composed of several domains: an N-terminal GTPase domain, adjacent to a coil-coil heptad repeat1 (HR1) domain, a transmembrane region anchoring Mfns to the mitochondrial outer membrane, followed by a C-terminal domain (Huang, Galloway, & Yoon, 2011; Rojo, Legros, Chateau, & Lombes, 2002; Santel & Fuller, 2001), illustrated in [Figure 1.4]. Human Mfns share around ~80% sequence similarity, and both can mediate mitochondrial fusion. Both Mfns accumulate at contact sites between the two opposing mitochondria leading to mitochondrial fusion (Hoppins et al., 2011). Mfn1 and Mfn2 seem to play a redundant role in mitochondrial fusion, and both can functionally replace each other.

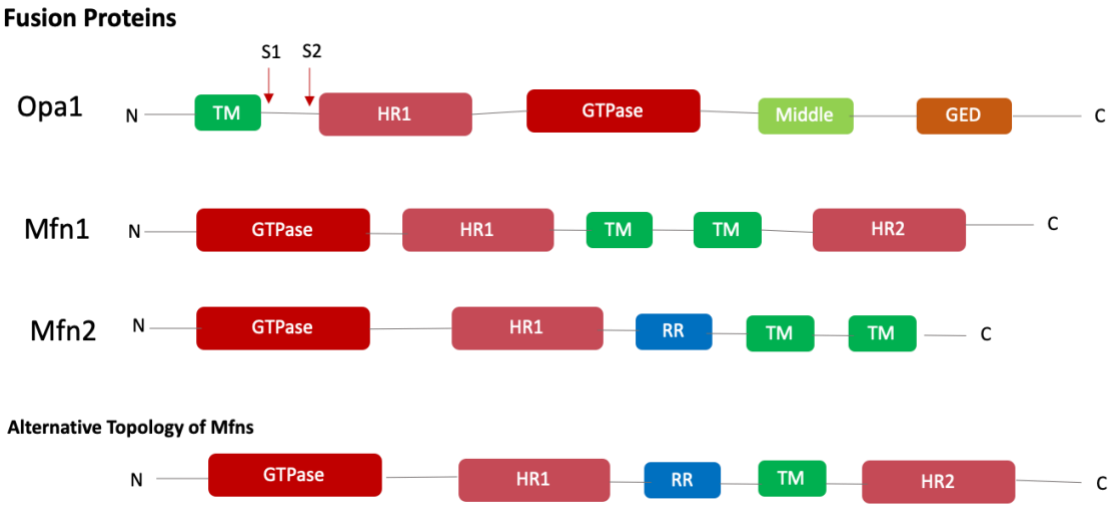

Figure.1.4 Schematic representation of the structural domains of Fusion proteins. Illustration of the core machinery proteins involved in mitochondrial fission and fusion. In regards to Mfns; The classical model proposes that Mfn2 contains two transmembrane (TM) domains in between HR1 and HR2 domains. Alternatively, Mfns have been recently demonstrated to only have one TM that lies between the two HR domains. Domains are depicted in different colors. BSE, bundle signalling elements; CC, coil-coi; GED, GTPase effector domain; HR, heptad repeats; NTD, nucleotidyl transferase; PH, Pleckstrin homology; PR , Proline rich; RR, Repeat region; TRP, tetratricopeptide repeat; TM, transmembrane. S1 : splicing variant site 1. S2: splicing variant site.

Cells lacking both Mfn1 and Mfn2 show no mitochondrial fusion activity and exhibit excessive fragmentation of the mitochondrial network (Chen, Chomyn, & Chan, 2005; Chen et al., 2003). The overexpression of each Mfn alone causes a marked clustering of fused mitochondria in the perinuclear space (Pich et al., 2005; Rojo, Legros, Chateau, & Lombes, 2002; Santel & Fuller, 2001). In mouse embryonic fibroblasts (MEF) lacking either Mfns, mitochondria show variable sizes of fragmented rounded mitochondria (Chen et al., 2003; 2005). Collectively, observations from these studies indicate the significant role of Mfns in the processes of mitochondrial fusion.

Mfns are also involved in many other mitochondrial–linked functions, such as mitochondrial transport along the axon (Cartoni et al., 2010; A. L. Misko, Sasaki, Tuck, Milbrandt, & Baloh, 2012), and the tethering of mitochondria to ER (Szabadkai, 2006; de Brito and Scorrano, 2008). The tethering between these two organelles facilitates the Ca++ intake from the ER into mitochondria (Rizzuto et al., 1993, 1998). This particular tethering of mitochondria to ER is also essential for lipid synthesis and its exchange (S. Lee & Min, 2018; Scharwey, Tatsuta, & Langer, 2013). However, the molecular mechanism underlying ER-mitochondria interaction and its involvement in lipid biosynthesis or hemostasis is not fully understood.

Mitochondrial Dynamin Like GTPase (OPA1). OPA1, which localizes at the MIMs, belongs to the dynamin protein family and regulates MIMs fusion and mitochondrial cristae architecture (Alexander et al., 2000; Delettre et al., 2001; Delettre et al., 2000; Olichon et al., 2002). Earlier studies documented that OPA1 loss causes mitochondrial fragmentation (Chen, Chomyn, & Chan, 2005; Cipolat, Martins de Brito, Dal Zilio, & Scorrano, 2004; Griparic, van der Wel, Orozco, Peters, & van der Bliek, 2004). However, our understanding of the OPA1 function is complicated by the fact that OPA1 overexpression can lead to both mitochondrial

fragmentation or elongation (Chen et al., 2005; Cipolat et al., 2004; Griparic, van der Wel, Orozco, Peters, & van der Bliek, 2004). OPA1 is a conserved protein with eight identified splice variants. OPA1 contains at least two cleavage sites that generate short and soluble variants [Figure 1.4]. OPA1 cleavages are facilitated by specific metalloproteases (i.e., OMA1 and YME1L) to cleave OPA1 at specific sites, illustrated in [Figure 1.4] (Ehses et al., 2009; Griparic, Kanazawa, & van der Bliek, 2007; Head, Griparic, Amiri, Gandre-Babbe, & van der Bliek, 2009; Song, Chen, Fiket, Alexander, & Chan, 2007). Such proteolytic cleavages result in at least five OPA1 isoforms, two of them at higher molecular weights, known as long (L-OPA1), and the other three as short forms, known as short (S-OPA1). Initial studies highlighted the requirement of both L-OPA1 and S-OPA1 isoforms in mitochondrial fusion (Song et al., 2007). Later studies demonstrated that the L-OPA1 isoform alone is sufficient to drive fusion activity (Anand et al., 2014; Tondera et al., 2009). Another recent study suggested that the balanced orchestrion of OPA1 cleavage by OMA-1 and YME1-L metalloproteases plays a key role in fusion regulation (MacVicar & Langer, 2016).

In addition to its role in MIMs fusion, OPA1 plays a role in cristate morphogenesis, and protection against programmed cell death. In the absence of OPA1, mitochondria are fragmented, and mitochondrial cristae are deformed, facilitating cytochrome C release in response to apoptotic stimuli (Olichon et al., 2003; Frezza et al., 2006; Griparic et al., 2004; Meeusen et al., 2006; Olichon et al., 2006). These observations further complicate the role of OPA1 in cellular functions. Further studies are required to elucidate the functions of OPA1 in mitochondrial dynamics and other cellular functions.

1.2.2.2 Steps in Mitochondrial Fusion

The main proteins mediating the process of mitochondrial fusion are identified (e.g., Mfn1, Mfn2, and OPA1); however, the specific mechanisms by which mitochondrial membranes fuse remain unknown. Mitochondrial fusion is suggested to occur in three significant steps; tethering of the opposing MOMs, the fusion of the MOMs, followed by fusion of MIMs, where mixing of the internal contents occurs [Figure 1.5];

Step 1- Tethering of The Two Opposing Mitochondria. The two mitochondria destined for fusion first come in contact and become tethered. Because the full biochemical structure of Mfn2 is not fully recognized yet, many models were suggested for the initial tethering of mitochondria by Mfn2. An earlier report suggested that Mfns interact via an antiparallel *trans*-interactions through their HR2 domains (Koshiba et al., 2004). However, recent data suggests that the HR2 domain is not exposed to the cytosol, and the tethering is mediated primarily by the GTPase-domains found in Mfns (Cao et al., 2017; Y. Qi et al., 2016). This GTPase-dependent oligomerization is proposed to promote adjacent outer mitochondrial membranes merge (Cao et al., 2017; Y. Qi et al., 2016). Another recent study proposed that the tethering of the MOMs occurs via peptides mimicking the HR1 helixes to activate fusion events (Franco et al., 2016). The initiation of mitochondrial fusion is also suggested to involve redox-signaling (Griparic, van der Wel, Orozco, Peters, & van der Bliek, 2004; Norton et al., 2014; Shutt, Geoffrion, Milne, & McBride, 2012; Thaher et al., 2018). In redox-signaling, the HR2 domains are suggested to be oxidized at specified cysteine sites via increased levels of oxidized glutathione, leading to the formation of disulfide bonds between the two Mfns molecules. The initial oxidation of Mfn2 molecules oligomerizes these molecules and primes them for tethering (Mattie, Riemer, Wideman, & McBride, 2018).

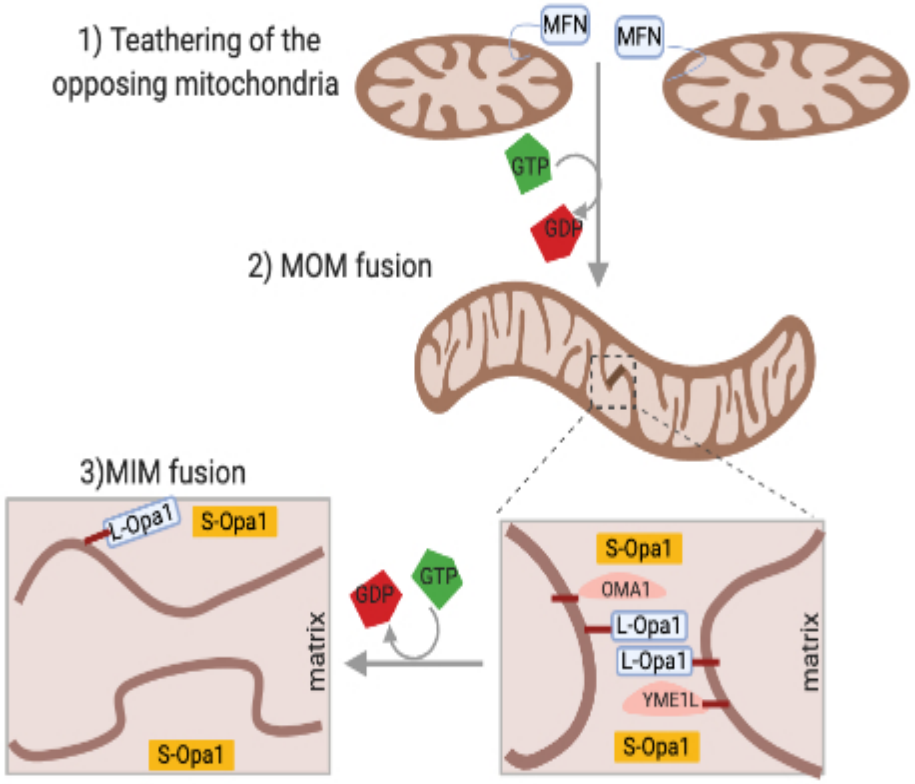

Figure 1.5 Steps in Mitochondrial Fusion.
Mitochondrial fusion is a three-step process consisting of MOM fusion, mediated Mfn1 and Mfn2 GTPases, followed by MIM fusion mediated by the Opa1 GTPase. Opa1 is present in two forms; L-Op1, which is an integral membrane form and a shorter processed form S-Opa1. Proteolytic cleavage of Opa1 can be achieved by either OMA1 or YME1L proteases. Adapted and modified from (Tilokani, Nagashima, Paupe, & Prudent, 2018). Illustration created by app/biorender.com.

Once Mfns are tethered, the distance between the two opposing mitochondria is suggested to be decrease; promoting further fusion steps (Brandt, Cavellini, Kuhlbrandt, & Cohen, 2016).

Step 2 – Fusion of the Mitochondrial Outer Membranes (MOMs). Based on recent literature, mitochondrial tethering occurs through the interactions between the fully extended Mfns molecules in the opposing adjacent mitochondria. The fusion of the MOMs is suggested to be facilitated by GTP binding (Brandt et al., 2016; Ishihara, Eura, & Mihara, 2004). GTP hydrolysis (GDP bound) is proposed to close the hinge between the two opposing mitochondria, bringing MOMs of both mitochondria together for fusion (Ishihara et al., 2004). GDP release may augment membrane fusion by inducing additional conformational changes that promote mitochondrial membrane merging (Low, Sachse, Amos, & Lowe, 2009).

Step 3- Fusion of the Mitochondria Inner Membranes (MIMs). MIMs fusion occurs after the MOMs fusion. OPA1 drives the fusion of the MIMs (Ban et al., 2017). The negatively charged lipid cardiolipin, which resides at the MIMs, interacts with L-OPA1 in a heterotypic fashion to drive MIMs fusion. The S-OPA1 is also suggested to facilitate L-OPA1-cardiolipin binding and membranes fusion (DeVay et al., 2009). Recent studies suggested that fusion of the MIMs is dependent on Mfn1, but not Mfn2. This suggestion raises the possibility of a cross-talk between the MOMs and the MIMs and the potential interaction between Mfn1 and OPA1 (Cipolat, Martins de Brito, Dal Zilio, & Scorrano, 2004; Mattie, Riemer, Wideman, & McBride, 2018; Tondera et al., 2009).

1.3 Mitochondrial Dynamics: Why?

Responsive mitochondrial dynamics are essential in many cellular processes, including cell cycle, responding to induced stress, mitophagy, and motility. Herein, I focus on the importance of mitochondrial dynamics in mitophagy, mitochondrial transport, and quality control.

1.3.1 Mitochondrial Mitophagy

In autophagy, cellular components are degraded by lysosomes. Initially, cellular components are engulfed by autophagosomes, which fuse with lysosome to break down cellular materials utilizing hydrolytic enzymes. Autophagy plays a vital role in maintaining cellular quality control by promoting protein turn over and degradation of damaged organelles (Glick, Barth, & Macleod, 2010). In mitophagy, mitochondria are specifically degraded. In fact, mitophagy can occur as a part of the generalized autophagic response to dysfunctional organelles. Mitophagy happens in response to a variety of signals reviewed in (L. Liu et al., 2012; Melser et al., 2013)

Currently, the most studied mitophagy pathway is the PTEN-induced kinase 1 (Pink 1)/Parkin-mediated mitophagy, which occurs in response to changes in mitochondrial membrane potential. In this model, Pink1 is constitutively targeted to mitochondria and imported. In the absence of mitochondrial membrane potential, Pink1 accumulates at the damaged MOMs. This, in turn, activates the phosphorylation of the Parkin E3 ubiquitin ligase, which is found in the cytosol (Matsuda et al., 2010; Narendra et al., 2010). Parkin is then recruited to the MOMs to ubiquitinate several proteins. As a result, adaptor proteins are translocated to the MOMs for proteasomal degradation (Chan et al., 2011). At this point, mitochondria are ready to be removed by autophagosomes. Few reports suggest that “mitophagy occurs selectively for damaged

mitochondria "(Kim, Rodriguez-Enriquez, & Lemasters, 2007; Twig et al., 2008). Therefore, compromising mitophagy may lead to the accumulation of oxidized proteins, and results in mitochondrial respiration deficits (Billia et al., 2011; Pickles, Vigie, & Youle, 2018).

1.3.2 Mitochondrial Axonal Transport and Mitochondrial Dynamics

In addition to fission and fusion events, mitochondria need to move throughout the cell. Mitochondrial motility is highly critical in cells that demanding higher energy needs or requiring mitochondria at a distance from the cell body, i.e., neurons. Neuronal axons contain microtubules organized in a linear uniformly polarized orientation with a minus terminus at the cell body and plus terminus at distal tips (Schwarz, 2013). The axonal flow is defined by the anterograde and retrograde movements. While, cellular elements move toward the terminal ends in anterograde flow, cellular elements travel back to neuron's soma in retrograde flow (Schwarz, 2013).

Mitochondrial transport in mammalian cells is largely microtubule-based (Ligon & Steward, 2000). Microtubules serve as a track with other molecular complexes to carry mitochondria along the neuronal axon (Hollenbeck & Saxton, 2005). Microtubule filaments, which are composed of the α-tubulin and the β-tubulin subunits, form a cytoskeleton for mitochondrial transport and distribution (Hollenbeck & Saxton, 2005). Polymerization of the α- and β- tubulin subunits are fundamental for proper axonal transport and motors shuttling in each direction (Dombeck et al., 2003; Nirschl, Ghiretti, & Holzbaur, 2017). Recently, a motor adaptor complex was identified as a mediator for mitochondrial transport in neurons, and possibly in most other cells (Brickley & Stephenson, 2011; Glater, Megeath, Stowers, & Schwarz, 2006; X. Guo et al., 2005; Hollenbeck & Saxton, 2005). The core of this complex consists of several proteins: (a) Kinesin, a motor protein that moves along microtubule filaments carrying cellular material and utilizes ATP hydrolysis, (b) Miro, a protein anchored to the outer surface of the

mitochondria and facilitates mitochondrial shuttling, (c) Milton, which is a protein that works as a bridge linking Kinesin and Miro, (d) Dynein, a cytoskeleton protein that transfers cellular cargo, also interacts with Milton and Miro. Mutations in motor proteins that cause mitochondrial transport deficits are associated with CMT disease and peripheral neuropathies (Beijer, Sisto, Van Lent, Baets, & Timmerman, 2019).

1.3.3 Fusion, Fission, and Mitophagy as a Quality Control Mechanism

Mitochondrial homeostasis requires an equilibrium between mitophagy (mitochondrial degradation) and mitochondrial biogenesis. Excessive mitophagy can lead to bioenergetic failure. Also, extreme mitochondrial biogenesis generates harmful levels of reactive oxygen species (ROS) and activates apoptotic signalling(East & Campanella, 2016). Therefore, a balanced interchange between both processes is essential for proper cellular function and cell survival (Kanki et al., 2009; Mao, Wang, Liu, & Klionsky, 2013).

Mitophagy regulates mitochondrial dynamics directly. For instance, the Pink1-Parkin pathway modifies several MOMs' proteins via protein phosphorylation, ubiquitination, and degradation. For example, Miro and Mfn2 proteins are phosphorylated by Pink1 and ubiquitinated by Parkin for further degradation by phagosome (Chan et al., 2011; X. Wang et al., 2011). Thus, the Pink1/Parkin pathway facilitates the shutting down of mitochondrial fusion machinery. Also, the Pink1/Parkin pathway serves to transport mitochondria across the cytoplasm to be sequestrated for further efficient degradation without spreading the damaged components (Cai, Zakaria, Simone, & Sheng, 2012). Interestingly, recent reports suggested that mitophagy also facilitates mitochondrial fission (Burman et al., 2017; Ni, Williams, & Ding, 2015; Twig & Shirihai, 2011). The balanced interaction between fusion and fission is also essential for maintaining mitochondrial DNA.

Generally, high levels of mutant DNA increase the odds and severity of mitochondrial diseases or neuropathies (Taylor & Turnbull, 2005). Mitochondrial fusion and fission are thought to play a "protective role" for the mtDNA genome (Tam, Gruber, Halliwell, & Gunawan, 2015). In fusion-deficient cells, mitochondria progressively lose their mtDNA, most likely due to its inability to share necessary materials during fusion (Chen, McCaffery, & Chan, 2007). Protection of mtDNA and mitochondrial functions occur through fusing healthy mitochondria to the damaged organelles. Fusion allows defective mitochondria to be exchanged by healthy materials from healthy mitochondria. This, in turn, allows the compensation of non-functioning elements and promote repair machinery for dysfunctional mitochondrial.

Fission also protects mitochondrial elements in several ways. For instance, the segregation of depolarized mitochondrial segments allows dysfunctional segments to be separated from active and healthy mitochondria for further degradation by mitophagy (Twig, Hyde, & Shirihai, 2008). Also, fission or inhibited-fusion ultimately prevents damaged mitochondria from merging with other healthy mitochondria (Twig, Elorza, et al., 2008). Failure to properly remove damaged components impairs mitochondrial functions or dynamics. Impairments in mitochondrial dynamics increase mutant mtDNA in specific disorders (Suarez-Rivero et al., 2016; Tam et al., 2015). Intriguingly, dysfunctions in mitophagy have been reported in several cellular and animal models of neurodegenerative diseases (Shefa et al., 2019; Y. Wang, Liu, & Lu, 2019); highlighting an indirect link between mitophagy and mitochondrial dynamics.

1.4 The Endoplasmic Reticulum (ER) and Links to Mitochondria

The ER is a large membrane-bound organelle that is involved in many cellular functions. ER is the site where luminal, secretory, and membrane proteins are synthesized and shuttled to other cellular organelles. The ER also functions as intracellular storage for Ca^{++} and lipid synthesis enzymes (Elbaz & Schuldiner, 2011). Recent studies demonstrated that ER has contact sites with many other cellular organelles. The contact sites between mitochondria and ER are known as the mitochondria-associated membrane (MAMs). Specific proteins mediate MAMs on each organelle. Cellular materials trafficking occurs between the mitochondria and ER (Friedman, Webster, Mastronarde, Verhey, & Voeltz, 2010). Despite the fact that each organelle has distinct roles, the tight juxta-positioning of these two organelles suggests its importance for the normal cellular functioning. Primary functions of MAMs include lipids biosynthesis, mitochondrial fission, Ca^{++} signaling, and coordinated dynamics of the two organelles. The next few paragraphs are focusing on functions pertaining to this thesis.

1.4.1 ER -Mitochondria Contact Sites Promotes Mitochondrial Fission and Possibly Fusion

As mentioned above, the MAMs are essential regulators for mitochondrial fission. The ER is strongly suggested to drive mitochondria's initial constrictions prior to fission complex machinery arrival at division sites. In mammalian cells, the two opposing mitochondria are joined by both Mfns at the MOMs (Chen et al., 2003). The mitochondria and ER tethering are facilitated mainly by Mfn2. In fact, mouse embryonic fibroblasts (MEF) lacking the *MFN2* gene show disrupted ER-mitochondria contacts, which were rescued by ectopic expression of Mfn2 (de Brito & Scorrano, 2008). Currently, it is not clear whether Mfn2 promotes tethering of ER to mitochondria during fusion events or not. Considering that Mfn2 governs tethering of mitochondria to ER, MAMs may also regulate mitochondrial fusion.

1.4.2 Mitochondria-ER Contact Sites may be Involved in and Lipid Droplets Synthesis and Lipid Exchange and Hemostasis

Lipid droplets are spherical organelles found in the cytoplasm and serve as lipid and energy storage (Guo, Cordes, Farese, & Walther, 2009). Lipid droplets are composed of: (a) a hydrophobic core consisting natural lipids, (b) an outer monolayer of embedded proteins that are involved in lipid transport, synthesis, and degradation (Bartz et al., 2007; Brown, 2001; Ohsaki, Cheng, Suzuki, Fujita, & Fujimoto, 2008). The number, size, composition, and functions of lipid droplets vary depending on tissues or organs in which cells reside (Thiam & Beller, 2017). Earlier reports documented the role of lipid droplets in moderating energy shifts within the cell. For example, in times of excess fatty acid availability, lipids are stored in lipid droplets in the form of triacylglycerols (TAG) (Brasaemle, 2007). In contrast, when lipid storage is low, the fats are released from lipid droplets to be utilized as energy resource (Ducharme & Bickel, 2008). However, the exact molecular mechanisms in these cellular conditions are not fully understood yet.

Lipid droplets are highly dynamics organelles and communicate with many cellular organelles, including mitochondria and ER (Ozeki et al., 2005; Sturmey, O'Toole, & Leese, 2006; Turro et al., 2006). Lipid droplets are synthesized at the ER membrane. Once a lipid droplet sphere formed, budding and detachment of the droplet occur. Lipid droplets then shuttle in the cytoplasm to other organelles like mitochondria. It is suggested that mitochondria utilize fatty acids released from lipid droplets to generate ATP (Benador, Veliova, Liesa, & Shirihai, 2019). Degradation of lipid droplets for further usage of its constituents occurs via cytosolic lipases (Lass, Zimmermann, Oberer, & Zechner, 2011) or lipophagy (Cingolani & Czaja, 2016).

MAMs are strongly suggested to be involved in lipid droplet formation (Fujimoto & Hayashi, 2011). The majority of enzymes involved in lipid biosynthesis are located at the ER, the MOMs, or the shared MAMs between these two organelles. For instance, the phosphatidylserine (PS) synthase, an enzyme involved in lipid synthesis, is located at the MAMs (Stone & Vance, 2000; Vance, 1990; Voelker, 2000). Indeed, biosynthesis of the cell's most abundant lipids and phospholipids occurs at the ER-mitochondria interface. This process is coordinated by uncharacterized complexes (van Meer, Voelker, & Feigenson, 2008). The exchange of lipids between these two organelles' membranes is bidirectional and suggested to facilitate cellular energy homeostasis, and lipid and protein trafficking (Flis & Daum, 2013; Rizzuto et al., 1998; Voelker, 2005). The mechanisms of lipid exchange between the two organelles are not explored fully in mammalian cells and are still under research (Iwasawa, Mahul-Mellier, Datler, Pazarentzos, & Grimm, 2011; Kornmann, 2013; Simmen et al., 2005; Szabadkai et al., 2006). An aberrant accumulation of lipid droplets was observed in multiple human diseases (Onal, Kutlu, Gozuacik, & Dokmeci Emre, 2017). Given that not all *MFN2*-CMT mutations cause impairments in mitochondrial fusion, it is tempting to speculate that other functions of Mfn2, such as mitochondria-ER contacts, might be relevant to CMT pathogenesis.

1.5 Peripheral Neuropathies (PNs) and Mitochondrial Dynamics

1.5.1 Neurons, Mitochondria, and Peripheral Neuropathies (PNs): A Brief Overview

Neurons need higher energy due to their large extensions. The relative metabolic requirements of peripheral neurons are frequently changing. Therefore, mitochondria play significantly as a source of energy (Hollenbeck & Saxton, 2005). As a result, it is critical to maintain an ideal distribution of mitochondria within the neuron's body and its axonal extensions. Delivering mitochondria to areas that require higher metabolites is essential and should be met at the right balance without depleting energy in other cellular parts. In neurons, mitochondria travel in anterograde and retrograde pathways to accommodate energy demands at several parts at the same time (Schwarz, 2013). Because mitochondria are involved in many primary cellular functions, their dysfunction causes various disorders, including mitochondrial diseases. Mitochondrial proteins are encoded either by mitochondrial or nuclear DNA. Therefore, mutations in mitochondrial or nuclear genomic DNA can cause mitochondrial diseases (McFarland, Taylor, & Turnbull, 2010). Mitochondrial diseases have a broad spectrum of phenotypes manifesting in organs and tissues requiring higher energy, including neuronal, skeletal muscle, heart, and kidney tissues (Wallace et al., 1999). Also, mitochondrial disease can affect multiple systems at the onset of the disease or during disease progression (Finsterer, 2005, 2011; Rahman & Hanna, 2009). Usually, the severity and symptoms of associating mitochondrial diseases range from mild to life-threatening.

One of the commonly affected systems in mitochondrial diseases is the peripheral nervous system leading to peripheral neuropathies (PNs). PNs are a group of disorders characterized by degeneration of peripheral motor, sensory, and autonomic axons (Bussmann & Storkebaum, 2017). PNs in mitochondrial diseases occur as a direct consequence of hereditary genetic

mutations and considered as primary mitochondrial PNs. Mitochondrial diseases may also manifest as a secondary phenotype to an underlying disorder, such as diabetes and thyroid disease (Pareyson, Piscosquito, Moroni, Salsano, & Zeviani, 2013). One of the significant hereditary neuropathies is the motor and sensory neuropathy (HMSN), also known as Charcot-Marie-Tooth (CMT).

1.5.2 Charcot-Marie-Tooth (CMT) Disease

CMT disease is a heterogeneous group of inherited PNs affecting motor neurons, sensory neurons, and Schwan cells. CMT is characterized by distal limb muscle wasting weakness with sensory loss, reduced or absent deep tendon reflexes, and foot deformities. CMT disease is the most common inherited neuromuscular disorder with a prevalence of 1/2500 in the North America (Barreto et al., 2016). According to electrophysiological criteria, CMT disease is classified into two main categories: demyelinating PNs with motor nerve conduction velocity (MNCV) less than 38 m/s and axonal neuropathies affecting mostly axons with normal MNCV (>3m m/s). There are also other CMT sub-classifications beyond this simple classification reviewed in (Pareyson, Saveri, Sagnelli, & Piscosquito, 2015).

CMT2A is the most prevalent form of the dominant axonal CMT with a 20-36% frequency among CMT patients (Barreto et al., 2016). Typical clinical manifestations of CMT2A include progressive distal limb muscle weakness, atrophy, distal sensors loss, mobility difficulties that may end up to wheelchair dependency. Surprisingly, the disease onset varies diversely among affected patients and seems to be related to disease severity. Early-onset of the disease is often associated with the most severe forms. A hallmark of the CMTA diseases is that they target neurons with the “longest axons” (Juarez & Palau, 2012). Nerve biopsies from typical CMT2A patients show axonal degeneration for both myelinated and unmyelinated fibers with an

accumulation of round, small, fragmented mitochondria at neurons tips (Calvo et al., 2009; Chung et al., 2006; Pareyson, Piscosquito, Moroni, Salsano, & Zeviani, 2013; Sole et al., 2009; Vallat et al., 2008; Verhoeven et al., 2006; Vital et al., 2012). In the following section, GDAP and MFN2 are discussed in detail as classic examples of genes regulating mitochondrial dynamics, and its mutations are associating with CMT diseases.

1.5.2.1 GDAP1 and CMT-PNs

Up To Date, more than 40 mutations associated with GDAP1-CMT have been reported (A. M. Martin, Maradei, & Velasco, 2015). GDAP1 is localized at the MOMs and is involved in fission via an unknown mechanism. GDAP1 is expressed in the central and peripheral nervous systems. However, data for GDAP1 localizing at axons or at myelinating cells are still in conflict (Cuesta et al., 2002; Detmer & Chan, 2007b; Milone & Benarroch, 2012; Niemann, Wagner, Ruegg, & Suter, 2009; Pedrola et al., 2008). Because GDAP1 regulates mitochondrial fission, functions downstream of fission events might be affected by GDAP1 mutations. For instance, GDAP1 silencing showed an impaired mitochondrial-ER interaction, changes in Ca^{++} influx, abnormal mitochondrial distribution, and dysfunction of the respiratory complex I (Gonzalez-Sanchez et al., 2017; Pla-Martin et al., 2013). In fact, GDAP1 mutations have been linked to the most severe form of the CMT disease (Pareyson, Saveri, Sagnelli, & Piscosquito, 2015). In GDAP1-CMT patients, neuropathy is the most dominant observed feature, starting early at infancy, and progresses rapidly to a complete loss of movement. Nerve biopsies from patients carrying GDAP1 mutations demonstrate axonal degeneration with loss of large myelinated fibers (Cassereau, Chevrollier, Gueguen, et al., 2011; Moroni et al., 2009; Nelis et al., 2002).

1.5.2.2 Mitofusin2 and CMT-PNs

Mfn2 is a mitochondrial fusion protein that is linked to PNs. Mutations in the *MFN2* gene are commonly associated with CMT disease (S. M. Murphy et al., 2012; Zuchner et al., 2006; Zuchner et al., 2004). Most of the *MFN2*-CMT2A cases show a severe phenotype with rapid onset and during disease progression. In *MFN2*- CMT2A disease, motor neurons are primarily affected, leading to disabilities and severe proximal weakness (Feely et al., 2011; Verhoeven et al., 2006; Zuchner et al., 2006; Zuchner et al., 2004). Other patients with late-onset show mild disabilities (Zuchner et al., 2006). Also, *de novo* mutations occur with high frequency in CMT2A (Chung et al., 2006; Feely et al., 2011; Renaldo et al., 2012). Some CMT2A patients develop other complex phenotypes, including tremor, deafness, vocal cord plays, and up to 20% of the patients develop optic atrophy (Banchs, Casasnovas, Montero, Martinez-Matos, & Volpini, 2008; Chung et al., 2006; Pareyson & Marchesi, 2009; Verhoeven et al., 2006; Zuchner et al., 2006; Zuchner et al., 2004).

Up To Date, more than 100 different mutations in *MFN2* gene have been identified, accounting for at least 20% of CMT2A (Pareyson, Saveri, Sagnelli, & Piscosquito, 2015). The spectrum of *MFN2* mutations related to phenotypes is rapidly expanding, and a complex clinical picture has been reported at the mean time. The majority of *MFN2* mutations are missense mutations located at critical functional regions close to or at the GTPase domains and coiled-coil motifs of the protein (Cartoni & Martinou, 2009; Feely et al., 2011; Pareyson, Piscosquito, Moroni, Salsano, & Zeviani, 2013). Many other mutations are considered polymorphisms or variants of undetermined significance (Cho, Sung, Kim, & Ki, 2007; Engelfried et al., 2006; McCorquodale et al., 2011). Although Mfn2 is ubiquitously expressed in human tissues, Mfn2 mutants are restricted to neurological dysfunction. Notably, the Mfn1 protein is suggested

to be sufficient to compensate for Mfn2 functions in most tissues, but not in peripheral neurons, where Mfn1 is expressed at a lower level. However, how *MFN2* mutations result in CMT2A or other complex phenotypes is not clear yet. Some studies suggest that PNs occur due to impaired mitochondrial fusion (Detmer & Chan, 2007b; El Fissi et al., 2018; Franco et al., 2016). Other studies suggest that abnormal mitochondrial transport underlies PNs and eventually leads to distal axonal degeneration (Cartoni & Martinou, 2009; Misko, Sasaki, Tuck, Milbrandt, & Baloh, 2012). In this thesis, a novel *MFN2* mutation (MFN2 Q367H) that does not cause neuropathy was studied, and our findings suggest MAMs as a possible player in PNs pathogenesis- discussed in Chapter four.

1.5.3 CMT-PNs: Possible Underlying Mechanisms

Currently, more than 40 genes associating CMT-PNs or distal hereditary motor PNs have been recognized; highlighting myelination and axonal transport as critical processes for axonal health (Vallat, Mathis, & Funalot, 2013). While many different cellular pathways can contribute to impairments in myelination and axonal transport, I focus in the few next paragraphs on mitochondrial dynamics and MAMs as possible players in PNs pathogenesis.

1.5.3.1 Impaired Myelination

Abnormal myelination or axon demyelination are of the classical causes of CMT-PNs. Mutations in genes required for the synthesis of myelin sheath provide an unprecedented opportunity to perturb axon myelination. For instance, mutations in *PMP22*, which is an integral constituent of compact myelin and expressed by Schwan myelinating cells, cause severe peripheral demyelinating CMT1A (Li, Parker, Martyn, Natarajan, & Guo, 2013; Sancho, Young, & Suter, 2001). Also, alterations to sphingolipids, which are essential lipids for myelination, contribute to axonal or motor sensory PNs. For instance, dominant mutations in the gene

encoding the Serine Palmitoyltransferase (SPT), which is critical to sphingolipid biosynthesis, cause hereditary sensory neuropathy type IA (HSAN1A) and hereditary sensory neuropathy type IC (HSAN1C) (Bejaoui et al., 2001; Dawkins, Hulme, Brahmbhatt, Auer-Grumbach, & Nicholson, 2001; Rotthier et al., 2010). Another factor that may affect myelination is protein translation. Myelination requires high protein synthesis (Müller, Bauer, Schäfer, & White, 2013). Therefore, protein synthesis inhibition may also contribute to PNs. Dominant mutations in cytosolic domains of the aminoacyl-tRNA synthetases (aaRSs,) which is a catalyzing agent required in the early protein translation process, are correlated with axonal or intermediate forms of CMT diseases (Hyun et al., 2014; Ibba & Soll, 2000; Jordanova et al., 2006; Latour et al., 2010; Motley et al., 2011). Protein translation requires catalyzing aminoacylation of tRNAs along its cognate via the aaRSs (Ibba & Soll, 2000).

1.5.3.2 Defects in Axonal Transport May Contribute to PNs

Mutations in the primary anterograde or retrograde transport machinery are associated with PNs. In human, mutations in Kinesins, which are involved in the anterograde transport, cause CM, and hereditary sensory or autonomic PNs. Also, mutations in Dynein, which is involved in the retrograde transport, result in distal hereditary motor neuropathy (dHMN) (Eschbach et al., 2013; Pilling, Horiuchi, Lively, & Saxton, 2006). In *Drosophil*a models, mutations in the Kinesins or Dynein exhibit disrupted axonal transport and lead to axonal PNs-like phenotypes (Duncan & Goldstein, 2006). These phenotypes encompass progressive loss sensory responsiveness, axonal swellings, morphological defects in mitochondria and lysosome and neuromuscular junction, and impaired synaptic transmission (Hurd & Saxton, 1996; Martin et al., 1999; Ray et al., 1999).

How mitochondrial transport machinery interacts with the fusion or fission machinery is not clear yet. Loss of the Dynein protein function inhibits the translocation of Drp1 into MOMs and leads to the clustering of elongated mitochondria in the perinuclear area (Varadi et al., 2004). Also, Miro manipulation in mammalian cells results in mitochondrial morphology changes (Fransson, Ruusala, & Aspenstrom, 2006; Saotome et al., 2008). These observations suggest that mitochondrial transport is affected primarily by defects in motor proteins and, possibly, secondary by deficits in mitochondrial dynamics.

1.5.3.3 Aberrant mitochondrial Fusion or Fission Are Linked to Peripheral Neuropathies

Observations from clinical studies in GDAP1 and *MFN2*-CMT patients and their cell lines suggest that impaired mitochondrial dynamics contribute to PNs pathogenesis. In an earlier study, cultured Purkinje cells obtained from *MFN2* knockout mice showed an improper distribution of mitochondria in dendritic branches (Chen, McCaffery, & Chan, 2007). In this pervious study, dendrites lacked mitochondria and showed fewer spines than usual. Also, the presence of Mfn2 mutant in primary rat dorsal root ganglion (DRG) cells resulted in mitochondria accumulation in the cell body and at distal axons. Besides, an increased number of stationary mitochondria were observed in these cells (Baloh, Schmidt, Pestronk, & Milbrandt, 2007; Cartoni et al., 2010; Misko, Sasaki, Tuck, Milbrandt, & Baloh, 2012; Villegas et al., 2014). In recent studies, overexpressing the R94Q (Mfn2 mutant) also resulted in the accumulation of mitochondria at distal parts of the nerve (Bernard-Marissal et al., 2019; Zhou et al., 2019).

Similarly, dominant GDAP1 mutations caused an impaired mitochondrial fusion (similar to the one associated with *MFN2* mutations), and increased apoptosis (Niemann, Wagner, Ruegg, & Suter, 2009). Recessive GDAP1 mutations were observed to be associated with decreased

mitochondrial fission. Significantly, in both inherence patterns, altered mitochondrial dynamics might led to altered transport of mitochondria to distal axons, and eventually resulting in axonal degeneration (Niemann et al., 2009).

Based on these observations, a recent review hypothesized that impaired fusion or fission dynamics as significant players in the pathogenesis of PNs (Chen & Chan, 2009). In this model, defective fusion or fission causes the accumulation of stationary or dysfunctional mitochondria in the cell body or distal axons. This accumulation, in turn, impedes anterograde and retrograde transport along the axon, including proper mitochondrial transport, eventually leading to the degeneration of the highly polar and lengthy axon of peripheral nerves (Chen & Chan, 2009), illustrated in [Figure 1.6]. This model was challenged by data from another recent report showing the inability of CMT2A-associated *MFN2* mutations to induce axonal transport defects in sensory and motor neurons (Strickland et al., 2014). In this report, sensory neurons isolated from homozygous or heterozygous R94W-*MFN2* knockout mice showed healthy mitochondria with mitochondrial trafficking similar to mitochondria in wild type animals (Strickland et al., 2014). In support to observation from the report discussed above, mitochondrial trafficking in motor neurons differentiated from induced pluripotent stem cells (iPSCs) from CMT2A-R94Q patients was only mildly affected (Rizzo et al., 2016; Saporta et al., 2015). In both studies, neither axonal length nor survival was reduced. Collectively, these observations suggest impairments to mitochondrial motility may not solely underly PNs- associated *MFN2* mutations and raises the possibility of other involved mechanisms in PNs pathogenesis.

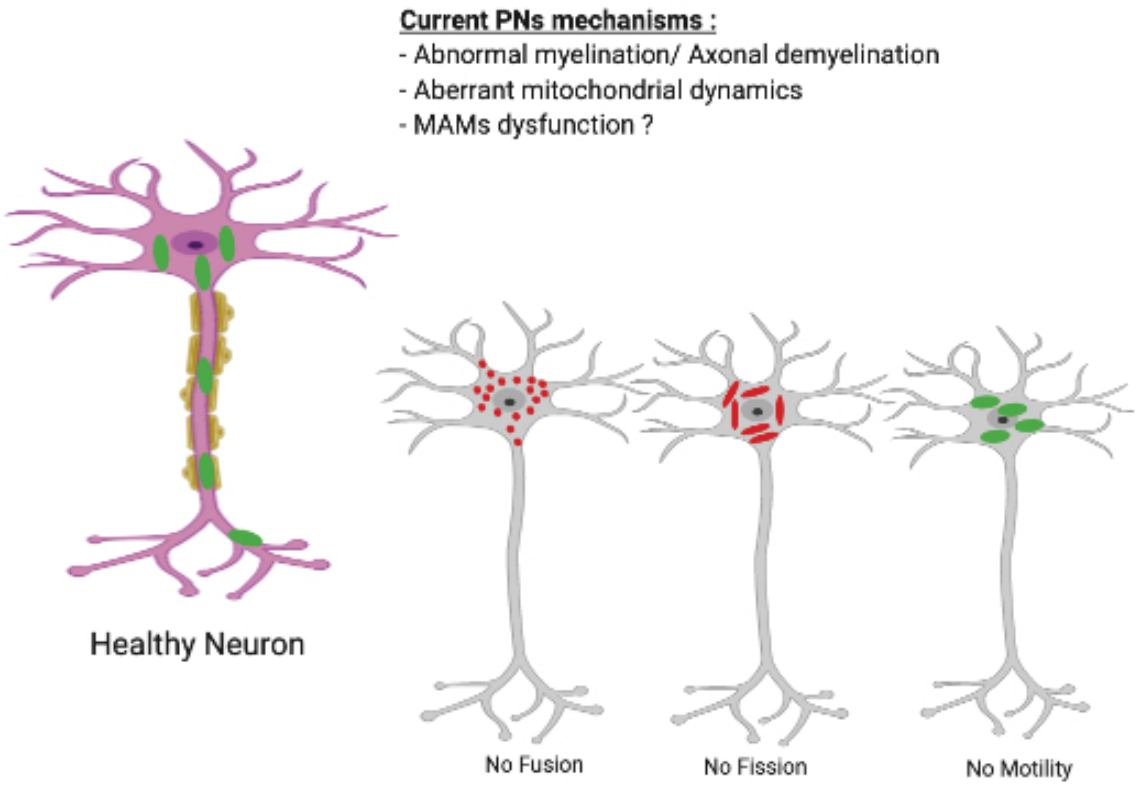

Figure 1.6 Possible mechanisms underlying Neuropathies.
In healthy neurons, mitochondria are motile and move long distances from the cell body to dendritic and back from dendrites to cell body. In the absence of fusion, excessive fragmentation occurs and mitochondria may accumulate in cell body, distal axon or axon The mitochondria secondarily have transport defects that prevent proper distribution to the periphery. In the absence of fission, the mitochondria excessively fused and may cluster within the cell body and cannot efficiently travel to the dendrites. Defects in mitochondrial motility prevent distribution of mitochondria to the periphery. In the absence of mitophagy, abnormal mitochondria accumulate. Adapted and modified from (Cartoni & Martinou, 2009; Chen & Chan, 2009). Illustration created by app/biorender.com

Last but not least, mitochondrial fusion and fission play a pivotal role in mtDNA maintenance. Therefore, it is conceivable that impairments in fusion or fission machinery lead to mtDNA instability, and possibly contributing to PNs pathogenesis. Because mtDNA encodes 13 proteins of the respiratory chain, mtDNA depletion or defects are expected to impair oxidative phosphorylation processes. For instance, a decrease in cytochrome C oxidase was observed in Purkinje cells of conditional *MFN2* knockout mice (Chen et al., 2007). This decline occurred possibly due to mtDNA loss caused by impaired mitochondrial fusion function (Chen et al., 2007). Studies with fibroblasts from CMT2A patients carrying *MFN2* mutations have often shown mitochondrial coupling defects leading to reduced OXPHOS (Loiseau et al., 2007). These observations implicate that bioenergetics alterations occur as an indirect result of fusion abnormalities. Hence, impairments in mitochondrial fusion or fission may alter mtDNA stability, which may, in turn, cause mitochondrial respiratory chain defects, that might be involved in CMT-PNs pathogenesis mechanism.

1.5.3.4 Impaired Mitochondria Associated Membrane (MAMs) May Underlie PNs

In addition to mitochondria, dysfunction of the ER may also facilitate the development of PNs. ER interacts with mitochondria at the MAMs. Multiple proteins make up the composition of the MAMs and play as an exchange grid for many elements important for mitochondria and ER functions (Bernard-Marissal, N). Interestingly, alterations to MAMs are observed in many neurodegenerative diseases (Area-Gomez et al., 2018; Lau et al., 2018). Intriguingly, both the ER and mitochondria become dysfunctional during the early phases of neuronal degeneration (Duffy, Chapman, Shaw, & Grierson, 2011). Therefore, it possible to propose that defects or alterations at MAMs may also be involved in PNs pathogenesis.

Mfn2 is a significant player in the ER-mitochondrial connection at the MAMs. Mfn2 mediates the tethering of ER−mitochondria via homo- or heterotypic interactions at the MOMs (de Brito & Scorrano, 2008). In cells carrying *MFN2*- CMT mutations or lacking *MFN2,* an altered ER-mitochondria juxtaposition is observed; indicating the significance of Mfn2 in maintaining MAMs biology and architecture (Cosson, Marchetti, Ravazzola, & Orci, 2012; Larrea et al., 2019; Naon et al., 2016). Therefore, it would not be surprising to expect that alterations to MAMs due to *MFN2* mutation may factor in PNs pathogenicity. Thus, it is still not clear whether the CMT2A pathogenesis occurs due to mutations in *MFN2* affecting mitochondrial dynamics, MAMs biology, or other mechanisms.

1.6 Hypotheses:

Although several studies identified mutations in the fusion and fission dynamics genes, our understanding of PNs pathogenesis mechanisms is not complete. In my studies, I sought to examine the role of NMIIC in mitochondrial fission. I also looked into a novel Mfn2 Q367H mutation and how this mutation impacted mitochondrial functions and its possible correlation to CMT disease's pathogenicity.

1.6.1 Hypothesis for Study 1-

"NMIIC regulates mitochondrial fission, and the R941L variant alters mitochondrial morphology".

The project was divided into two objectives:

1) To assess the role of NMIIC in mitochondrial fission.

2) To assess mitochondrial morphology in cells harboring the R941L mutation.

1.6.2 Hypothesis for Study 2-

"The Q367H Mfn2 variant alters mitochondrial dynamics and or other mitochondrial-linked functions".

The project was divided into three objectives:

1) To evaluate whether Mfn2 Q367H is associated with mitochondrial dysfunction.

2) To assess mitochondrial morphology in cells harboring the Mfn2 Q367H mutation.

3) To screen for the effect of Mfn2 Q367 on bioenergetic profile and lipid metabolism.

Chapter Two

Materials and Methods

2.1 Patients

For the NMIIC study, informed consent for enrollment in the Care4Rare project and publication was obtained by the examined members of this 3-generation pedigree. This study was approved by the conjoint ethics board of the University of Calgary (CHREB). All participants provided informed consent for the publication and identified the underlying genetic basis of their condition and for publication. Patients were enrolled primarily from the Alberta Children's Hospital Genetics Clinic and Foothills' hospital. For the MFN2 study, appropriate written informed consent was obtained from the patient. Research ethics approval was obtained for this study from the University of Calgary Conjoint Health Research Ethics Board (REB15-2763 and REB16-2196). Fibroblasts from three healthy donors were run as parallel controls for experiments done in this thesis. Matching donors at ages of second, third, and sixth decades, named hereafter, control 1, control 2, control 3.

2.2 Cloning and Plasmids

The wild-type NMIIC-EGFP plasmid was a gift from Dr. John Hammer at the National Institutes of Health, which was created in the lab of Dr. Adelstein of the National Institutes of Health. The NMIIC R941L mutant was generated by overlapping PCR mutagenesis and verified by Sanger sequencing. The wild-type mCh-Drp1 plasmid was purchased from Addgene (plasmid# 49152), which was initially created by Dr. Gia Voeltz. The R941L mutation in NMIIC was generated by Christ Smith utilizing overlapping PCR mutagenesis and further verified by Sanger sequencing.

2.3 Cell lines and Culture Conditions

Fibroblast cells were generated from skin biopsies obtained from patients harboring the R941L and Q367H mutations and obtained healthy donors. Fibroblasts from two healthy donors at matching age and gender were obtained for the NMIIC project as parallel control lines for the experiments. Fibroblasts from two healthy male donors at the age of 28 and 68 years old were used as control cell lines. The human skin fibroblast HFF-1 cell line (male, newborn) was used as a third running control for NMIIC project studies. For the MFN2 project, fibroblasts obtained from the healthy male donor at age 68 were used as a parallel control. All obtained fibroblasts from donors were cultured in Dulbecco's Modified Eagle Medium (DMEM) containing 10% Fetal Bovine Serum (FBS) (Life Technologies), supplemented with Penicillin/Streptomycin (100 IU/mL/100 µL/mL). Once the cells reached 90 % confluency, cells were re-passaged in DMEM, supplemented with 10 % FBS and Penicillin/Streptomycin (100 IU/ml/100 µL/mL) at 37°C and in a 5% CO2 humidified atmosphere. For MFN2 project experiments, fibroblasts were grown either in the regular medium; DMEM, 10% FBS, referred as glucose media, or in nutrient-deprived medium, hereinafter, referred as galactose media; DMEM glucose-free containing 5mM galactose (Sigma), 5mM pyruvate (Life Technologies), 2% FBS, and Penicillin/Streptomycin (100 IU/ml/100 µL/mL).

For the human osteosarcoma (U2OS) cells, cells were grown in McCoy's 5A (modified) media containing 10% FBS and supplemented with Penicillin/Streptomycin. Initially, for transfection experiments, cells were seeded in McCoy's 5A (modified) media containing 10% FBS and supplemented with Penicillin/Streptomycin (100 IU/ml/100 µL/mL). Once cells reached 90% confluency, they were seeded onto glass coverslips in 24 well plates (for fixed-cells imaging studies) and onto glass bottomed-dishes at a density of 8x104 cells/well (Mattek, P35G-

1.5-14-C) (for live imaging studies). The following day, cells were transfected with 0.5 g of plasmid DNA of wtNMIICEGFP or mutNMIICEGFP with or without mCherry-DRP1 plasmid using Lipofectamine®3000 according to the manufacturer's recommended protocol. A parallel control set of the U2OS cells transfected with an empty vector (pcDNA) was run parallel. Finally, U2OS cells were imaged 24 hours following transfection.

For the BE (2)-M17 neuroblastoma cells (hereafter M17), cells were initially seeded in a 1:1 mixture of Eagle's Minimum Essential Medium (EMEM) and Ham's *F-12* Nutrient Mixture (F-12) medium with 10% FBS and supplemented with non-essential amino acids and Penicillin/Streptomycin in 10 cm2 dishes. For M17 transfection, cells were passaged on to glass bottomed-dishes (Mattek, P35G-1.5-14-C) and differentiated as previously described (Andres et al., 2013). Briefly, cells were seeded on pre-coated glass with poly-D- Lysine for 24 hours. Retinoic acid at a concentration of 15 µM was added, and the cells incubated for 72 hours. Following the 72 hours, M17 cells were transfected with 2 µg of plasmid DNA (wild-type or R941L mutant NMIIC- EGFP, or empty pcDNA vector as a control) using Lipofectamine®3000. Twelve hours after transfection, the media was changed, and M17 cells were stained with selected Mito-trackers and imaged after 24 hours.

2.4 Immunofluorescence

Cells were grown on glass coverslips in related media conditions. For mitochondrial morphology, cells were imaged either fixed or live. For fixed cells images, cells were fixed with 4% Paraformaldehyde (PFA), quenched with 50 mM ammonium chloride, permeabilized with 0.25 % Triton X-100, blocked with 10 % FBS in *Phosphate-buffered* saline (PBS), and incubated over-night TOMM-20 (rabbit-anti tomm20, Sigma, HPA011562, 1:500 dilution in 5% FBS in PBS), Calnexin (mouse anti-calnexin, EMD Millipore, MAB 3126, 1:500 dilution in 5% FBS in

PBS). Cells were then incubated for 1 hour at room temperature with matching secondary antibodies (Alexa Flour 488 goat-anti mouse, Thermo Fisher Scientific, A11029, or 647 Alexa Flour 488 goat-anti-rabbit, Thermo Fisher Scientific, A21245, 1:500 dilution in 5% FBS in PBS). Cells were incubated at room temperature for 10 minutes in Hoechst 33342 staining (ImmunoChemistry, 639, 1:500 dilution in BPS).

2.5 Live Cell Imaging

Approximately 24 hours prior to imaging, cells were seeded at 8×104 cells/mL onto glass-bottom dishes. Immediately before imaging, cells were treated with the indicated dyes as follows; to label mitochondria, cells were stained for 40 minutes at 37°C with 50 nM MitoTracker Red (Thermo Fisher Scientific®, M7512), or MitoTracker Deep Red (Thermo Fisher Scientific®, M22426), as indicated. After incubation, cells were washed 3 times with PBS and imaged. To label mDNA nucleoids, cells were co-stained with the DNA dye PicoGreen (Thermo Fisher Scientific®, P11495, 3 μL/mL), as previously described by [Ashley et al., 2005], and with MitoTacker Red. After staining, cells were washed 3 times with pre-warmed PBS, and regular growth media was added before imaging.

For the phototoxic-dependent mitochondrial fission assay using the Olympus SD-OSR microscope, MitoTrackerRed-labelled fibroblasts were repeatedly exposed (100 ms at one frame per second intervals) to higher levels of the 561 nM excitation laser (100 mW at 4% power), for a total of 5 minutes.

2.6 Lipid Droplet Staining

Cells were fixed in pre-warmed 4% PFA for 10 minutes at 37°C, quenched with 50 mM ammonium chloride, permeabilized for 10 minutes in 0.1 % Saponin (Harris, Skinner, & Wolins, 2013). Cellular proteins were blocked 10% FBS in PBS.

Cells were incubated overnight at 37oC with HSC LipidTox Green (Thermo Fisher Scientific, H34350, 1:200 dilution in 5% FBS in PBS). Cells were washed with PBS and mounted. All coverslips were mounted on glass slides with Dako mounting media (Agilent, S3023), and images were obtained by Zeiss LSM confocal microscopy.

2.7 Microscopy

Cells were imaged as indicated with either of the following two microscope setups. A Zeiss LSM 710 confocal microscope (plan-Apochromat 63x/1.4 oil objective) with image capture and processing performed with Zen Blue and Black software (Carl Zeiss, Jena, Germany). For live-cell imaging with the Zeiss microscope, cells were supplemented with 50 mM HEPES and incubated at 37°C. Alternatively, an Olympus spinning disc confocal system (Olympus SD-OSR) (UAPON 100XOTIRF/1.49 oil objective) operated by Metamorph software was utilized. The SD-OSR was equipped with a CellVivo incubation module to maintain cells at 37ºC and 5% CO2 during live-cell imaging.

2.8 Image Analysis

Images were cropped, globally adjusted for contrast and brightness, and median filtered using ImageJ (https://imagej.nih.gov/ij/index.html). Mitochondrial morphology was assessed in a blinded fashion by qualitatively assigning morphology into three or four categories, as explained in the text. Quantification was performed in 100 cells from multiple technical and experimental replicates, as indicated. Results are presented as mean ± SD, and *P* values were based on Student's t-tests.

The mitochondrial length was quantified from 30 cells from each patient, as described previously (Ouellet, Guillebaud, Gervais, Lupien St-Pierre, & Germain, 2017), using the

Tubeness plugin from FIJI for mitochondrial segmentation. For nucleoid analysis, images were cropped, globally adjusted for contrast and brightness, and median filtered using ImageJ.

Mitochondrial DNA nucleoid size and number were analyzed in 10 fibroblast cells from each group using the particle analysis tool on ImageJ FIJI (Schindelin, Rueden, Hiner, & Eliceiri, 2015). Briefly, images were scaled and binarized. A region of interest enclosing the entire cell was selected, and the particle analysis tool was used to generate surface area and total nucleoid count measurements. Nuclear and non-specific signals outside the mitochondrial network were manually excluded from the analysis.

Lipid droplet intensity was measured in cells as described previously (McFie, Ambilwade, Vu, & Stone, 2016). Briefly, cells were converted into an 8-bit monochrome image. ImageJ software was set to read the image in grayscale and thus considered only brightness as the factor analyzed. The window of brightness/darkness is more or less representative of the lipid droplets in the image. The software is very sensitive to counting grainy background pixels, but this can be minimized to a great extent by this threshold setting. For the threshold setting, a manual threshold was used to define brightness/darkness. All the images were converted to binary images to ease black and gray pixels based on the intensity. The minimum and maximum size of lipid droplets were detected, and the areas were calculated in numerical data. The average size of lipid droplet per cell was copied to Excel software, from which the average of all analyzed cells was calculated and graphed.

2.9 Mitochondrial Membrane Potential

Mitochondrial membrane potential and mitochondrial mass were assessed in control and patient fibroblasts by flow cytometry, as described previously (Zhao et al., 2019). Briefly, fibroblasts were seeded at 1×105 cells in 6 well plates and allowed to grow for 72 hours.

On the day of the experiment, a set of negative control was prepared by discarding old media and adding 20 uM FCCP to regular growth media to cells for 10 minutes before adding TMRE or Mito-tracker green. Before analysis, cells were stained with Tetramethylrhodamine, ethyl ester(TMRE) (50 nM, 20 minutes) (T669; Life Technologies), or MitoTracker Green (50 nM, 20 minutes) (M7514; Life Technologies). Cells were subsequently washed with 1× PBS, trypsinized and harvested. Cell pellets were resuspended in media and analyzed using the BD LSR II flow cytometer (BD Bioscience) and the BD FACSDiva software. Signal intensity was recorded from at least 20,000 events, and data is presented percent control. Analyses were performed in triplicates for each fibroblast line.

2.10 mtDNA Copy Number Analysis

Genomic DNA (gDNA) from control and patient fibroblasts was extracted using PureLink Genomic DNA Mini Kit (Thermo Fisher Scientific, K182001) according to the manufacturer's instructions. Relative mtDNA copy number was assessed by real-time quantitative PCR (qPCR) using the QuantStudio 6 Flex Real-Time PCR system (Thermo Fisher Scientific). Primer sequences to amplify mtDNA, the nuclear-encoded housekeeping gene 18S, and thermocycling conditions were exactly as described previously (Eaton, Lin, Sartorelli, Bonawitz, & Shadel, 2007). The 20 μL reactions contained 10 μL PowerUp SYBR Green Master Mix (Thermo Fisher Scientific, A25742), 100 ng gDNA, and a final concentration of 500 nM forward and 500 nM reverse primers.

2.11 Long-Range PCR

To examine mtDNA deletions, the following primers were used to amplify nearly full-length mtDNA (16.3 kb) (1482-1516) as reported previously (Nishigaki, Marti, & Hirano, 2004);

Forward: ACCGCCCGTCACCCTCCTCAAGTATACTTCAAAGG;1180-1146

Reverse: ACCGCCAGGTCCTTTGAGTTTTAAGCTGTGGCTCG

Long-range PCR reactions were performed using the Takara LA Taq polymerase (Takara Bio, RR002M), with 250 ng genomic DNA, 200 nM forward and reverse primers. The PCR cycling conditions were as follows: 94°C for 1 minutes; 98°C for 10 s and 68°C for 11 minutes (30 cycles); and a final extension cycle at 72 °C for 10 minutes. PCR products were visualized by electrophoresis on a 0.6% agarose gel, run for approximately 12 hours at 20V.

2.12 Measurements of Mitochondrial Bioenergetics

Measurements of endogenous respiration rates in intact cells were performed using SeaHorse XF96 Analyzer (Seahorse Bioscience) according to the manufacturer's instructions. Cells were seeded in a Seahorse XF 24-well assay plate at a cell density between 2-3×104 in the regular growth medium. After overnight attachment, the medium was washed and replaced with pre-warmed running medium (non-buffered DMEM supplemented with 1 mM sodium pyruvate and 10 mM glucose, pH 7.4) and incubated in a non-CO2 incubator at 37°C for 40 minutes. Basal levels of OCR for 24 minutes, followed by a mitochondrial stress test (1 μg/ml oligomycin, 0.75 μM FCCP, 1 μM rotenone/1 μM antimycin A). Cells were lysed post-measurement and protein content estimated using BCA Assay for normalization.

2.13 Western Blot

To examine fusion and fission protein expression, obtained fibroblasts from patients and healthy donors were grown in 10 cm2. At 95 -100% confluency, cells washed 3 times with cold PBS. Cells were then scraped following the addition of 150 μL Radioimmunoprecipitation assay

buffer (RIPA) buffer to each dish. Cell harvest was collected from two 10 cm2 for each cell line and was collected into a 1.5 ml tube. Protease inhibitor was added to each sample. 10 % Sodium Dodecyl (lauryl) Sulfate (SDS), resolved on polyacrylamide gel electrophoresis (PAGE) and transferred to Polyvinylidene Fluoride (PVDF) membrane overnight at 22 V at 4°C.

Membranes were blocked for 1 hour at room temperature with 5% skim milk in TBS buffer (50 mM Tris-HCl, 150 mM NaCl, 0.1% Tween-20; pH 8.5). The proteins of interests were probed with the following antibodies: anti-DLP-1 (1:500, BD Transduction Laboratories™, 611112) overnight, MFN1 (1:500 dilution in 5 % milk, cell signaling, D6E2S) overnight, MFN2 (1:500 dilution in 5 % milk, Abnova,661-757) overnight, OPA-1(1:500 dilution in 5 % milk, BD Transduction Laboratories™,612607). Blots were then incubated in 5% skim milk–TBS containing matching horseradish-peroxidase-conjugated second antibody (Santa Cruz Biotech., Santa Cruz, CA, USA, 1:1000 dilution in 5 % milk) for 2 hours at room temperature. Membranes were stripped and re-probed with secondary antibodies against actin (Sigma, A5316, 1:000 dilution in 5 % milk), followed by incubation with matching horseradish-peroxidase-conjugated secondary antibody (1:1000 dilutions in 5 % milk). The blots were illuminated with enhanced chemiluminescence reagents (ClarityÔ, WesternECL substrate# 1705060) between 1-5 minutes and detected by AmershamÔ imager 680.

2.14 Statistical Analysis

Quantification was performed in at least 50 cells from multiple technical and experimental replicates, as indicated. To quantify the peripheral hyper-connectivity in fibroblasts, the presence/absence of hyperconnected mitochondrial networks at the cell periphery was scored from three independent experiments. At least 70 cells were assessed per replica.

mtDNA nucleoid sizes are presented as the average size of all nucleoids per cell ± SD. Nucleoid counts are presented as mean ± SD. mtDNA copy number relative to 18S was analyzed using the ΔΔCt method and expressed as percent control from at least three independent biological replicates as done previously in (Hartley et al., 2018).

Lipid droplet analysis was presented as fluorescence intensity in percentage and analyzed from at least two independent biological replicates. Quantification was performed in 100 cells from multiple technical and experimental replicates, as indicated. Results are presented as mean ± SD, and p-values were based on Student's t-tests. All results are presented as mean ± SD. The p-*values* were based on unpaired, 2-tailed Student's *t*-tests comparing data from each patient or experiment to the control to assess statistical significance.

Chapter Three
The R941L Mutation in *MYH14* Disrupts Mitochondrial Fission and Associates with Peripheral Neuropathy

In the following manuscript, Walaa Almutawaa contributed to the experimental design, data collection and analysis of (Figures 3.5, Figure 3.6, Figure 3.8, Figure 3.9, Figure 3.11, Figure 3.14, Figure 3.15, Figure 3.16), and preparation of the manuscript.

3.1 Abstract

Background

Peripheral neuropathies are often caused by disruption of genes responsible for myelination or axonal transport. In particular, impairment in mitochondrial fission and fusion are known causes of peripheral neuropathies. However, the causal mechanisms for peripheral neuropathy gene mutations are not always known. While loss of function mutations in *MYH14* typically cause non-syndromic hearing loss, the recently described R941L mutation in *MYH14*, encoding the non-muscle myosin protein isoform NMIIC, leads to a complex clinical presentation with an unexplained peripheral neuropathy phenotype.

Methods

Confocal microscopy was used to examine mitochondrial dynamics in MYH14 patient fibroblast cells, as well as U2OS and M17 cells overexpressing NMIIC. The consequence of the R941L mutation on myosin activity was modeled in *C. elegans*.

Findings

We describe the third family carrying the R941L mutation in *MYH14*, and demonstrate that the R941L mutation impairs non-muscle myosin protein function. To better understand the molecular basis of the peripheral neuropathy phenotype associated with the R941L mutation,

which has been hindered by the fact that NMIIC is largely uncharacterized, we have established a previously unrecognized biological role for NMIIC in mediating mitochondrial fission in human cells. Notably, the R941L mutation acts in a dominant-negative fashion to inhibit mitochondrial fission, especially in the cell periphery. In addition, we observed alterations to the organization of the mitochondrial genome.

Interpretation

As impairments in mitochondrial fission cause peripheral neuropathy, this insight into the function of NMIIC likely explains the peripheral neuropathy phenotype associated with the R941L mutation.

3.2 Introduction

Peripheral neuropathies are generally caused by defects affecting myelination and/or axonal transport. Mutations in genes regulating mitochondrial fission or fusion are a known cause of Charcot-Marie-Tooth (CMT) disease, a heterogeneous group of inherited peripheral neuropathies (Pareyson et al., 2015). It is hypothesized that peripheral neuropathy is a consequence of mitochondria that are too fragmented or too fused, such that mitochondria are not efficiently transported down the long axons of peripheral neurons (Chen & Chan, 2009). A key regulator of mitochondrial fission is the dynamin-related protein DRP1 (encoded by *DNM1L*), which is recruited from the cytosol to mitochondrial tubules, where it forms a ring to constrict mitochondria. While Drp1 is generally regarded as the major protein mediating mitochondrial fission, recent studies have shown that additional factors, such as the endoplasmic reticulum (ER) and Dynamin2 (*DNM2*), also regulate key steps in fission (Friedman et al., 2011; Kraus & Ryan, 2017; Lee, Westrate, Wu, Page, & Voeltz, 2016).

We now appreciate that a pre-constriction step, mediated by the ER, is required to reduce the mitochondrial circumference such that DRP1 rings can encircle mitochondria (Friedman et al., 2011). Non-muscle myosin family II proteins A and B (NMIIA/B) are ATP-dependent molecular motors that interact with actin and provide the necessary mechanical force for this pre-constriction and promote DRP1 recruitment to mitochondria (Hatch, Ji, Merrill, Strack, & Higgs, 2016; Ji, Hatch, Merrill, Strack, & Higgs, 2015; Prudent & McBride, 2016). In contrast to muscle myosins, which form the contractile filaments in smooth, skeletal, and cardiac muscle, NMII proteins are present in all cells, where they regulate intracellular processes. The human genome contains three NMII isoforms: NMIIA, NMIIB and NMIIC, encoded by the genes *MYH9*, *MYH10*, and *MYH14*, respectively. These NMII isoforms are thought to be partially redundant. However, while NMIIA/B are known to regulate cellular processes such as cytokinesis, cell motility, cell polarity, mtDNA regulation, and mitochondrial fission, the cellular functions of NMIIC have not been thoroughly investigated (Golomb et al., 2004). Additionally, the interplay and redundancy of NMII proteins regarding their role in mitochondrial fission is unknown.

Recently, the R941L mutation in NMIIC has been linked to a complex phenotype including peripheral neuropathy and hearing loss and has been reported in two distinct families from different geographic regions, and in single individual from a larger study (Choi et al., 2011; Gonzaga-Jauregui et al., 2015; Iyadurai et al., 2017). The role of NMIIA/B in mediating mitochondrial fission (Korobova, Gauvin, & Higgs, 2014) led us to hypothesize that NMIIC is also involved in mitochondrial fission, and that the pathogenic R941L mutation would impair fission. While several other pathogenic variants in *MYH14* are known to cause autosomal dominant hearing loss *via* haploinsufficiency (Donaudy et al., 2004; B. J. Kim et al., 2017; K. Y. Kim, Kovacs, Kawamoto, Sellers, & Adelstein, 2005; S. J. Kim et al., 2016; Yang et al., 2005)],

the peripheral neuropathy phenotype is unique to the R941L mutation. Moreover, *MYH14* null mice are reported to have increased susceptibility to hearing loss (Fu et al., 2016) but no peripheral neuropathy phenotype has been reported.

Prior to this study, the cellular functions of NMIIC, and the molecular mechanism by which the R941L mutation might cause peripheral neuropathy were unknown. Here, in addition to describing a novel family pedigree harbouring the R941L mutation, we address two unanswered questions, namely how the R941L mutation causes peripheral neuropathy, and how this mutation has appeared independently in multiple families. Mechanistically, we describe a previously uncharacterized role for the NMIIC as a mediator of mitochondrial fission, which is impaired by the pathogenic R941L mutation.

3.3 Results

3.3.1 Clinical Evaluation and Modeling of the R941L Pathogenicity

3.3.1.1 A Novel Family Carrying The R941L Mutation

We report a novel family carrying the R941L mutation in MYH14, which has been followed in the Neurogenetics clinic at the Alberta Children's Hospital in Calgary for many years. Across three generations, there are four affected individuals showing a pattern of autosomal dominant inheritance [Fig 3.1. a]. Details regarding available clinical features are summarized in Table 3.1. Individual II-5 was not directly examined in this study but was diagnosed 'late-in-life' with CMT, with a long-standing history of high arches, hearing loss, and mild progression of her disease.

All individuals directly examined in this study (III-2, IV-1, IV-2) have symptoms and clinical signs consistent with peripheral neuropathy manifesting in 2nd and 3rd decades of life, and sensorineural hearing loss manifesting in early childhood (this was diagnosed in infancy in subject

IV-1 and resulted in language delay). Nerve conduction studies in patient III-2 revealed a borderline reduction in conduction velocity and amplitude in the tibial nerve, which was considered to be consistent with axonal polyneuropathy rather than demyelinating polyneuropathy. Limited electromyography study in tibialis anterior identified polyphasic motor units but was unremarkable in vastus lateralis. Neurophysiology was not obtained in patients IV-1 and IV-2, but the motor neuropathy diagnosis was based upon the length dependent weakness/atrophy pattern, pes cavus, and family history in the mother who had confirmed neuropathy on nerve conduction studies. Echocardiogram and muscle MRI in the upper and lower legs did not show evidence for cardiac involvement or a coexistent myopathy. After filtering through established peripheral neuropathy genes, exome sequencing in three individuals (II-5, III-2, and IV-2) identified the c.2822G>T (p. Arg941Leu) (NM_001077186.1) mutation (referred to hereafter as R941L). Sanger sequencing confirmed heterozygosity for the pathogenic variant in all four affected individuals: II-5, III-2, IV-1, IV-2 [Fig.3.1. b].

3.3.1.2 Recurrence of The R941L Mutation.

As the R941L variant has been reported in several geographically discrete regions, we hypothesized that it could be the result of a recurrent mutation rather than identity by descent. Genome-wide methylation studies have identified the recurrently mutated guanine nucleotide (c.2822G) as part a CpG methylation site (Kent et al., 2002; Maunakea et al., 2010). Notably, we were able to confirm that this site is indeed methylated [Fig. 3.2. a], [Fig. 3.2. b].

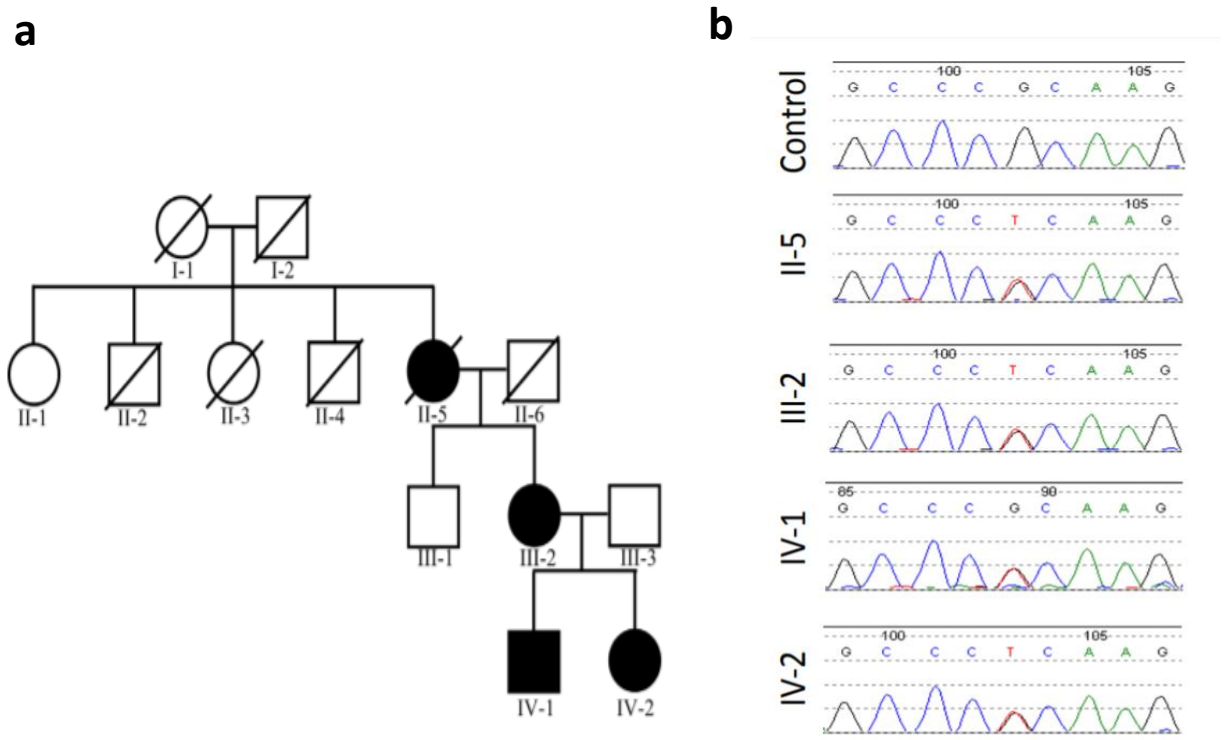

Fig 3.1 Genetic analysis of patients of the R941L mutation.
(a) Pedigree of a three-generation family with peripheral neuropathy and hearing loss. Shaded sections indicate the presence of both CMT and hearing loss, which were always seen together in the pedigree. Exome sequencing was performed on individuals II-5, III-2 and IV-2. The c.2822G>T p. Arg941Leu mutation was identified in individuals II-5, III-2, IV-1 and IV-2. Note that for subsequent fibroblast studies individuals III-2, IV-1, and IV-2 are patients 1-3, respectively. (b) Sanger sequencing confirms the presence of the c.2822G>T p.Arg941Leu mutation in individuals II-5, III-2, IV-1 and IV-2. Sanger sequencing confirms the presence of the c.2822G>T p.Arg941Leu mutation in individuals II-5, III-2, IV-1 and IV-2. ©courtesy of Christopher Smith.

Table.3.1 Detailed clinical features of R941L patients

	II-5	III-2	IV-1	IV-2
Age at last assessment		58	23	24
Sex	F	F	M	F
Onset age (years)		9	<1 (hearing loss), 10 (foot weakness)	4 (hearing loss), 10 (foot weakness)
Age deceased	86	N/A	N/A	N/A
Initial symptom		Tripping	Hearing loss	Hearing loss
Other medical history		Diabetes type II (age 55)	Mild language delay	Attention-deficit disorder
Atrophy		Intrinsic hand muscles, anterior/posterior calf and intrinsic foot muscles; pes cavus present	Atrophy calves and feet, mild.	Intrinsic hand muscles, calf muscles and intrinsic foot muscles
Reflexes		Hyporeflexia arms, areflexia in legs	Absent Achilles reflex	Reduced in arms and Achilles tendon
Muscle power (MRC scale)				
Shoulder abduction		5	5	5
Elbow flexion		5	5	5
Elbow extension		4	5	5
Wrist extension		4	5	4
Wrist flexion		4	5	4
Finger extension		3	5	4
Finger flexion		3	5	4
Finger abduction		3	4	4
Hip flexion		5	5	5
Knee extension		5	5	5
Knee flexion		5	5	5
Ankle dorsiflexion		1	4	3
Ankle plantarflexion		3	4	4
Sensory symptoms		Numbness, dysesthesiae below kn	-	-
Sensory exam		Reduced cold sensation below kne	Normal	Normal
Sensorineural hearing loss	+	+	+++	++
Muscle MRI		Lipomatous atrophy of calf muscu	N/A	Fatty infiltration of gastrocnemius, soleus and extensor digitorum muscles. Asymmetric/mild involvement of left anterior compartment muscles in lower legs.
Neurophysiology		Consistent with axonal polyneuro	N/A	N/A

*Limited clinical data are available from Subject II-5 because the patient had not come to medical attention with her symptoms and was deceased at the time this research study began.

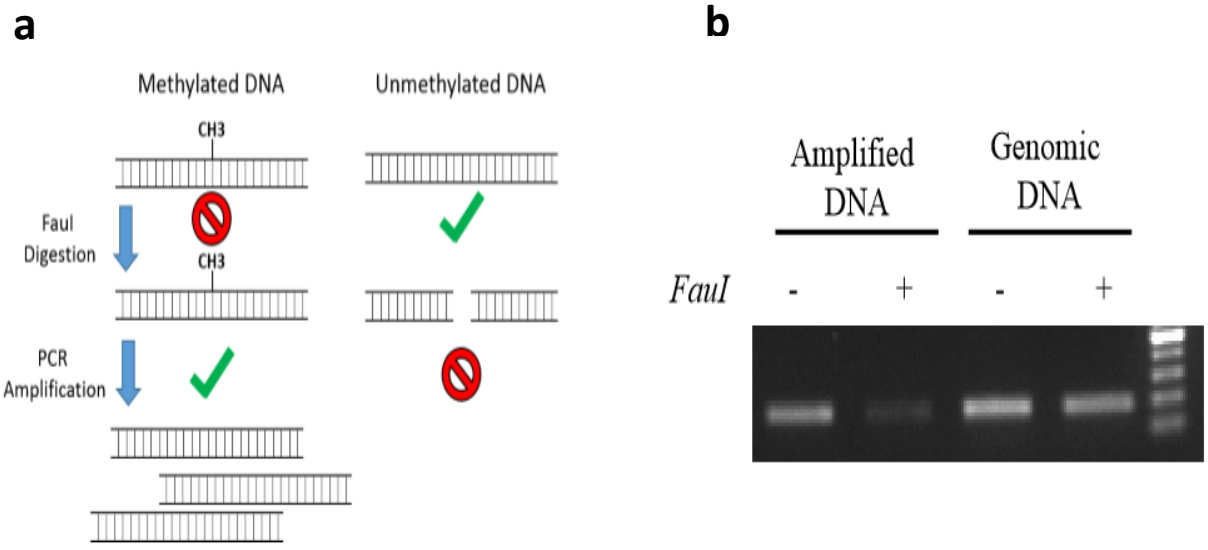

Figure 3.2 Evidence for CpG methylation at c.2822G of the *MYH14* gene.
To verify the presence of a methylated CpG site experimentally, we devised an assay based on the methylation selectivity of the restriction enzyme *FauI*.a) Schematic depicting the experimental strategy, where unmethylated genomic DNA is cleaved by the enzyme, such that the region cannot be PCR amplified.
b) Digestion with methyl sensitive enzyme shows methylation in whole blood extracted genomic DNA. As a control, DNA lacking methylation marks (i.e., PCR amplified prior to treatment) was digested by *FauI*, indicating that the enzyme was actively able to cleave the DNA. Meanwhile, the genomic DNA samples extracted from whole blood were readily amplified following incubation with *FauI* prior to PCR, indicating their resistance to digestion by the enzyme. This result was observed across a broad cross section of genomic DNA samples (data not shown) and is consistent with previous reports that the c.2822G>T mutation occurs at a methylated CpG site.
Courtesy of ©Christopher Smith.

3.3.1.3 Genetic Modeling of The R941L Mutation

As there are no established assays to study the function of NMIIC (B. J. Kim et al., 2017), we modeled the R941L mutation in *C. elegans*, where there is a sensitive assay for non-muscle myosin function (Piekny, Johnson, Cham, & Mains, 2003). The worm homolog of *MYH14*, NMY-1, is 48% identical to *MYH14*, and the R941 residue is conserved (R915 in *C. elegans* [Fig.3.3. a]. We used CRISPR technology to create an R915L allele, designated *sb139* [Appendix-A]. To measure NMY-1 function, we examined the effects of *nmy-1(sb139)* on *C. elegans* embryonic morphogenesis. NMY-1 participates in the contraction of the *C. elegans* epidermal cells, which squeezes the embryo from an ovoid into a long, thin larva (Piekny et al., 2003). *C. elegans* MEL-11 represents the myosin phosphatase targeting subunit/MYPT that moderates this contraction. Loss of MEL-11 thus results in death due to hypercontraction, and embryos fail to hatch. Mutations in genes such as *nmy-1*, which lessen the contractile force, rescue *mel-11* lethality.

Thus, we can use this rescue as a sensitive readout of NMII protein function. At 15°C, 19% of the homozygous embryos of the temperature-sensitive allele *mel-11(it26)* hatched [Fig. 3.3. b]. This value increased to 69% with the addition of *nmy-1(sb139)*. Rescue of *mel-11* lethality was also seen at 20°C and 25°C where *mel-11(it26)* function is even more compromised [Fig. 3.3 b]. This rescue of *mel-11* lethality shows that R915L results in decreased non-muscle myosin function and *nmy-1(sb139)* appears to act semi-dominantly [Fig.3.3.b]. We previously reported that an *nmy-1* null allele (Piekny et al., 2003), also shows semi-dominant rescue of *mel-11*. However, while null alleles of NMY-1 have a characteristic lumpy body shape (Piekny et al., 2003), *sb139* animals are wild-type, indicating retention of at least some myosin function.

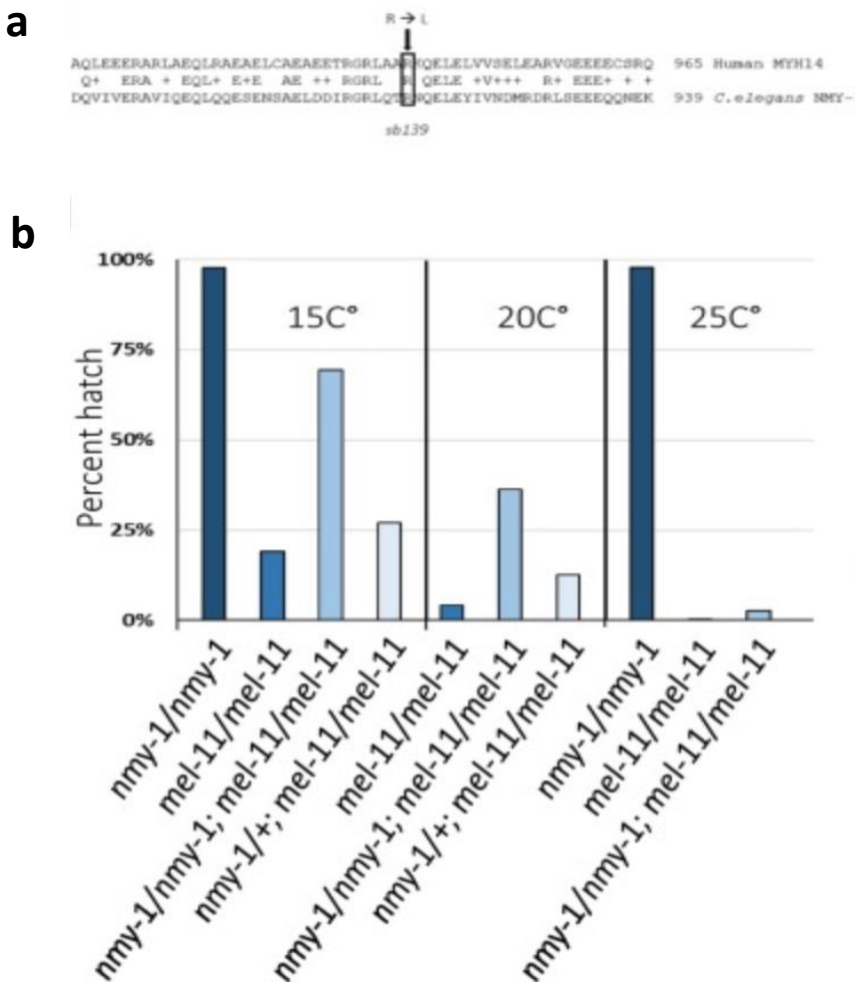

Figure 3.3 Modeling of the R941L mutation in the *C. elegans worm*.
a) Alignment of the human and worm genes showing the conservation in the region surrounding *MYH14* R941, which corresponds to R915 of the worm gene. (b) The R915L mutation in *C. elegans* NMY-1 decreases nonmuscle myosin function. *nmy-1(sb139)* acts semi-dominantly at all three temperatures to increase the hatching rate of *mel-11* mutations, indicating that *sb139*/R195L compromises NMY-1 function (the 2.6% hatching at 25° was significant as it represented 25/936 *vs.* 2/938 for the control). The 27% viability of *nmy-1(sb139)/+; mel-11/mel-11* embryos at 15 °C was inferred from the hatching rates of the progeny of mothers of that genotype. These animals segregate a mixture of *nmy-1(sb139)* homozygotes and heterozygotes, as well as *nmy-1*(+) homozygotes in a Mendelian 1:2:1 ratio. The hatching rates of homozygous *nmy-1(sb139)* and *nmy-1*(+) embryos in the *mel-11/mel-11* background are 69% and 19%, respectively. We observed 36% hatching from *nmy-1(sb139)/*+; *mel-11/mel-11* mothers and this corresponds to 27% hatching of their heterozygous offspring, an increase above the 19% hatching *nmy-1*(+)*/nmy-1*(+); *mel-11*/*mel-11*. Similar calculations demonstrated the semi-dominance at 20 °C. Courtesy of ©Paul Mains

3.3.1.4 Structural Modeling of the R941L Mutation

In order to begin to understand the consequences of R941L mutation on the tertiary or quaternary structure of the NMIC protein, we employed *in silico* protein modeling. In general, myosin proteins are comprised of a catalytic head domain, and a coiled-coil tail domain that is required for multimerization. The wild-type arginine residue is predicted to engage in hydrophilic interactions that could potentially influence myosin dimerization [Fig.3.4]. Our *in-silico* modeling suggests that the introduction of a leucine residue at position 941 eliminates a predicted hydrophilic interaction with residues on an opposite alpha helix. We thus speculate that this substitution could alter the formation of a functional dimer, which would be consistent with a possible dominant-negative effect, where a defective subunit poisons the complex.

3.3.2 A role for NMIIC in Mitochondrial Fission

3.3.2.1 Characterization of R941L Patient Fibroblasts

Given the established link between NMIIA/B isoforms and mitochondrial fission, and the fact that impaired mitochondrial fission can cause peripheral neuropathies, we hypothesized that the R941L mutation might impair mitochondrial fission. Thus, we examined mitochondrial morphology in fibroblast cells obtained from our R941L patients. We observed a significant shift towards a more fused mitochondrial network in all three patient fibroblast lines, consistent with impaired mitochondrial fission [Fig.3.5 a], [Fig.3.5 a b]. Notably, the mitochondrial morphology in the control fibroblast line we used is similar to other control fibroblast lines [Fig. 3.6].

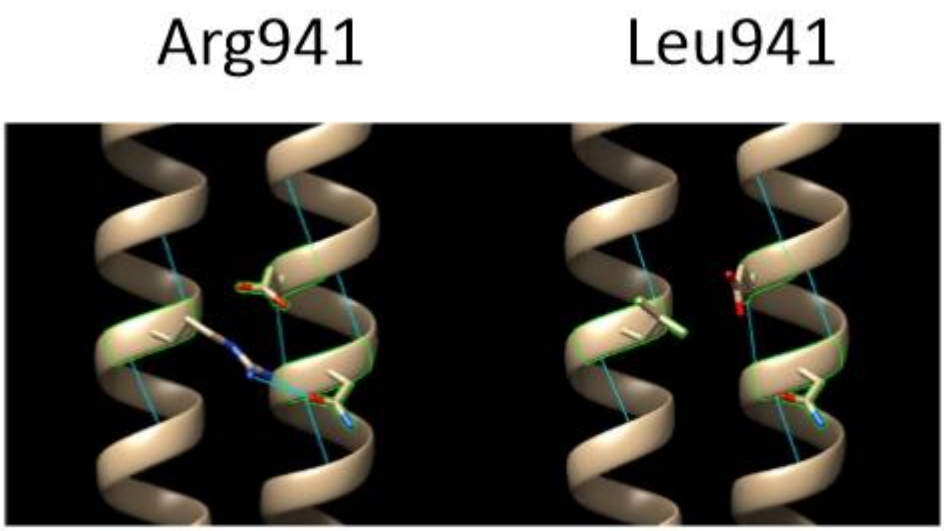

Figure 3.4 *In-silico* protein modeling for the R941L mutation
In silico modelling suggests that the wild-type arginine residue at position 941 (left) has hydrophilic interactions with residues on an adjacent alpha-helix during dimerization. The mutant leucine residue (right) is unable to form the same hydrophilic interactions with the opposite myosin chain.

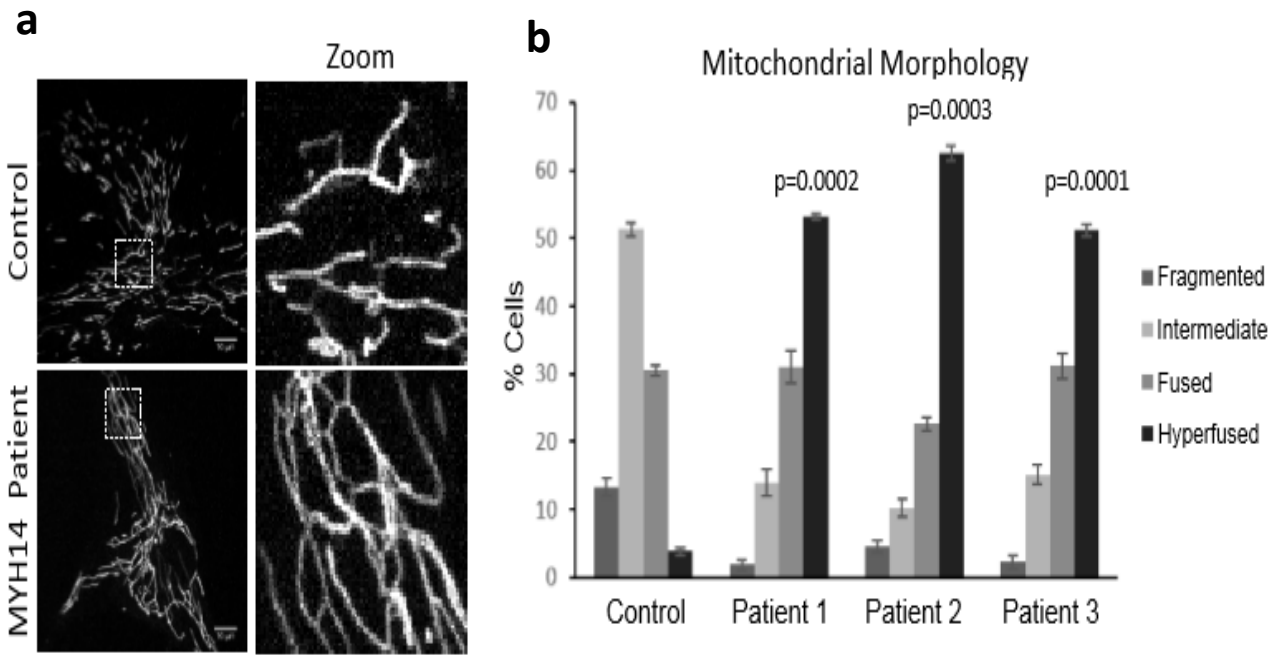

Figure 3.5. The R941L patient fibroblasts show hyperfused mitochondrial network. (a) Representative confocal images of mitochondrial networks taken with a Zeiss Olympus SD-OSR microscope. Mitochondria in fixed control and patient cells were stained *via* immunofluorescence using a TOMM20 antibody. Scale bars indicate 10 μm. (b) Quantification of mitochondrial morphology in control fibroblast and R941L patient fibroblast cells. One hundred cells were quantified in three technical replicates for two independent experimental replicates. Error bars indicate standard deviations, while p-values (Student's t-test) were determined by comparison to the number of cells with hyperfused mitochondria in control Fibroblast cells. Control 1 from [Figure 3.6] was run in the statistics of this figure.

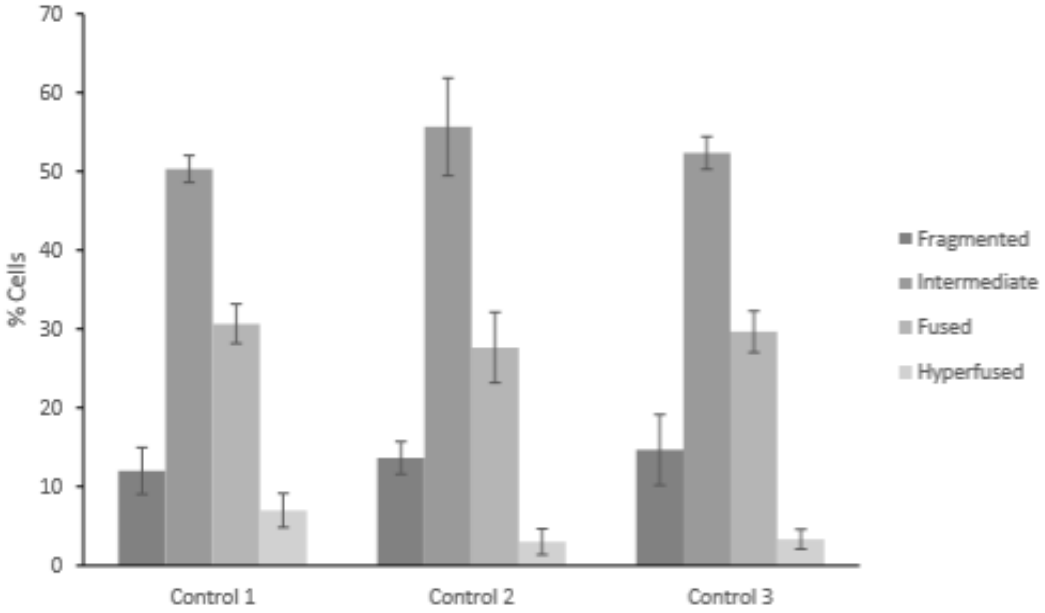

Figure 3.6 Mitochondrial morphology in control fibroblasts.
Quantification of mitochondrial morphology from three different control fibroblast lines. At least 100 cells were quantified in three independent experimental replicates. Error bars indicate standard deviations. No significant differences were observed between the three lines, as determined by Student's t-test compared to the number of cells in control. Control 1 was used for subsequent fibroblast cell analysis.

We confirmed these changes in mitochondrial morphology by quantifying the length of individual mitochondria, which were also longer in patient fibroblasts [Fig. 3.7. a], [Fig. 3.7. b]. As changes in mitochondrial morphology are sometimes linked to alterations in mitochondrial function (*e.g.* more fragmented mitochondrial tend to be less active), we looked at whether there were any functional consequences of reduced fission in MYH14 patient fibroblasts. To this end, we measured mitochondrial membrane potential with the potentiometric dye TMRE, and mitochondrial mass with the Mitotracker Green dye. Although we observed a slight ~20% increase in TMRE signal in MYH14 fibroblasts [Fig.3.8. a], [Fig.3.8. b], we also observed a corresponding ~20% increase in Mitotracker Green signal [Fig.3.8. a] [Fig.3.8. b], suggesting that the increased TMRE signal is due to increased mitochondrial mass rather than membrane potential. Given that there were no major global changes in mitochondrial function, combined with the notion that peripheral neuropathy linked to impaired mitochondrial fission and fusion are thought to be due to impaired mitochondrial transport, rather than decreased function *per se* (Chen & Chan, 2009), we decided to look at the distribution of mitochondria in MYH14 patient fibroblasts. Surprisingly, a close examination of mitochondrial morphology in patient fibroblasts also revealed an enrichment of hyper-connected mitochondrial networks in the periphery of greater than 60% of cells, compared approximately 20% of control fibroblasts [Fig.3.9]. This observation led us to hypothesize that fission may be more impaired at the cell periphery. To test this notion, we devised a fission assay that allowed us to induce mitochondrial fission and monitor the mitochondrial network throughout the cell. When mitochondrial fission was induced with a phototoxic stress, we found that these peripheral hyper-connected regions remained intact in R941L patient fibroblasts, even though central mitochondrial networks in the same cell were able to fragment [Fig. 3.10] and (supplementary video 1).

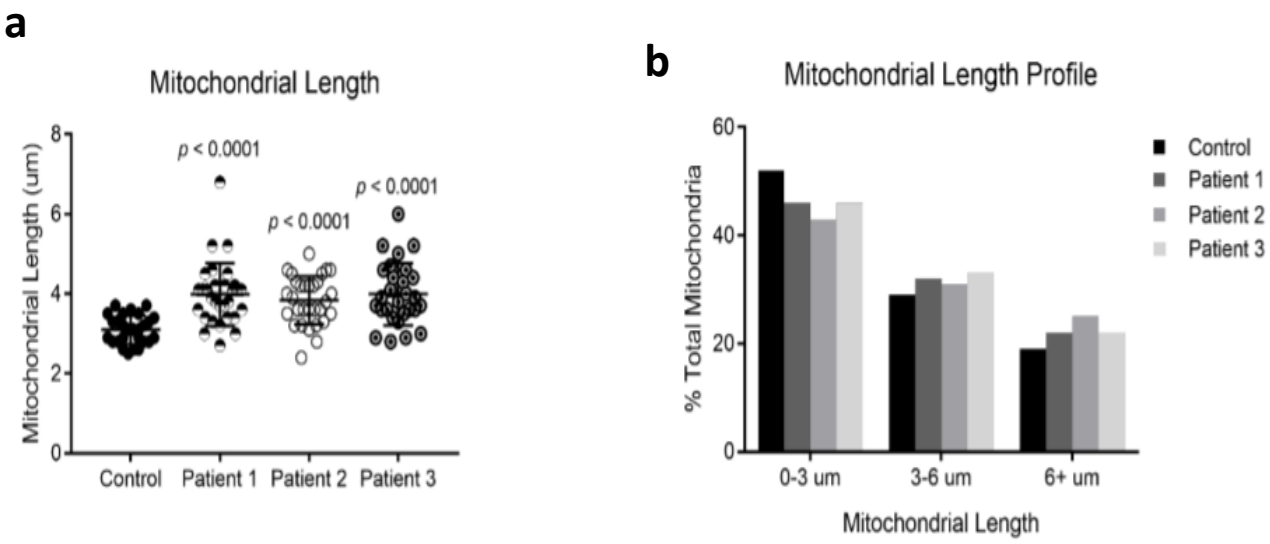

Figure 3.7 Quantification analysis of mitochondrial length.
a) Data represents automated analyses from at least 30 cells per fibroblast line. (b) Mitochondrial length profile from cells in (c), binned into 0–3 and 6+ μm bins and presented as % of total mitochondria. Error bars indicate standard deviations, and p-values (Student's *t*-test) determined by comparison to the control. Courtesy of ©Rasha Sabouny

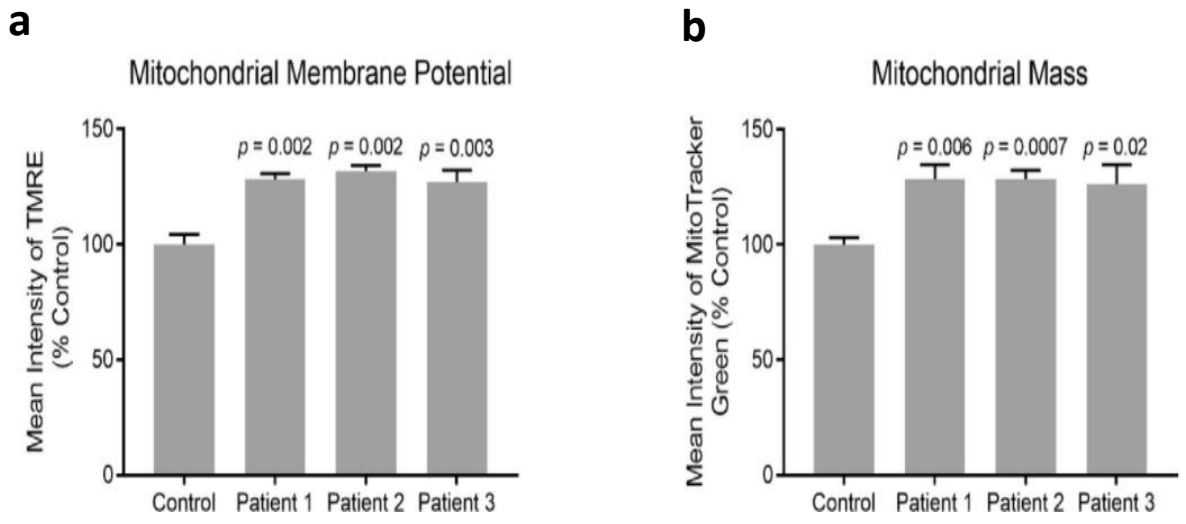

Figure 3.8 Mitochondrial membrane potential in control and patient fibroblasts measured with flow cytometry analysis of TMRE-stained cells.
a) mitochondrial membrane potential measured following staining cells with TMRE and measured by flowcytometry.
b) Mitochondrial mass measured in Mito-Tracker Green stained samples by flow cytometry. Data are presented as % control. Error bars indicate standard deviations, and p-values (Student's *t*-test) determined by comparison to the control.

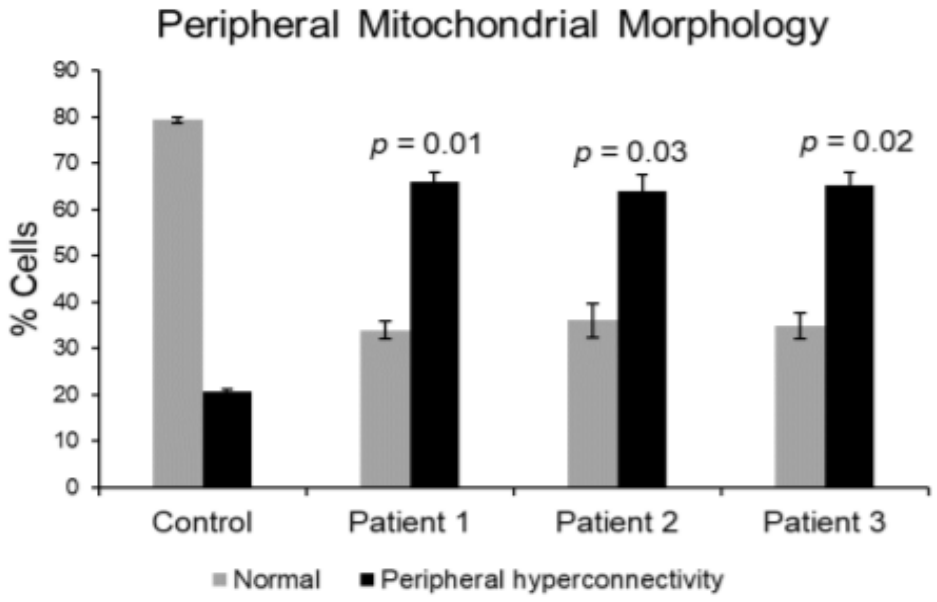

Fig. 3.9 Quantification of hyperconnected mitochondrial networks at the cell periphery in R941L in patient's fibroblasts show resistance to phototoxicity-induced fission. Quantification of control and patient cells containing hyperconnected mitochondrial networks at the cell periphery. At least 70 cells were quantified from two independent replicates. Error bars indicate standard deviations, and *p*-values (Student's *t*-test) were determined by comparison to the number of control cells with hyperfused mitochondria.

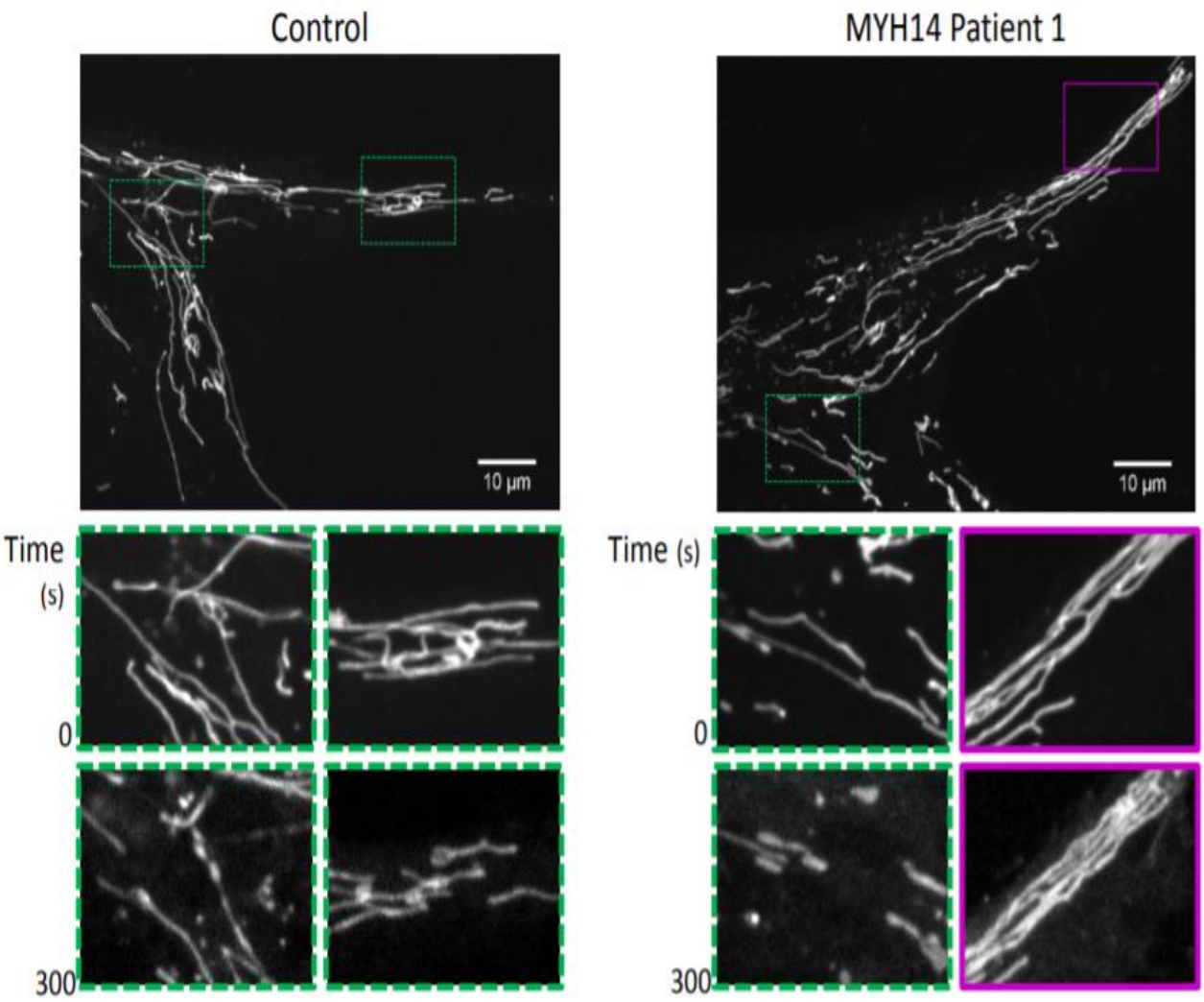

Fig. 3.10 Hyperconnected mitochondrial networks at the cell periphery in R941L in patient's fibroblasts show resistance to phototoxicity-induced fission.
Representative confocal images of mitochondrial networks taken with an Olympus SD-OSR microscope. Control and patient cells stained with Mito-Tracker Red were imaged continuously over 5 min with high laser power to induce fission. Inset zoomed boxes represent regions with fragmented mitochondria (green hashed boxes) or resistant to fission (magenta hashed boxes) when imaging commenced, and at the end of 5 min (full video available as Supplemental Video 1). Signal intensity was enhanced for later frames to adjust for photobleaching. Scale bars indicate 10 µm. (For interpretation of the references to colour in this figure legend, the reader is referred to the web version of this article.) Courtesy of ©Rasha Sabouny

In comparison, mitochondrial networks in control fibroblasts were able to undergo fission throughout the entire cell, even in the few hyper-connected peripheral regions that could be found. Thus, this peripheral mitochondrial fission defect phenotype is unique to R941L patient fibroblasts.

As an independent approach to look at whether mitochondrial fission was impaired in R941L patient fibroblasts cells, we also examined mitochondrial genomes, as mitochondrial fission is required for mtDNA maintenance (Garrido et al., 2003; Iborra, Kimura, & Cook, 2004; Lewis, Uchiyama, & Nunnari, 2016). Specifically, loss of fission leads to enlarged mtDNA nucleoid structures [(Ban-Ishihara, Ishihara, Sasaki, Mihara, & Ishihara, 2013). Moreover, NMIIA and B isoforms have also been implicated in regulating mtDNA(Reyes et al., 2011). Using live-cell imaging to visualize nucleoid size and distribution, we observed that patient fibroblast cells had fewer, but larger nucleoids than controls cells [Fig.3.11.a]. Moreover, the distribution of mtDNA nucleoids throughout the mitochondrial network was different in MYH14 fibroblasts. In control fibroblasts, mtDNA nucleoids are distributed evenly throughout the network, even in hyper-connected peripheral regions. In contrast, when we looked at the nucleoid distribution in the hyper-connected mitochondria in the cell periphery of R941L patient fibroblasts, we observed a marked lack of nucleoids within these regions [Fig.3.11.b].

Next, we quantified the average size and number of mtDNA nucleoids and found that MYH14 fibroblasts has fewer, but larger mtDNA nucleoids [Fig. 3.12]. As decreases in the total number of nucleoids can be due to either loss of mtDNA or clumping of several smaller nucleoids, we also looked at the total amount of mtDNA in these cells.

Quantification of the mtDNA copy number by qPCR showed that there were no significant changes in R941L patient fibroblast cells compared to control [Fig. 3.13. a]. Finally, we performed long-range PCR to rule out the possibility of mtDNA deletions in MYH14 fibroblasts [Fig. 3.13 b]. Altogether, these observations are consistent with impaired mitochondrial fission leading to mtDNA nucleoid alterations.

3.3.2.2 Wild-type NMIIC Induces Mitochondrial Fission While R941L Mutation Exerts a Dominant-negative Effect

Given the altered mitochondrial networks in patient fibroblast cells, which were both longer and more connected, we wanted to test whether NMIIC was directly involved in regulating mitochondrial structure. We expressed an EGFP-tagged NMIIC protein that has been used previously to study the role of NMIIC in U2OS cells (Beach et al., 2014). Consistent with a role for NMIIC in regulating mitochondrial fission, we saw that overexpression of wild-type NMIIC-EGFP in U2OS cells increased fragmentation of the mitochondrial network [Fig. 3.14]. In contrast, when we overexpressed NMIIC containing the R941L mutation, we saw a marked difference, as overexpression of R941L-NMIIC did not promote mitochondrial fragmentation. In fact, we observed a statistically significant increase in the number of cells with hyperfused mitochondrial networks. This finding shows that the R941L mutation not only abrogates the ability of NMIIC to promote mitochondrial fragmentation, but also demonstrates a dominant negative effect on the ability of endogenous wild-type protein to mediate fission.

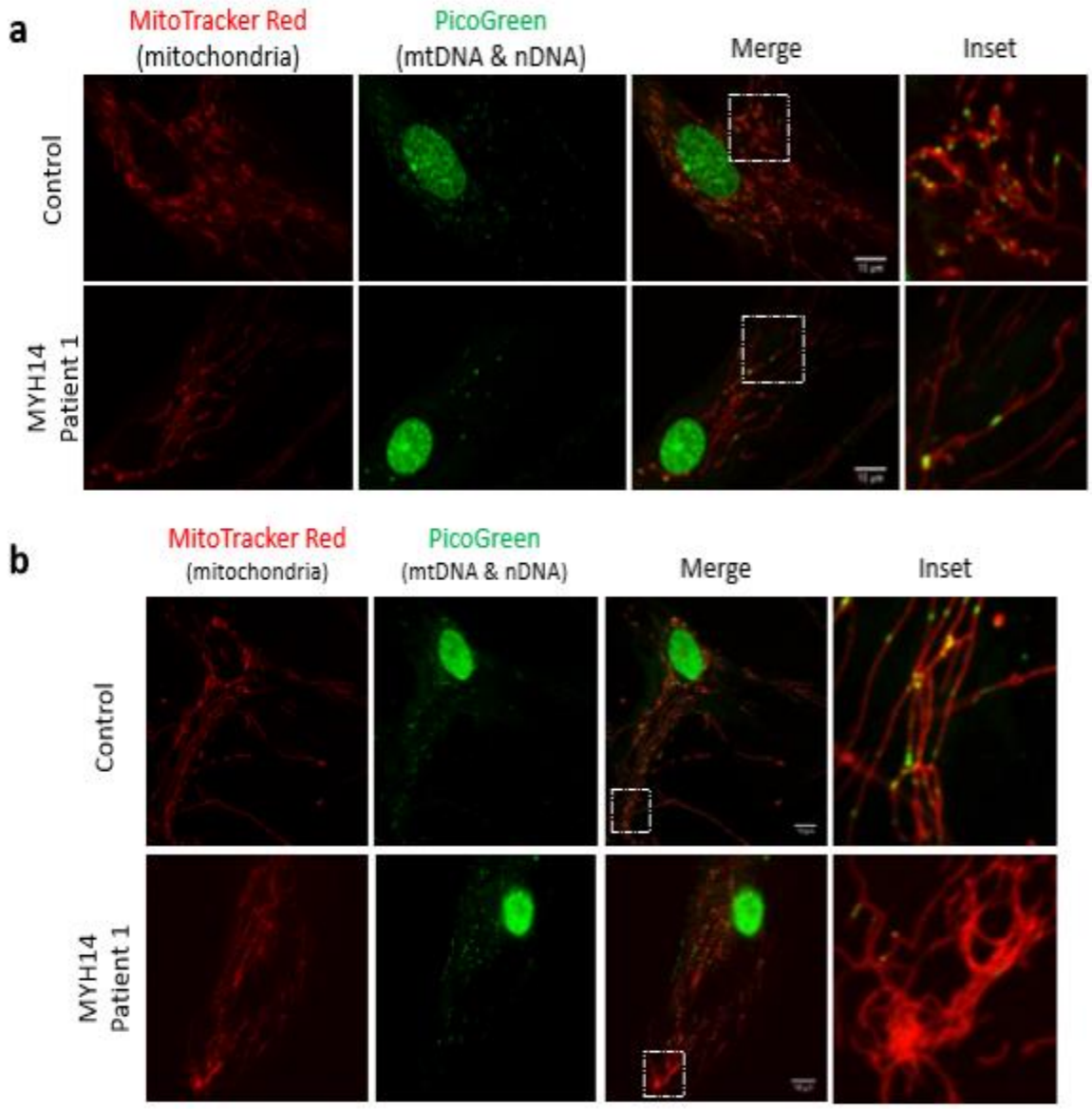

Figure 3.11 Altered mtDNA nucleoids' morphology in R941L patient's fibroblasts.

a) Representative confocal images of control and patient fibroblast cells taken with an Olympus SD-OSR microscope. Live cells were stained with Mito-Tracker Red (Red, mitochondria) and PicoGreen (Green, nuclear and mitochondrial DNA). Scale bars indicate 10 μm.

b) Representative confocal images of peripheral mitochondria and nucleoids as in (a).

a

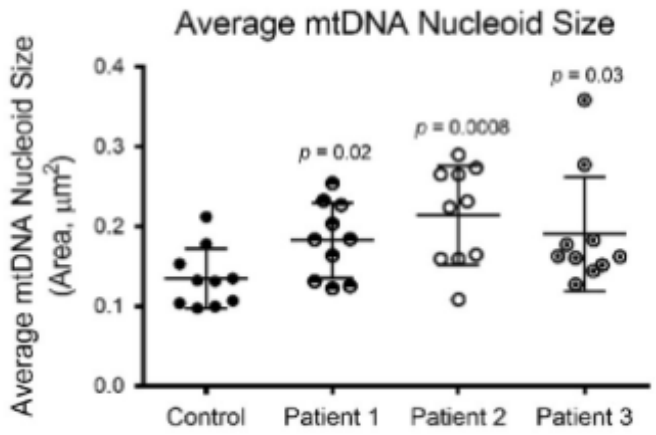

b

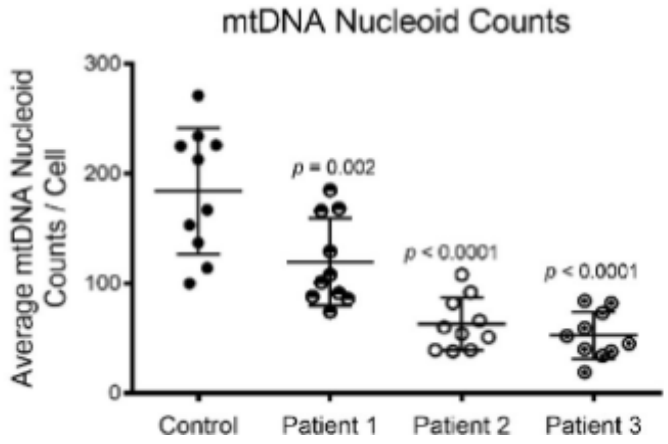

Figure 3.12 Quantitative analysis of mitochondrial nucleoid size and number in R941L patient's fibroblasts.

a) Quantification of mitochondrial nucleoid size from 10 cells obtained from each patient. b) Quantification of mitochondrial nucleoid from 10 cells obtained from each patient. Error bars indicate standard deviations, and *p*-values (Student's *t*-test) were determined by comparison to control fibroblasts. Courtesy of ©Rasha Sabouny

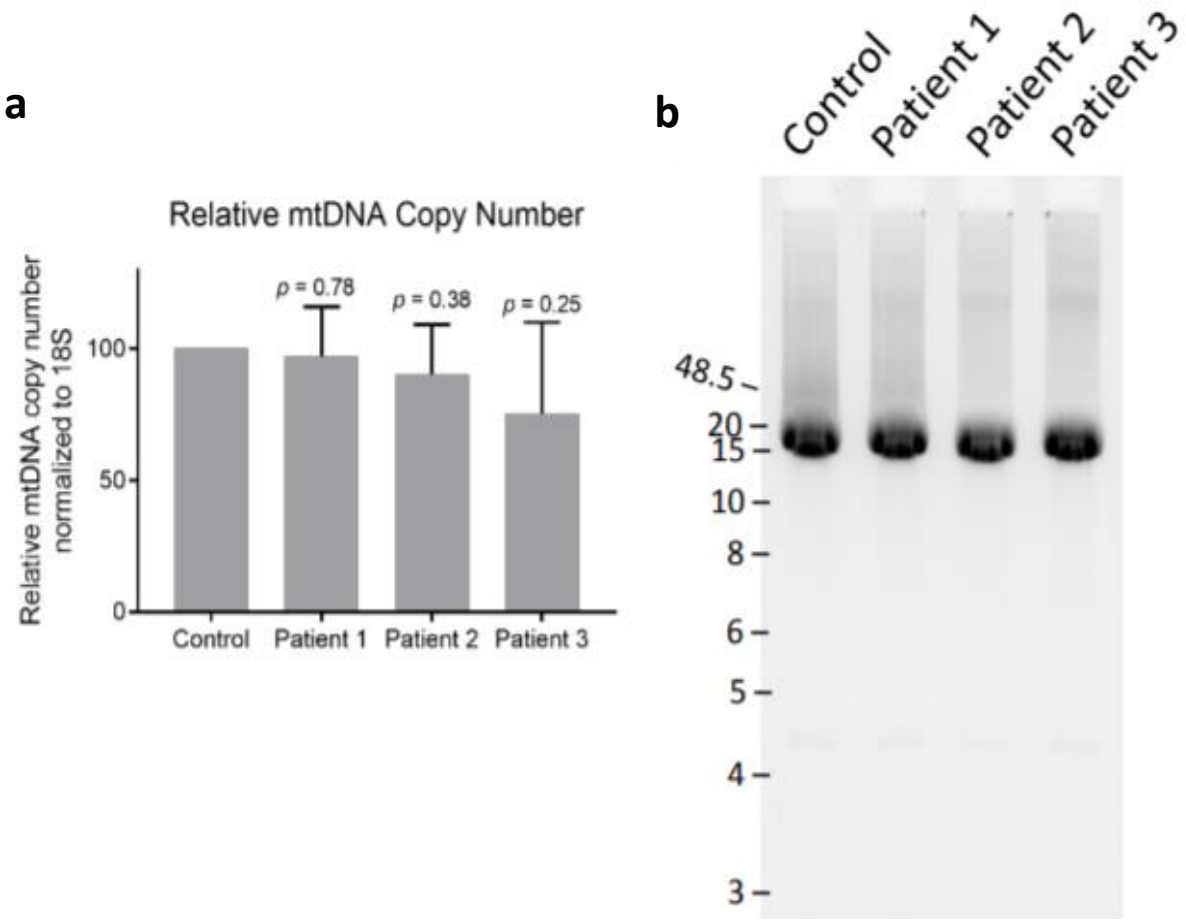

Figure 3.13 Analysis of mtDNA copy number in R941L patients' fibroblasts. a) Relative mtDNA copy number quantification by PCR in R91L and control fibroblast. mtDNA copy number was normalized to the housekeeping gene 18sRAN. Error bars indicate standard deviations, and *p*-values (Student's *t*-test) were determined by comparison to control fibroblasts. b) Long range PCR of mtDNA in control and patient fibroblasts showing 16.3 kb amplicons and no mtDNA deletions.

a

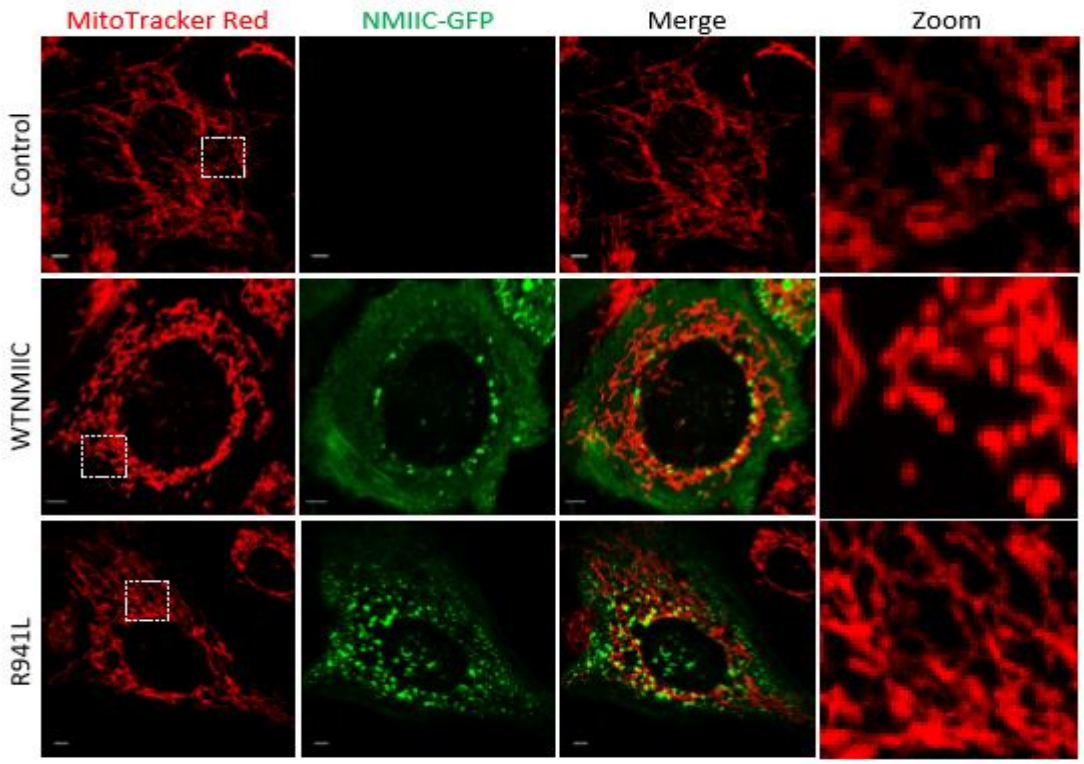

b

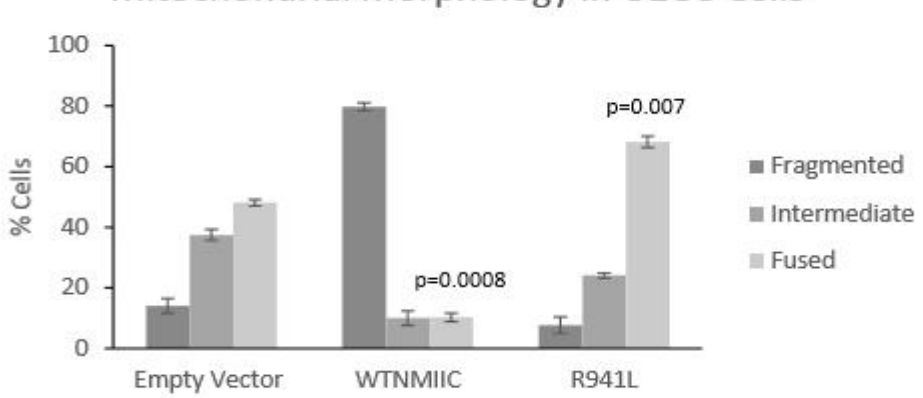

Fig. 3.14 NMIIC puncta localize to mitochondria at sites of mitochondrial fission.
(a) Representative confocal images from live U2OS cells transfected with empty vector (control) or NMIIC-EGFP constructs (WTNMIIC = wild-type, R941L = mutant). Mitochondria were stained with Mitotracker Red, and the EGFP signal represents wild-type or R941L mutant NMIIC. Images were captured with a Zeiss LSM microscope. Scale bars indicate 5 μm.
(b) Quantification of mitochondrial morphology in U2OS cells transfected as in (a). One hundred cells were quantified in three technical replicates for each of three independent biological replicates. Error bars indicate standard deviations, and *p*-values (Student's *t*-test) were determined by comparison to the number of cells with hyperfused mitochondria in the empty vector control.

3.3.2.3 NMIIC Localizes to Future Sites of Mitochondrial Fission

To further characterize the role of NMIIC in mediating mitochondrial fission, we examined the cellular distribution of the NMIIC-EGFP protein *via* microscopy. In addition to observing NMIIC-EGFP at the periphery of cells, in line with a role in cell migration, we also observed several NMIIC-EGFP puncta throughout the cell, several of which co-localized with mitochondria [Fig. 3.15.a]. Live-cell imaging allowed us to see that a subset of NMIIC-EGFP mitochondrial puncta were located at sites of mitochondrial fission, indicating that NMIIC-EGFP participates in mitochondrial fission (Fig. 3.15.a, Supplemental Video 2). To quantify how often NMIIC-EGFP was located at fission sites, we monitored fission events from 14 cells transfected with NMIIC-EGFP. We found that NMIIC-EGFP was located at fission sites in 62 of 216 total fission events that were observed (29%), over a total of 42 minutes of video. In addition, we were able to show that NMIIC-EGFP puncta at sites of fission precedes recruitment of the mitochondrial fission protein Drp1 tagged with an mCherry fluorescent protein (mCh-Drp1) (Fig. 3.15.b, Supplemental Videos 3 and 4). These findings demonstrate that NMIIC regulates mitochondrial fission in a similar manner as NMIIA and B, which mediate ER-mediated pre-constriction of mitochondrial tubules.

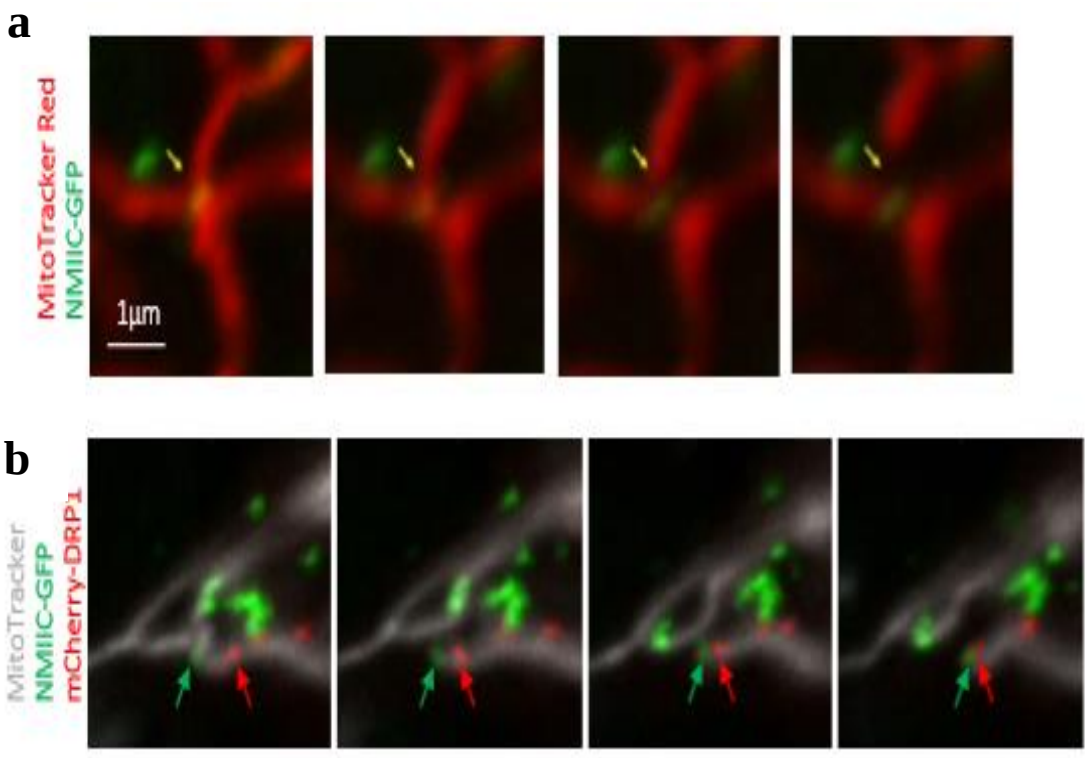

Figure 3.15 NMIIC-EGFP localization with mitochondrial at fission sites.
(a) A subset of NMIIC-EGFP puncta co-localize with mitochondria at sites of fission. Single frames from live cell imaging of wild-type NMIIC as described in Figure 3.13.a, with yellow arrow indicating fission site (full video available as Supplemental Video 2). (b) NMIIC puncta at fission sites precede Drp1 recruitment and fission. Single frames from live cell imaging of U2OS cell transfected with wild-type NMIIC-EGFP (green), mCherry-DRP1 (red), and mitochondria stained with Mito-tracker Deep-Red (grey) (full video available as Supplemental Video 3). Green arrow denotes the NMIIC puncta at the site of fusion. Red arrow indicates the DRP1 recruited to the site of fission. ©Christopher Smith & ©Walaa Almutawaa.

3.2.3 The R941L Mutation Disrupts Neuronal Mitochondria

Given the peripheral neuropathy phenotype in patients, which can be caused by impaired axonal mitochondrial transport in other peripheral neuropathies due to alterations to mitochondrial fission, we decided to look at the effects of R941L overexpression in a neuronal cell type. Thus, we turned to M17 neuroblastoma cells, which are amenable to transfection, and which can be differentiated into neuronal-like cells (Andres et al., 2013; Macias et al., 2014). Similar to U2OS cell, and consistent with a role for NMIIC in fission, overexpression of WT-NMIIC promoted mitochondrial fragmentation. Meanwhile, the R941L led to more hyperfused mitochondrial networks, again indicating a dominant-negative function [Fig. 3.16.a & b].

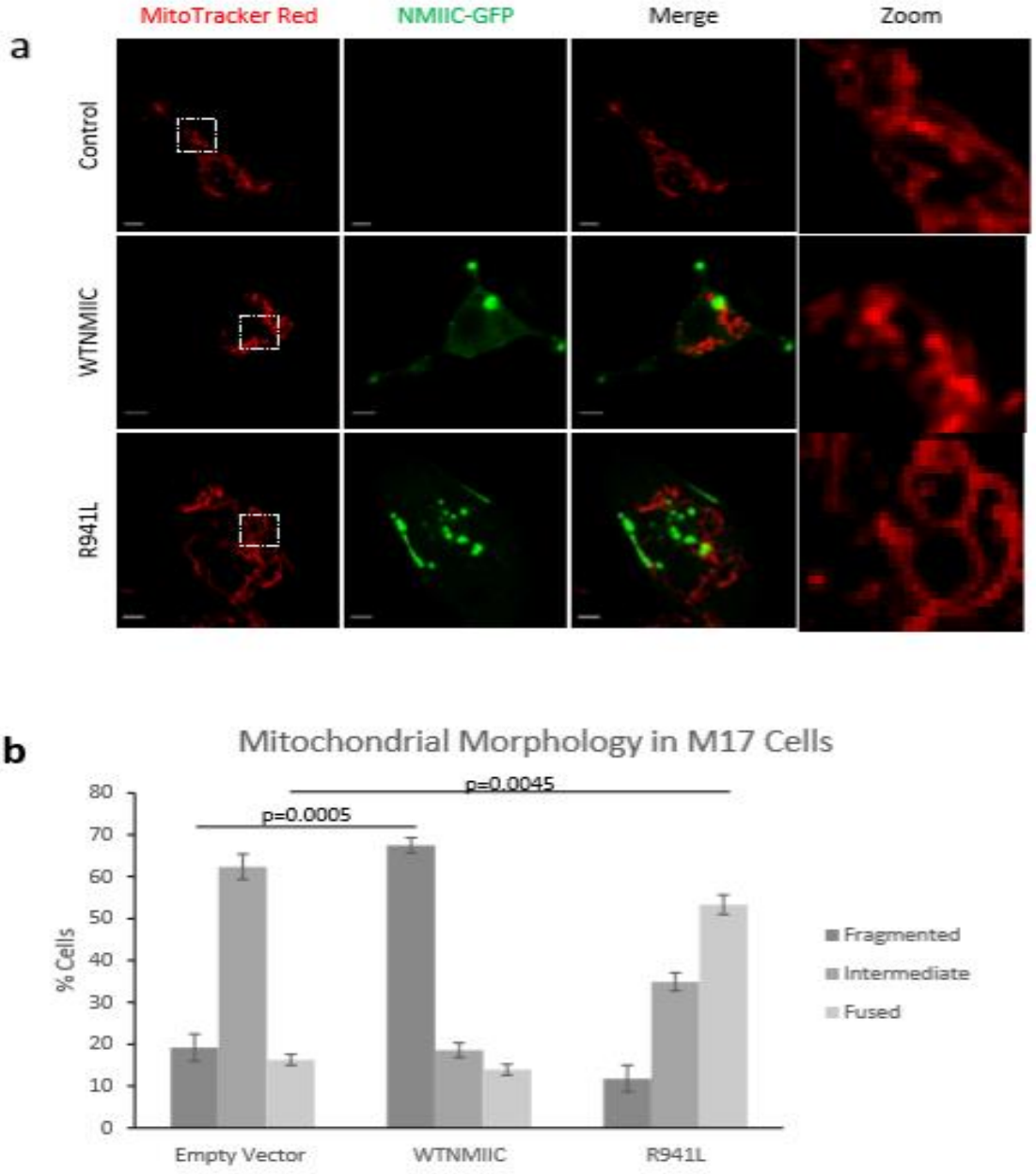

Fig. 3.16 The R941L NMIIC does not promote mitochondrial fission in differentiated M17 neuronal cells.

(a) Representative confocal images of live M17 cells transfected with empty vector (control) or NMIIC-EGFP constructs (WTNMIIC = wild-type, R941L = mutant). Mitochondria were stained with MitoTracker Red, and the EGFP signal represents wild-type or R941L mutant NMIIC. Images were captured with a Zeiss LSM microscope. Scale bars indicate 10 μm.

(b) Quantification of mitochondrial morphology in differentiated M17 cells as transfected as in (a). At least 40 cells were quantified in two independent experimental replicates. Error bars indicate standard deviations, and *p*-values (Student's *t*-test) were determined by comparison to the number of cells with fragmented or fused mitochondrial networks (as indicated) in the empty vector control.

3.4 Discussion

Prior to this study, although it was shown that the R941L mutation in NMIIC was associated with a peripheral neuropathy phenotype, there was little known about the molecular function of the NMIIC protein, and no insight into the underlying mechanism of the pathology. Here, we describe a third family where the R941L mutation segregates with a peripheral neuropathy phenotype, further strengthening the causal link between the mutation and the phenotype.

Identifying a causal gene ends a diagnostic odyssey for patients and can provide families answers, counselling and prognosis. Moreover, diagnosis is also the first step towards therapy, with the next step involving mechanistic studies to understand the molecular basis of the disease. In this context, we also demonstrate a previously unrecognized role for NMIIC in regulating mitochondrial fission, which is impaired by the R941L mutation, and which may explain the peripheral neuropathy phenotype.

Two previous reports of the R941L mutation occurring *de novo* in independent families exhibiting deafness and peripheral neuropathy have been described in the literature (Choi et al., 2011; Iyadurai et al., 2017). In addition, this mutation has also been reported as part of a larger study of peripheral neuropathies (Gonzaga-Jauregui et al., 2015). However, the reason for reoccurrence of the same base pair change was unexplained. In the current report, we describe a new family pedigree harbouring the c.2822G>T mutation resulting in the R941L amino acid substitution in the protein sequence. Thus, the c.2822G>T mutation in *MYH14* appears to have occurred *de novo* four times. Normally, it would be exceedingly rare for the exact same mutation to arise independently. However, our data support existing evidence that the locus in question is a methylated CpG site, increasing the chance of a mutation, and explaining the recurrence of this *de*

novo mutation. Consistent with this notion, there are multiple different nucleotide substitutions at this position in The Exome Aggregation Consortium (ExAC) (http://exac.broadinstitute.org/)(Lek et al., 2016) [Figure 3.17], suggesting an increased sensitivity to mutations. Though of note, the R941L variant itself does not appear In the ExAC database.

While several autosomal dominant loss of function mutations in *MYH14* have been linked to non-syndromic hearing loss (Donaudy et al., 2004; B. J. Kim et al., 2017; K. Y. Kim et al., 2005; S. J. Kim et al., 2016; Yang et al., 2005), the additional peripheral neuropathy phenotype in patients with the R941L mutation suggests that this neuronal phenotype is not likely to be due simply to haploinsufficiency. Nonetheless, it is possible that peripheral neuropathy was not closely examined in these other *MYH14* affected individuals with hearing loss alone, or that the disease had not progressed sufficiently to exhibit peripheral neuropathy when hearing loss was first diagnosed. However, the most likely explanation is that the non-syndromal hearing loss associated with other *MYH14* mutations is due to haploinsufficiency from loss of function in these alleles. The fact that *MYH14*-null mice are also susceptible to hearing loss (Fu et al., 2016) , but have no reported peripheral neuropathy phenotype supports this conclusion.

In contrast, our data suggest that the peripheral neuropathy phenotype associated with the R941L mutation is not simply due to loss of function. In this regard, *in silico* modeling of the R941L mutation suggests that the replacement of the arginine residue with a leucine could impair protein interactions required for dimer formation that could influence the functional activity of the NMIIC protein. Such structural changes that alter dimerization are consistent with a dominant-negative effect where a dimer of mutant with wild-type protein would be inactive.

Figure 3.17 MYH14 variants reported in the Exome Aggregation Consortium (ExAC). Alignment of various alleles that correspond to the methylated CpG site examined in this study., as reported in ExAC, an aggregation of exome sequencing data from a variety of large-scale sequencing projects. Notably, the c.2822G>T change leading to the R941L mutation is not in ExAC.

Meanwhile, our modeling of the R941L mutation in *C. elegans*, where there is a highly sensitive functional assay of NMII protein function, shows that the correlating R915L mutation acts semi-dominantly, but retains some myosin activity. However, our data does not allow us to conclude if the R915L mutation also has dominant-negative properties in *C. elegans*. Nonetheless, as it pertains to mitochondrial fission in human cell culture models, we see that overexpression of the R941L mutant protein has the opposite effect on mitochondrial morphology as the wild-type NMIIC protein. Taken together, these findings are consistent with a distinct dominant-negative mechanism underlying the peripheral neuropathy of the R941L mutation.

Critically, we demonstrate a role for NMIIC as a mediator of mitochondrial fission, a cellular function that is known to cause peripheral neuropathy when impaired (Pareyson et al., 2015). To characterize the role of the R941L mutation at endogenous levels, we examined mitochondria in patient fibroblasts.

We found that patient fibroblast cells exhibit several phenotypes that are consistent with impaired mitochondrial fission, most notably hyperfused mitochondrial networks. Although such hyperfused mitochondrial networks could be caused by either increased fusion or decreased fission, our data clearly show that NMIIC plays a previously unrecognized role in fission, which is impaired in patient fibroblasts harbouring the R941L mutation. Notably, impaired fission is even more prominent at the cell periphery, as central mitochondria in the same cell could still undergo fragmentation. This intriguing finding demonstrates a definitive defect in mitochondrial fission in the fibroblasts cells and suggests that NMIIC may play a more important role in mediating mitochondrial fission at the cell periphery. Such a role would be especially relevant in the context of the peripheral neuropathy phenotype in patients with the R941L mutation in *MYH14*.

A peripheral fission phenotype is also intriguing as it pertains to our understanding of how impaired fission leads to mitochondrial dysfunction and peripheral neuropathies. Rather than the proposed model where impaired mitochondrial fission in the cell body prevents the anterograde transport of large mitochondria down axons (Chen & Chan, 2009), impaired fission at the tips of axons could impact local mitochondrial quality control and function in a different fashion. Specifically, the fused state at the ends of axons could prevent the retrograde transport of mitochondria. Additionally, as fission is required for the autophagic removal of mitochondria (Twig et al., 2008), which has been reported to occur in axons (Ashrafi, Schlehe, LaVoie, & Schwarz, 2014; Maday, Wallace, & Holzbaur, 2012), impaired peripheral mitochondrial fission could also inhibit mitochondrial autophagy and thus impair neuronal function. The slight increase in mitochondrial mass that we observe in MYH14 fibroblasts would also be consistent with decreased turnover of mitochondria due to reduced mitochondrial autophagy.

In addition to mitochondrial network changes, we observed fewer and larger mtDNA nucleoids in patient fibroblasts, alterations that are also consistent with impaired fission (Ban-Ishihara et al., 2013). While the larger mtDNA nucleoids that we visualized could be due to clumping of multiple mtDNA genomes, it is notable that signal from the DNA intercalating dye picogreen can also reflect changes to the supercoiling or packaging state of the mtDNA, not just mtDNA abundance (Fukuoh et al., 2014; He et al., 2007). Meanwhile, the decrease in the number of nucleoids could also be due to clumping, or alternatively to loss of total mtDNA.

As our quantification of the mtDNA copy number in patient fibroblasts shows there is no significant mtDNA loss, we conclude that the larger nucleoids are most likely due to clumping of multiple nucleoids. This result is consistent with a previous report where inhibition of fission *via* acute knockdown of *DRP1* leads to fewer, but larger nucleoids composed of multiple

genomes, without any change in copy number (Ban-Ishihara et al., 2013). The notion that fission is playing a key role in the distribution of mtDNA throughout the network is also supported by the lack of mtDNA nucleoids that we observe in the hyper-connected mitochondrial networks in the cell periphery of R941L patient fibroblasts. The mtDNA nucleoid impairments we observed in R941L patient fibroblasts are also notable, as regulation of mtDNA is involved in peripheral neuropathies. For example, peripheral neuropathies can be due to mutations in the mtDNA or mutations in proteins that regulate mtDNA replication (Cassereau et al., 2011). In addition, a peripheral neuropathy is a side-effect of the chemotherapeutic agent cisplatin, which preferentially damages mtDNA (Canta, Pozzi, & Carozzi, 2015) and also impairs mitochondrial dynamics in peripheral nerves (Bobylev, Joshi, Barham, Neiss, & Lehmann, 2018).

Supporting the previously unrecognized role for NMIIC in mediating mitochondrial fission, we found that overexpression of a GFP-tagged NMIIC shifted mitochondrial networks to a more fragmented state. While there are always potential concerns about protein overexpression artifacts, we note that the R941L mutation is not competent to promote mitochondrial fission, arguing against the increased mitochondrial fragmentation resulting from an accumulation of NMIIC protein. In fact, overexpression of the R941L mutation shifted cells towards a more hyperfused network, consistent with a dominant-negative effect of the mutation. Moreover, we could directly visualize NMIIC-GFP puncta at mitochondrial fission sites preceding Drp1 recruitment, demonstrating that NMIIC mediates fission in the same fashion as NMIIA and NMIIB. Although we observed NMIIC-GFP at only 29% of total fission sites, it is important to remember that the U2OS cells express unlabeled NMIIC proteins (Beach et al., 2014) which likely mediate ER-mediated constriction at the remaining mitochondrial fission events.

The functional interplay and redundancy of the three NMII isoforms (A, B, and C) remains unknown in the context of regulating mitochondrial fission but has important implications to the peripheral neuropathy phenotype in patients. In this regard, the situation of NMII isoforms is reminiscent to that of the fusion proteins MFN1 and MFN2. Though MFN1 and MFN2 are functionally redundant for fusion, mutations in MFN2 are thought to lead to a peripheral neuropathy phenotype because MFN1 is not highly expressed in neurons (Detmer & Chan, 2007). Thus, it is notable that neurons predominantly express NMIIB and NMIIC (Kneussel & Wagner, 2013). As such, it might be expected that neurons are more sensitive to mutations affecting NMIIC function than other cell types. It is intriguing that the phenotype associated with the R941L mutation is primarily a distal motor neuropathy phenotype, and few reported patients have any sensory symptoms or signs (Patient III-2 from this report and Patient III-8 from (Choi et al., 2011). One possible explanation could be that the various NMII isoforms are differentially expressed in nerve fibers and sensory neurons.

In addition to expression differences, it is also possible that the cellular distribution and precise roles of the different NMII protein isoforms varies. Although little is known about the relative cellular functions of the NMII isoforms, based on our findings we would predict that NMIIC is more important for mediating fission at the cell extremities. Finally, it is notable that all three NMII isoforms can form homo or heterodimers with each other (Beach et al., 2014). Though our structural modeling suggests that the R941L mutation could affect dimerization, we do not know how this might affect homo *versus* heterodimers, let alone the resulting functional outcomes on fission.

Due to the fact that we do not know all of the cellular functions of NMIIC, a limitation of this study is that we cannot say with certainty that the peripheral neuropathy is caused specifically by impaired mitochondrial fission. Future work using a peripheral neuron model expressing the R941L mutant would allowing us to strengthen this connection. Nonetheless, the role of NMIIC in regulating mitochondrial fission, particularly at the cell periphery is likely to be relevant to the peripheral neuropathy phenotype in R941L patients. Notably, there is a growing list of peripheral neuropathy genes encoding proteins that regulate mitochondrial dynamics *via* fission (*e.g. GDAP1*, *DNM2*, *INF2*, and *MFF*), fusion (*e.g. MFN2*, and *OPA1*), or transport (*e.g. KIF1A*, *KIF1B*, and *KIF5A*) (Boyer et al., 2011; Pareyson et al., 2015) (Koch et al., 2016)]. Of particular relevance to the role of the NMIIC protein in fission, the INF2 protein regulates actin, which interacts with NMII proteins during the ER-mediated mitochondrial constriction that initiates fission (Korobova et al., 2014). Thus, the R941L is likely a second example of how impairing the actin/myosin contraction required for fission can lead to a peripheral neuropathy phenotype. Collectively, our findings provide evidence that NMIIC mediates mitochondrial fission. Moreover, the fact that the R941L mutation is deficient in the ability to promote mitochondrial fission provides additional evidence that impaired mitochondrial fission underlies the peripheral neuropathy in these patients. Thus, *MYH14* can be added to the list of genes regulating mitochondrial dynamics, mutations in which lead to peripheral neuropathy.

Supplementary Videos to this work can be found online at

https://doi.org/10.1016/j.ebiom.2019.06.018

Figures have been reinstalled and formatted in compliance to the Faculty of Graduate Studies' roles and regulation at University of Calgary .

Chapter Four

A Novel Pathogenic Mutation in *MFN2* (Mfn2 Q367H)

That Is Not Associated With Peripheral Neuropathy

In the following chapter, Walaa Almutawaa contributed to the experimental design, data collection and analysis of (Figures 4.2, Figure 4.3, Figure 4.4, Figure 4.5, Figure 4.6, Figure 4.7).

4.1 Introduction

During the past decade, our understanding of mitochondria has been revolutionized, and we now perceive mitochondria as highly dynamic organelles. In cells like peripheral neurons, efficient energy metabolism is required to maintain the energy demands required for anterograde and retrograde movements along the axon (Schwarz, 2013). The distribution of mitochondria along peripheral axons is regulated by mitochondrial dynamics. Abnormalities in mitochondrial dynamics are recognized to be one of several causes of peripheral nerve dysfunction (Ashrafi et al., 2014; Chen & Chan, 2009; Pareyson et al., 2015). Generally, mutations in genes encoding mitochondrial dynamics proteins are associated with hereditary neuropathies. Of note, mutations in the *MFN2* gene, a pivotal mitochondrial fusion protein, cause Charcot-Marie-Tooth (CMT) diseases, which is an autosomal dominant axonal peripheral neuropathy (Zuchner et al., 2006). Mfn2 plays a key role in mitochondrial fusion. Notably, Mfn2 is also involved in other mitochondrial functions such as mitochondrial respiration and oxidation activities (Glancy et al., 2015; Pich et al., 2005). Overexpression of Mfn2 in cells induces glucose oxidation and increases mitochondrial membrane potential (Kong et al., 2013; Pich et al., 2005; Wang et al., 2018).

On the other hand, Mfn2 knockdown causes a decrease in oxygen consumption and mitochondrial membrane potential, and decreases oxidation of substrates like pyruvate and fatty acids (Bach et al., 2003; Mourier et al., 2015). These observations suggest an indirect correlation of Mfn2 to respiratory chain machinery and oxidation functions.

Mfn2 is also known to maintain mitochondrial DNA integrity. For instance, *MFN2* knockout, along with *MFN1*, causes a significant mtDNA depletion (Vidoni, Zanna, Rugolo, Sarzi, & Lenaers, 2013). In the mouse model, *MFN2* mutants causing fusion dysfunction are associated with an increase in mtDNA mutations (Chen et al., 2010). Also, CMT-MFN*2* mutations are often associated with higher odds of mtDNA deletions or instability (Beresewicz, Charzewski, Krzysko, Kochanski, & Zablocka, 2018; Chen et al., 2010; Rouzier et al., 2012).

Recently, other Mfn2 mitochondrial-linked functions came to light. For instance, Mfn2 localizes to the MAMs and known for its function in tethering mitochondria to ER. Mfn2 monomers at the MAMs forms an intra-organellar bridge between mitochondria and ER (McFie, Ambilwade, Vu, & Stone, 2016). Cells lacking *MFN2* shows disfigurations in the MAMs (de Brito & Scorrano, 2008). Also, this special juxta-positioning, via the MAMs, maintains many cellular functions, such as calcium homeostasis, respiratory functions, and mitochondrial dynamics (Hayashi, Rizzuto, Hajnoczky, & Su, 2009; Larrea et al., 2019; Pera et al., 2017). In addition, Mfn2 is suggested to be involved in the synthesis and storage of several lipids at the MAMs (Hernandez-Alvarez et al., 2019; McFie, Ambilwade, Vu, & Stone, 2016). For example, Mfn2 appears to be involved in transferring the lipid phosphatidylserine (PS) into mitochondria for the synthesis of phosphatidylethanolamine (PE) (Hernandez-Alvarez et al., 2019). Mfn2 deficiency causes a reduction in PS transfer and phospholipid synthesis, leading to development

of cancer-like cells (Hernandez-Alvarez et al., 2019). Also, Mfn2 regulates interactions between mitochondria and lipid droplets, an important regulator of fat reservoirs within the cell (Fujimoto & Parton, 2011; Krahmer, Farese, & Walther, 2013). Intriguingly, MFN2 mutations cause alterations in lipid droplet morphology (Larrea et al., 2019; McFie et al., 2016).

Despite what is known about the role of Mfn2 in mitochondrial fusion and other cellular functions, the exact role of Mfn2 mutation in CMT disease pathogenesis is still elusive. Some earlier studies proposed that the axonal degeneration occurs due to impaired mitochondrial fusion. In this model, *MFN2* mutations are thought to impair mitochondrial fusion functions, which in turn impedes proper mitochondrial anterograde and retrograde transport along the axon, eventually leading to a degeneration of the highly polar and lengthy axon of peripheral nerves (Baloh, Schmidt, Pestronk, & Milbrandt, 2007; Beresewicz, Charzewski, Krzysko, Kochanski, & Zablocka, 2018; Cartoni & Martinou, 2009; Chen, McCaffery, & Chan, 2007). Surprisingly, not all Mfn2 mutants seem to impair mitochondrial fusion (Larrea et al., 2019; Loiseau et al., 2007; Misko, Sasaki, Tuck, Milbrandt, & Baloh, 2012; Pich et al., 2005). Instead, some *MFN2* mutations seem to promote mitochondrial fusion (de Brito & Scorrano, 2008; Detmer & Chan, 2007a), raising doubts about the loss of mitochondrial fusion as a significant player in CMT pathogenesis. Notably, we know that defects in fission can also lead to neuronal degeneration (Li, Okamoto, Hayashi, & Sheng, 2004; Vallat et al., 2008; Verhoeven et al., 2006; Verstreken et al., 2005; Chen & Chan, 2009). In these instances where fusion is increased, the notion behind what is causing peripheral pathogenesis is that highly fused interconnected mitochondria leads to inefficient mitochondrial motility, specifically into smaller neuronal processes.

To date, little attention has been paid to the role of MAMs, how they are affected by *MFN2* mutations, and if MAMs also contribute to CMT pathogenesis. Importantly, structural or functional changes in MAMs are suggested to be involved in neurodegenerative disease pathogenesis (Lee & Min, 2018). In this study, we detected a novel mutation of *MFN2* c.1101G>C, p. (Gln367His), hereafter referred to as Mfn2 Q367H, in a patient with atypical pathological features of CMT phenotype. Instead of the usual CMT phenotype associated with mutations in *MFN2*, the patient presented only with myopathy, which is not the hallmark peripheral neuropathy typically associated with *MFN2* mutations.

Prior to this study, the Mfn2 Q367H was not reported in the literature as a pathogenic variant; rather, it was classified as a variant of uncertain significance (VUS) (Xie et al., 2016), dbSNP report: rs373211062. This online report did not reveal sufficient data to determine the pathogenicity of theMfn2 Q367H variant, nor its role in mitochondrial fusion or other mitochondrial linked functions. Some questions, therefore, arose as follows; Does the Mfn2 Q367H mutation affect mitochondrial morphology? Does the Mfn2 Q367H mutant impact other mitochondrial functions? Dos Mfn2 Q367H mutant lead to the different observed clinical manifestations in this patient? We, therefore, sought to examine the effect of the Mfn2 Q367H mutation on mitochondrial morphology and other Mfn2 mitochondrial-linked functions. Interestingly, the Mfn2 Q367H variant is located close to the previously identified pathogenic variants K357N (p.Lys357Asn) and *R364W (*p.Arg364Trp), associated with CMT autosomal dominant axonal neuropathy. Results in this study suggest that Mfn2 Q367H leads to altered lipid homeostasis and altered bioenergetic profile, but does not disrupt ER-mitochondrial contacts. Taken together, these findings support an earlier proposal in literature suggesting MAMs dysfunction as a possible player in CMT disease pathogenesis.

4.2 Results

4.2.1 Case Report and Whole Exome Sequencing (WES) For The Mfn2 Q367H Mutation[1]

A male patient of 73 years was referred to Dr. Pfeffer's clinic at the Foothills Hospital in Calgary, with a two-year history of slowly progressive weakness affecting his lower extremities. Initial symptoms included difficulty walking uphill, and he eventually developed difficulty with stairs and limitations with walking on the ground level and rising from a chair. There were no cramps, fasciculations, or contractures. No sensory loss or coordination. Dysarthria, dysphagia, ptosis, or diplopia were not present.

The patient was medically well and did not have any history of cardiac disease. The mother of the patient developed weakness in her lower legs in her 60s, with progressive limitations in her mobility. Apparently, she was diagnosed with CMT disease, but her clinical profile was not available for review. The mother died at the age of 81 due to congestive heart failure. The mother's two siblings, aged 80 and 78, and her other two sons of ages 45 and 43 were all unaffected. Clinical examination of the patient demonstrated a cognitively normal individual. Cranial nerve examination was normal. Motor examination revealed MRC grade 4+ strength for ankle dorsiflexion and 4+ plantarflexion bilaterally. Proximal and axial muscle testing was normal, except for Achilles tendon reflexes. The sensory examination was normal. Creatine kinase enzyme check was ordered and reflected an elevated to a maximum of 455 U/L (reference range ≤ 195 U/L). The muscle biopsy showed necrotic and regeneration myofiber, myofiber hypertrophy, multifocal endomysia, and perimysial fibrosis, and extensive infiltration by adipose tissue. Immunostaining for dystrophin, alpha/gamma sarcoglycan, sceptrin, α-laminin, desmin, and α-β- crystallin was unremarkable. There was no inflammatory cell

[1] This case was evaluated clinically by Dr. Gerald Pfeffer

infiltrate. For the magnetic resonance imaging (MRI) examination, upper and lower legs revealed atrophy in the adductor longus gluteus minimus, tibialis anterior, and inferior gastro-soleus bilaterally [Figure 4.1]. The case was interpreted as a chronic myopathy without other known pathological features. A complete exosome sequencing analysis was done, and identified a heterozygous novel variant in the MFN2 gene, c.1101G>C, p. (Gln367His) [Table 4.1]. Therefore, this patient was finally diagnosed with a late-onset distal myopathy and a heterozygous Gln367His mutation in the *MFN2* gene. This sequence change in *MFN2* replaces glutamine with histidine at codon 367 of the Mfn2 protein (Q367H). The glutamine residue is highly conserved, and there is a small physicochemical difference between glutamine and histidine, implying a hypermorphic change. The Mfn2 Q367H variant is present in population databases with a very low allele frequency ExAC 0.001% by dbSNP report (rs373211062, https://www.ncbi.nlm.nih.gov/snp/rs373211062), including at least one homozygous individual. Also, this *MFN2* variant was not reported previously in the literature in individuals with related diseases.

Notably, exome sequencing also identified another two variants of uncertain significance (VUS)in the SYNE1 and the DYSF genes [Table 4.1]. While mutations in SYNE1gene are associated with autosomal dominant neuromuscular disease, this novel variant in SYNE1 was not considered to be likely as an explanation for this patient's disease for several reasons: (a) the mutation is not in the same domain as other mutations previously associated with autosomal dominant disease, (VUS)in the SYNE1 and the DYSF genes [Table 4.1] (b) other reported SYNE1 mutations in this region of the gene have only been associated with autosomal recessive disorders, while our patient is heterozygous, (c) no characteristic of nuclear abnormalities under

a

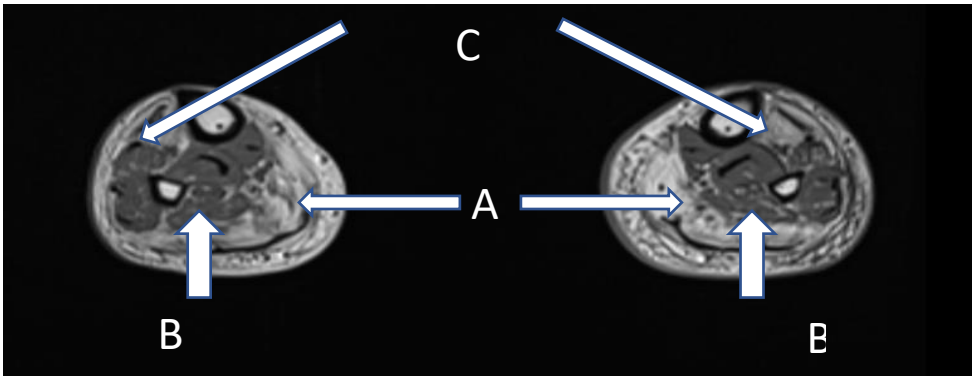

b

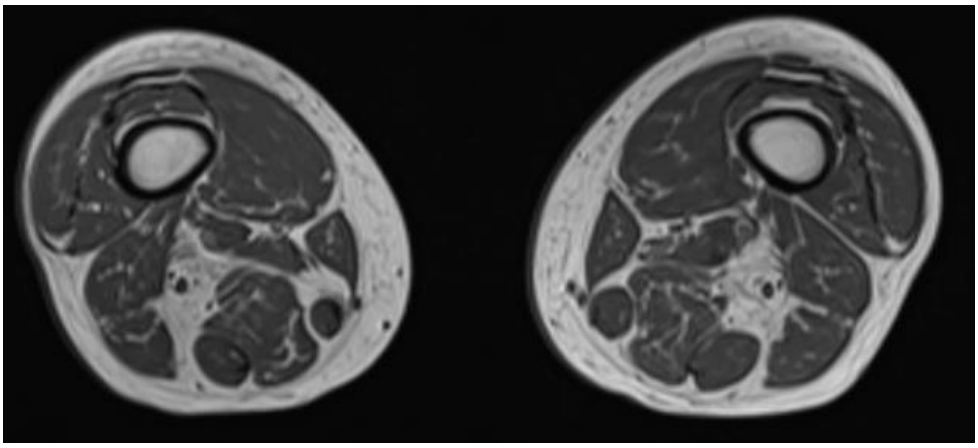

Figure 4.1 Magnetic Resonance Imaging (MRI) of lower extremities from the patient.

(a) MRI image at the level of the legs demonstrating predominant atrophy in white arrows; Gastrocnemius (A) , Soleus (B)and Tibialis Anterior (C) bilaterally.

(b) MRI image of upper Thighs demonstrating predominant atrophy of adductor longus gluteus minimus (Non shown here). Courtesy of ©Gerald Pfeffer.

Table 4.1 Identification of variants in fibroblast obtained from c.1101G>C (Gln367His) patient[2]

Gene	Disease/ Inheritance pattern	Coding variant	Amino acid change	rsID	Max reported MAF	ClinVar	Zygosity	Polyphen2 prediction	Mutation-taster prediction
MFN2	CMT neuropathy 2A; AD	c.1101G>C	pGln367His	rs373211062	0.00011	VUS	Hetero-zygous	B	D
DYSF	LGMD 2B; AR	c.5180G>C	p.Gly1727Ala	rs146153532	1.16E-04	VUS	Hetero-zygous	P	D
SYNE1	EDMD 4; AD/AR	c.9934G>A	p.Asp3312Asn	rs147281213	2.33E-04	VUS	Hetero-zygous	D	D

AD=autosomal dominant; AR=autosomal recessive; B= benign; CMT=Charcot Marie Tooth; D=deleterious; EDMD=Emery Dreyfuss muscular dystrophy; LGMD=limb girdle muscular dystrophy; P=possibly tolerated; VUS=variant of uncertain significance.

[2] Information provided by Dr. Gerald Pfeffer

microscopy associated with SYNE1 mutations in patient fibroblasts were observed by Dr. Pfeffer's group, (d) the myopathy phenotype is not in keeping with the SYNE1-related disease phenotype, which includes proximal weakness and contractures. Meanwhile, the DYSF variant was not considered to be likely as an explanation for this patient's disease for several reasons: (a) mutations in the DYSF gene are associated with autosomal recessive disorders and our patient is heterozygous for this gene, (b) our patient did not show symptoms of the sarcolemma, (c) the muscles affected in our patient do not match DYSF muscle disorders, which affect voluntary muscles, pelvic muscles, or the shoulder girdle, (d) DYSF mutations usually affect patients at young adulthood (20 years old), which was not the case in our patient, (e) autosomal recessive DYSF mutations are associated with 10-100 fold increase in Creatine kinase enzyme and altered cardiac markers, parameters that were not markedly changed in our patient. Based on the reasons mentioned above, the American College of Medical Genetics and Genomics (ASMG) guidelines, the reported patient phenotype (Richards et al., 2015), and the altered mitochondrial-linked functions detected in this study (discussed in the upcoming sections), the Mfn2 Q367 is a *pathogenic allele.*

Since *MFN2* mutations are typically associated with CMT, a question arose of whether the Mfn2 Q367H mutation affects Mfn2 functions and if it is responsible for the patient's atypical clinical symptoms. To address this question, we sought to examine several mitochondrial functions in fibroblast cells obtained from the patient.

4.2.2 Mitochondrial Morphology

In most cell types, including fibroblasts, mitochondria form a connective network of tubules spread-out through the cytosol. This mitochondrial network is maintained by a continuous balance between fusion and fission events. Given the well-established role for Mfn2

in mitochondrial fusion, we examined the effect of the Mfn2 Q367H mutation on mitochondrial network morphology. Mitochondria of early passages (5-9) in control and Mfn2 Q367H fibroblasts were observed by Mitotracker ™ Green staining. No substantial differences were observed in mitochondrial morphology or distribution between control or Mfn2 Q367H fibroblast cultured in regular glucose-containing media. In this media, mitochondria tend to reflect a more fused network in both cell lines, represented as a 55-60 % fused network [Figure 4.2] and [Figure 4.3]. However, fibroblast cells also express Mfn1, which can compensate for Mfn2 deficiency (Chen et al., 2003), and this fact may explain why fibroblast cells from patients with *MFN2* mutations do not always exhibit altered mitochondrial morphology. Also, impaired mitochondria morphology in *MFN2*-CMT patient fibroblasts might not be detected in cells grown under these conditions (Beresewicz, Charzewski, Krzysko, Kochanski, & Zablocka, 2018; Marroquin, Hynes, Dykens, Jamieson, & Will, 2007). Galactose media is frequently utilized as an alternative for revealing mitochondrial dysfunctions that are detected in cells grown in glucose media (Aguer et al., 2011; Beresewicz et al., 2018; Marroquin et al., 2007). In glucose free-media, galactose, which cannot be fermented to produce ATP via glycolysis, is added to the media as an alternative energy source. Galactose oxidation is proposed to push the cells to rely on oxidative phosphorylation to produce ATP for cellular revival (Kase et al., 2013). Thus, to further test whether the Mfn2 Q367H is affecting mitochondrial fusion under different growth conditions, we used the glucose-free media model to study mitochondrial fusion function. In glucose-free media, mitochondria in cells harboring the Mfn2 Q367H mutation remained in a fused state compared to control fibroblasts, which showed a significant mitochondrial fragmentation [Figure 4.2] and [Figure 4.3]. In order to further confirm our observations, a second control fibroblast line was characterized along with the mutant Mfn2 Q367 fibroblast

cells. In glucose-free media, a fused mitochondrial morphology was observed for Mfn2 Q367 cells compared to control fibroblast lines (40 % increase in fusion compared to control) [Figure 4.4]. Our data collectively showed an alteration in mitochondrial response to applied stimuli compared to control, suggesting that fusion is unchanged under glucose conditions but activated under starvation conditions.

4.2.3 ER-Mitochondria Interactions

Recent data in the mitochondrial field highlight the link between Mfn2 protein and the biology of the ER (Merkwirth & Langer, 2008; Naon et al., 2016). Thus, I sought to examine whether or not the Mfn2 Q367H mutation affects ER morphology and ER-mitochondria contact sites in the fibroblasts cultured in either glucose or glucose-free media for 72 hours. Cells were fixed, and mitochondria and ER stained by immunofluorescence for microscopy. No obvious changes in ER morphology or mitochondrial-ER contacts were observed in glucose or glucose-free media and compared to control fibroblast grown in the same conditions [Figure 4.5].

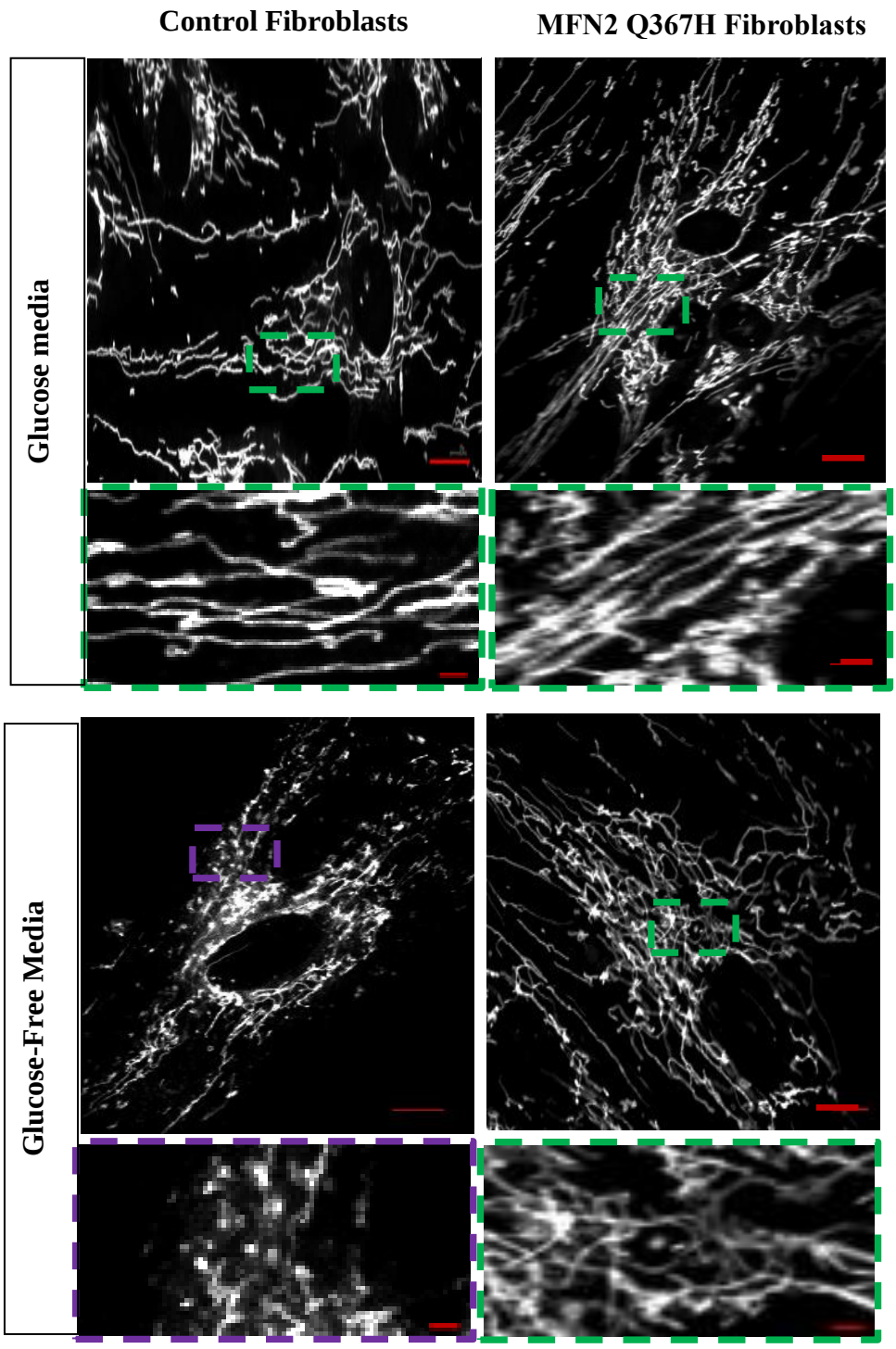

Figure 4.2 Mitochondrial morphology of Mfn2 Q367H fibroblast cultured in glucose and glucose-free media. Representative confocal images of mitochondrial networks in Mfn2 Q367H control fibroblast cultured in glucose media . All images were taken with a Zeiss LSM microscope. Live cells were stained with 50 nM Mito-tracker green for 40 minutes in 37 ºC. Scale Bar =20 µM.In magnified areas, Scale Bar = 2 µM.

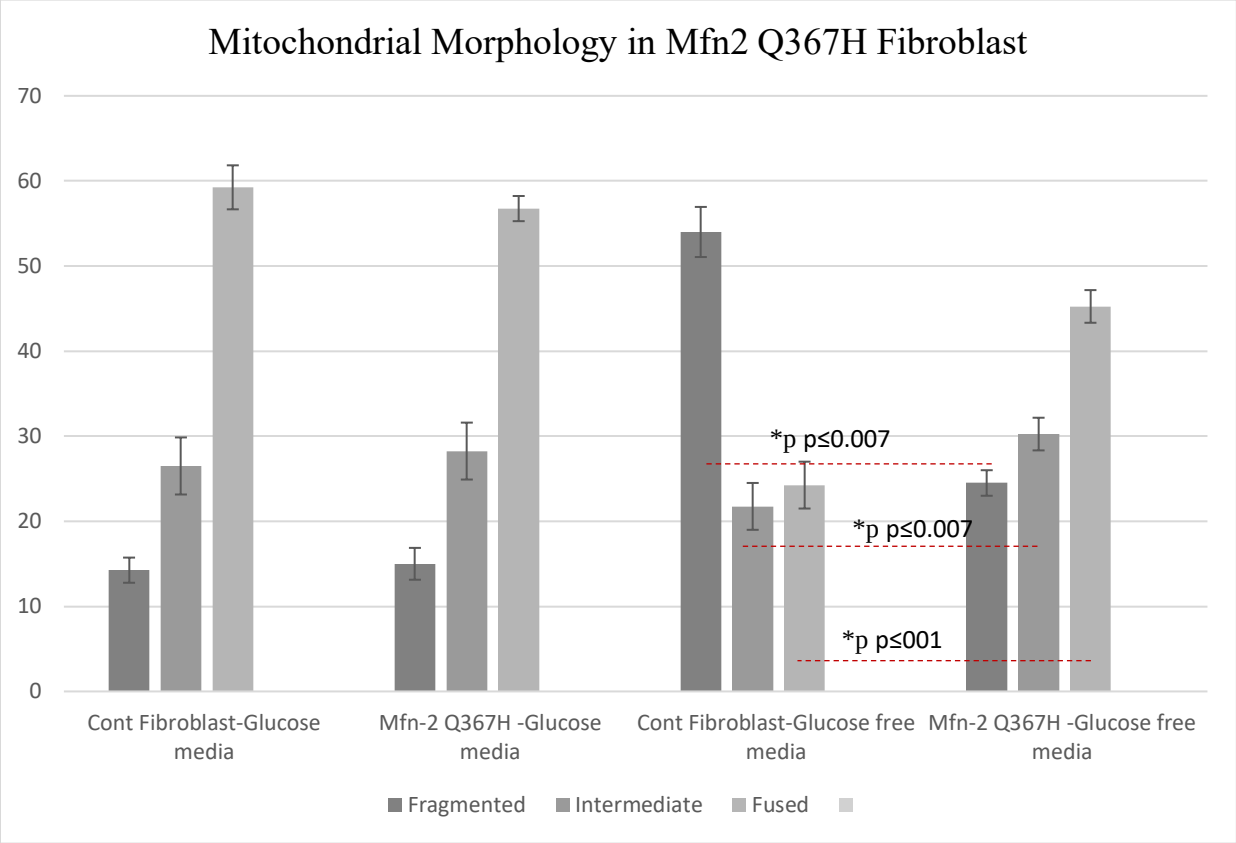

Figure 4.3 Mfn2 Q367 shows fused mitochondrial morphology in glucose and glucose-free media.

Quantification of mitochondrial morphology in control fibroblast and patient fibroblast cells in examined growth conditions (glucose and glucose -free media). One hundred cells were quantified in two technical replicates for two independent experimental replicates. Quantification was done in fixed cells stained with the mitochondrial marker TOMM-20. *** denotes $p<0.05$ as determined by Student's t-test.

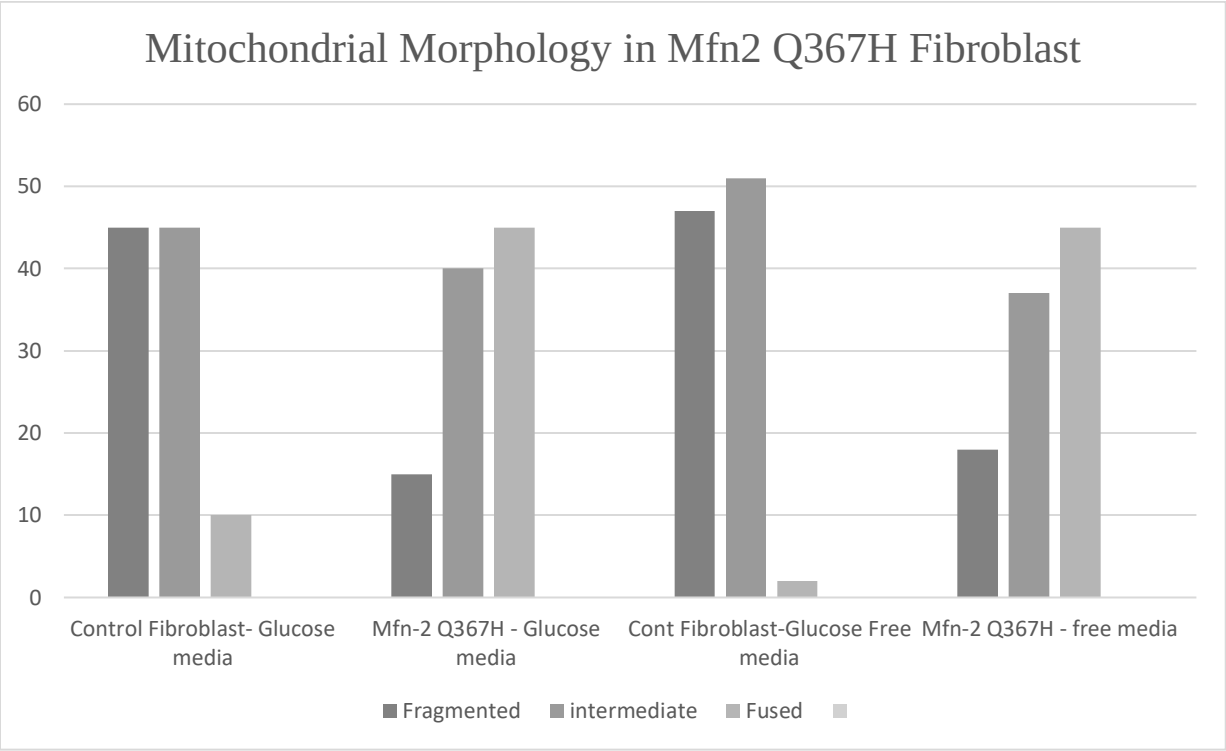

<u>Figure 4.4 Preliminary data for mitochondrial Morphology in MFN2 Q367H fibroblasts along with Control 2 cultured in glucose and glucose-free media.</u>
Quantification of mitochondrial morphology in another control fibroblast line (control 2) and Mfn2 Q367H fibroblast cells cultured in glucose and glucose-free media for 72 hours. One hundred cells were quantified in only one biological replicate. Control and patient cells were stained via immunofluorescence using a TOMM20 mitochondrial. n=1.

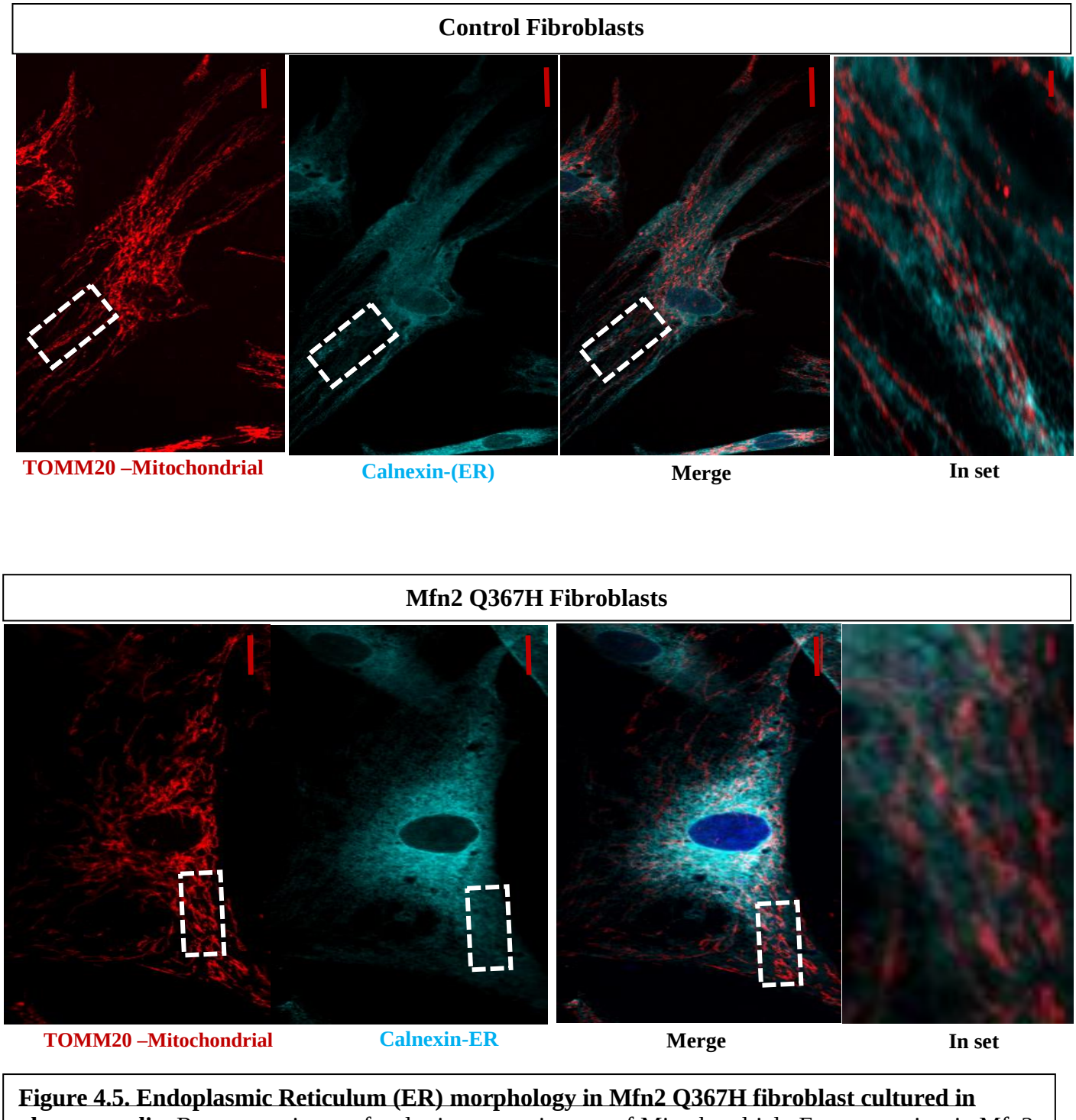

Figure 4.5. Endoplasmic Reticulum (ER) morphology in Mfn2 Q367H fibroblast cultured in glucose media. Representative confocal microscopy images of Mitochondrial –Er contact sites in Mfn2 Q367H fibroblast cultured for 72 hours in glucose media. Deep Blue: Hoechst 3330 staining, Red: Anti-TOMM-20 (Mitochondrial marker), Cyan Blue: anti-Calnexin (ER marker). Scale Bar =20 µM, in zoomed areas 2 µM. (n= 1 100 cells counted / each condition).

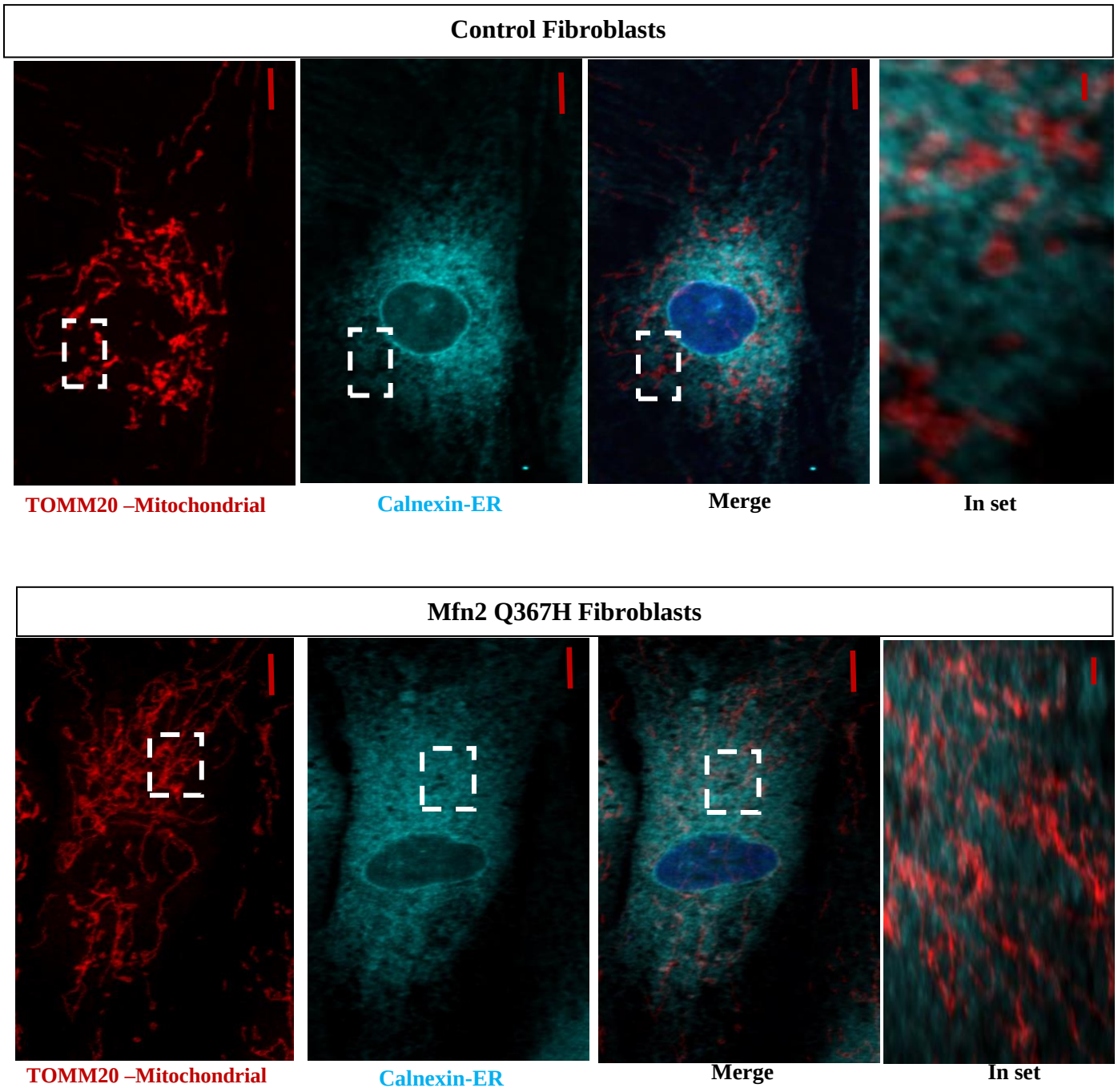

Figure 4.6 Endoplasmic Reticulum (ER) morphology in Mfn2 Q367H fibroblast cultured in glucose-free media. Representative confocal microscopy images of Mitochondrial –Er contact sites in Mfn2 Q367H fibroblast cultured for 72 hours in glucose-free media. Deep Blue: Hoechst 3330 staining, Red: Anti- TOMM-20 (Mitochondrial marker), Cyan Blue: anti-Calnexin (ER marker). Scale Bar =20 µM, in zoomed areas 2 µM. (n= 1 100 cells counted / each condition).

4.2.4 Mitochondrial DNA Content

MFN2 mutations have been linked to severe mtDNA depletion (Chen et al., 2010); therefore, we examined the effect of the Q367H mutation on mtDNA copy number. To assess mtDNA copy number, the ratio of mitochondrial DNA to nuclear DNA was measured in Mfn2 Q367H and control fibroblast cultured for 72 hours in either glucose or glucose-free media. Relative mtDNA levels were not found to differ significantly between control and Mfn2 Q367H fibroblasts cultured in glucose media [Figure 4.7]. However, in glucose-free media, a significant 50% depletion in the mtDNA/18sRNA ratio was observed in Mfn2 Q367H compared to control ($p < 4.47E-14$). Lastly, no significant differences were observed between control cells growing in the different growth conditions ($p > 0.05$).

4.2.5 Lipid Droplet Morphology in Mfn2 Q367H

Considering recent data showing a link between *MFN2* mutations and alterations in lipid homeostasis (Boutant et al., 2017; Larrea et al., 2019), I sought to examine the effect of the Mfn2 Q367H mutation on lipid droplet abundance. Fibroblasts harboring the Mfn2 Q367H mutant were cultured in both glucose and glucose-free media for 72 hours and then processed for immunofluorescence using a marker to label lipid droplet (HSC LipidTox™ Green). Notably, we observed a significantly higher signal for lipid droplets in fibroblasts harboring the Mfn2 Q367H regardless of culture conditions [Figure 4.8]. Specifically, we observed a 30% increase in the average fluorescence intensity in glucose media ($p \leq 0.04$), and a 40% increase in glucose-free media ($p \leq 0.008$) [Figure 4.9]. This finding suggests that the Mfn2 Q367H mutation affects the lipid droplet abundance or Mfn2-linked lipid functions regardless of growth conditions (Glucose media or glucose-free media).

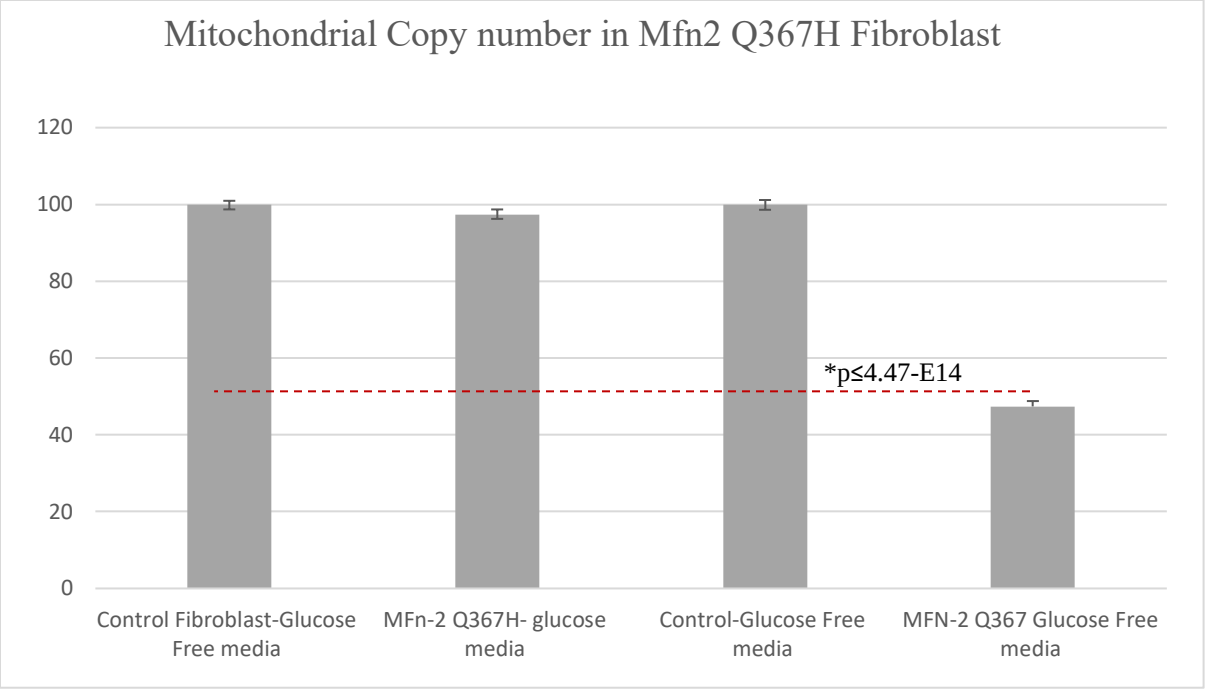

Figure 4.7 Mitochondrial DNA content expression of control and Mfn2 Q376H fibroblasts cultured for 72 hours in glucose and glucose-free media and quantified by Real Time PCR.

A histogram representing relative quantification of mtDNA expression to the housekeeping 18S RNA gene expression. Mean value and standard deviation were calculated from at least 3 independent experiments. P-value calculated by tow-tailed t-test and are shown as *, P-value calculated by tow-tailed t-test and are shown as *P = 4.47-E14.

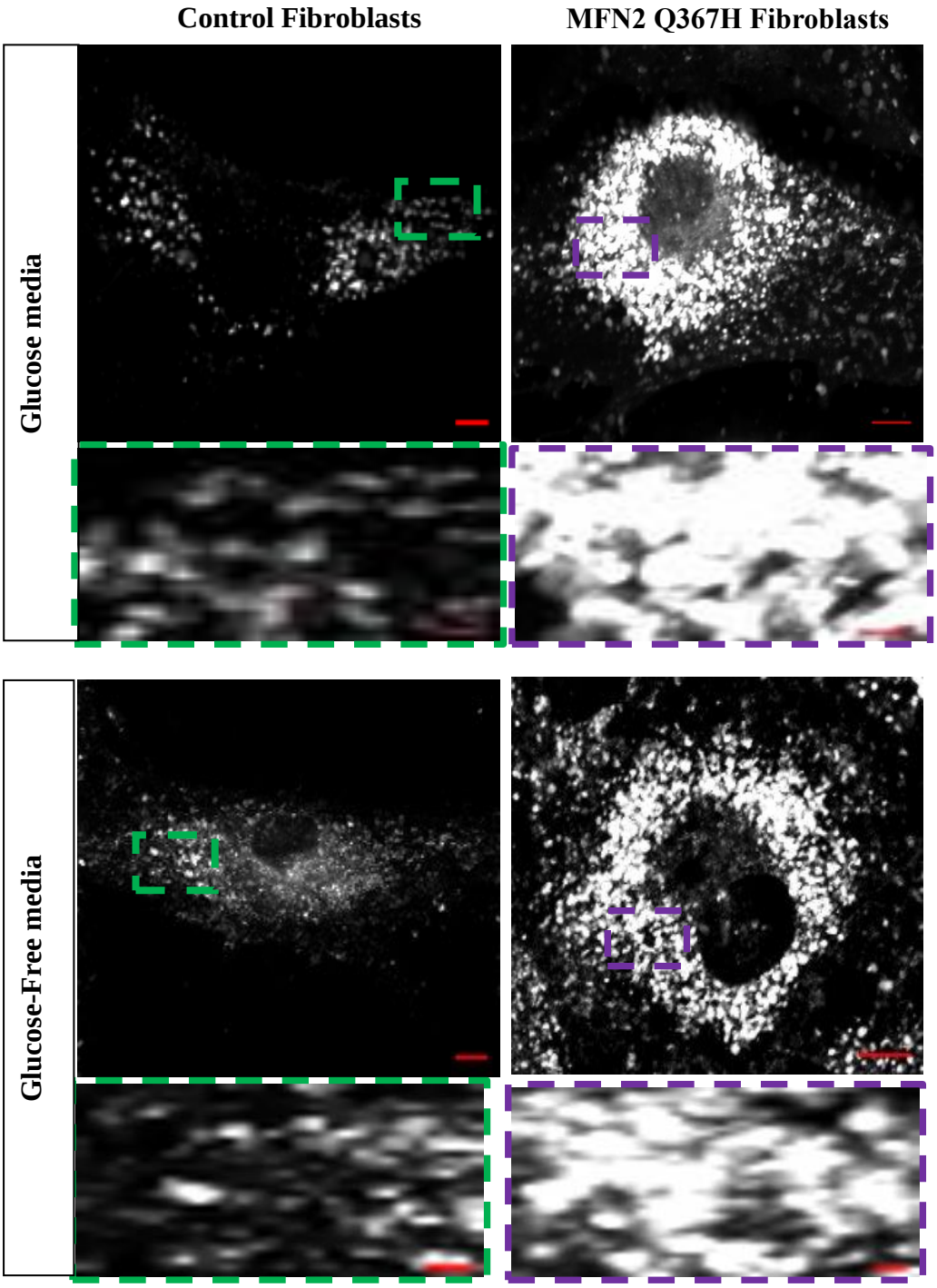

Figure 4.8 Lipid droplet phenotype in Mfn2 Q367H Fibroblast and control fibroblast cells cultured in glucose media and glucose free media.
Cells were fixed by 4% PFA and incubated overnight with HSC lipid TOX (Lipid droplet marker) and imaged with confocal microscopy taken by Zeiss. Scale Bar =20 µM, in zoomed areas 2 µM.

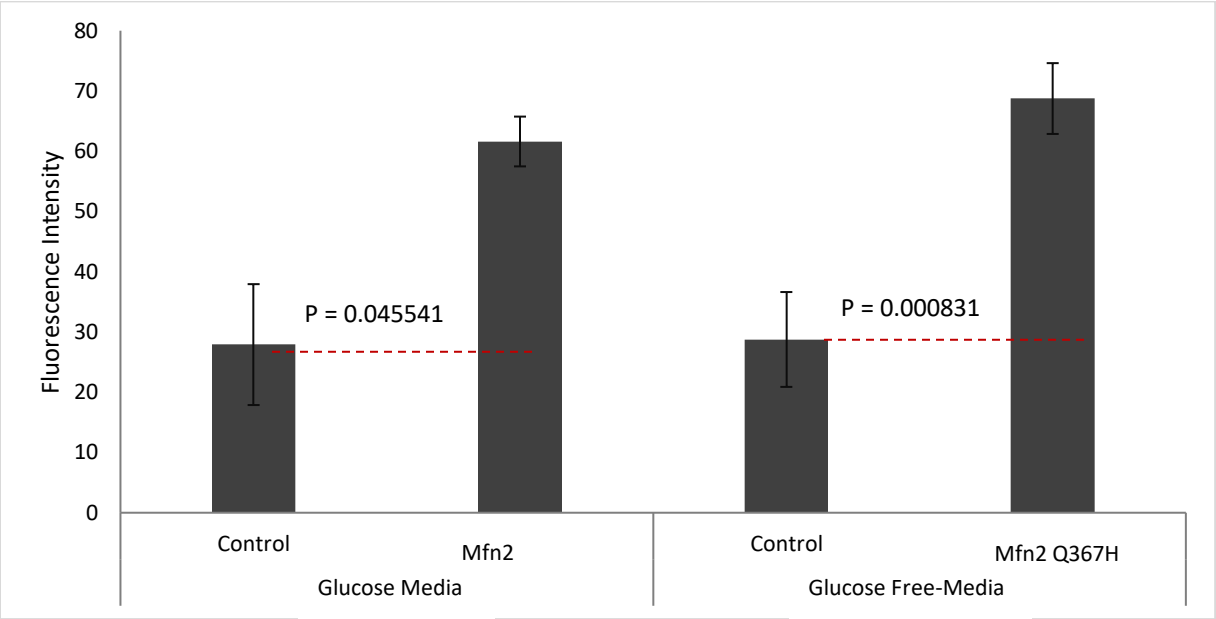

Figure 4.9 High fluorescence intensity of lipid droplets in the Mfn2 Q367H fibroblasts. Representative histogram for fluorescence intensity quantification. Fluorescence intensity was quantified according to a series set of control images as threshold, n= 1 100 cells counted / each condition). *p denotes $p<0.05$ as determined by Student's t-test. At least three independent experiments were run (n=100 cells / conditions).

4.2.6 Bioenergetic Profile for Mfn2 Q367H Fibroblasts

Next, I sought to investigate the impact of the Mfn2 Q367H mutation on mitochondrial bioenergetics. The respiration analysis in Mfn2 Q367H and control fibroblasts was performed using a Seahorse Metabolic Flux Analyzer, which measures oxygen consumption rate (OCR) in adherent cells or isolated mitochondria. Changes in oxygen concentration are interpreted according to the provider's suggested calculation and reported as Oxygen Consumption Rate (OCR) [Figure 10. a]. In the absence of inhibitors, mitochondrial respiration is measured as basal respiration. The first inhibitor to be added is oligomycin, which inhibits ATP complex from shuttling protons across the electron gradient chain for phosphorylation of ADP to ATP (Hong & Pedersen, 2008); causing a decrease in respiration. To calculate the "ATP production", the OCR after oligomycin addition is subtracted from OCR before oligomycin addition. Next, the carbonyl cyanide-4-(trifluoromethoxy)phenylhydrazone (FCCP) is added to measure the maximal mitochondrial respiration. The addition of the ionophore FCCP ionophore abolishes mitochondrial membrane potential and forces mitochondrial-dependent respiration to work at maximum. The "spare respiratory capacity" is calculated for the difference between maximal and basal respiration outcomes. The last inhibitors to be added are antimycin and rotenone to cease electrons transfer for mitochondrial respiration. The non-mitochondrial respiration is calculated for the difference of OCR at the final point (once the reaction is stopped) and zero. Finally, the "proton leak" is calculated for the difference between OCR after oligomycin and after respiration machinery inhibition.

In our study, all OCR readings were normalized to cellular protein levels. The overall respiratory responses of Mfn2 Q367H and control fibroblasts are illustrated in [Figure 4.10. a].

A comparison of these parameters in mutant Mfn2 Q367H and control fibroblasts is provided in [Figure 4.13.b]. After correcting non-mitochondrial respiration, a slightly lower basal mitochondrial respiration was observed in Mfn2 Q367H fibroblasts ($P \leq 0.04$) [Figure 4.10.c]. Also, ATP production was lower in Mfn2 Q367H fibroblasts than the control fibroblast ($P \leq 7.2$ E-12) [Figure 4.10.d]. In this study, the Mfn2 Q367H cells had a markedly lower maximum respiratory rate than control fibroblasts ($p \leq 8.3$E-9) [Figure 4.10.e.]. Finally, the spare respiratory capacity was significantly lower in Mfn2 Q367H fibroblast than the control fibroblast ($p \leq 1.4$E-10) [Figure 4.10.F]. Overall, these data suggest that Mfn2 Q367H may affect the mitochondrial respiratory capacity and lower its ability to produce ATP efficiently.

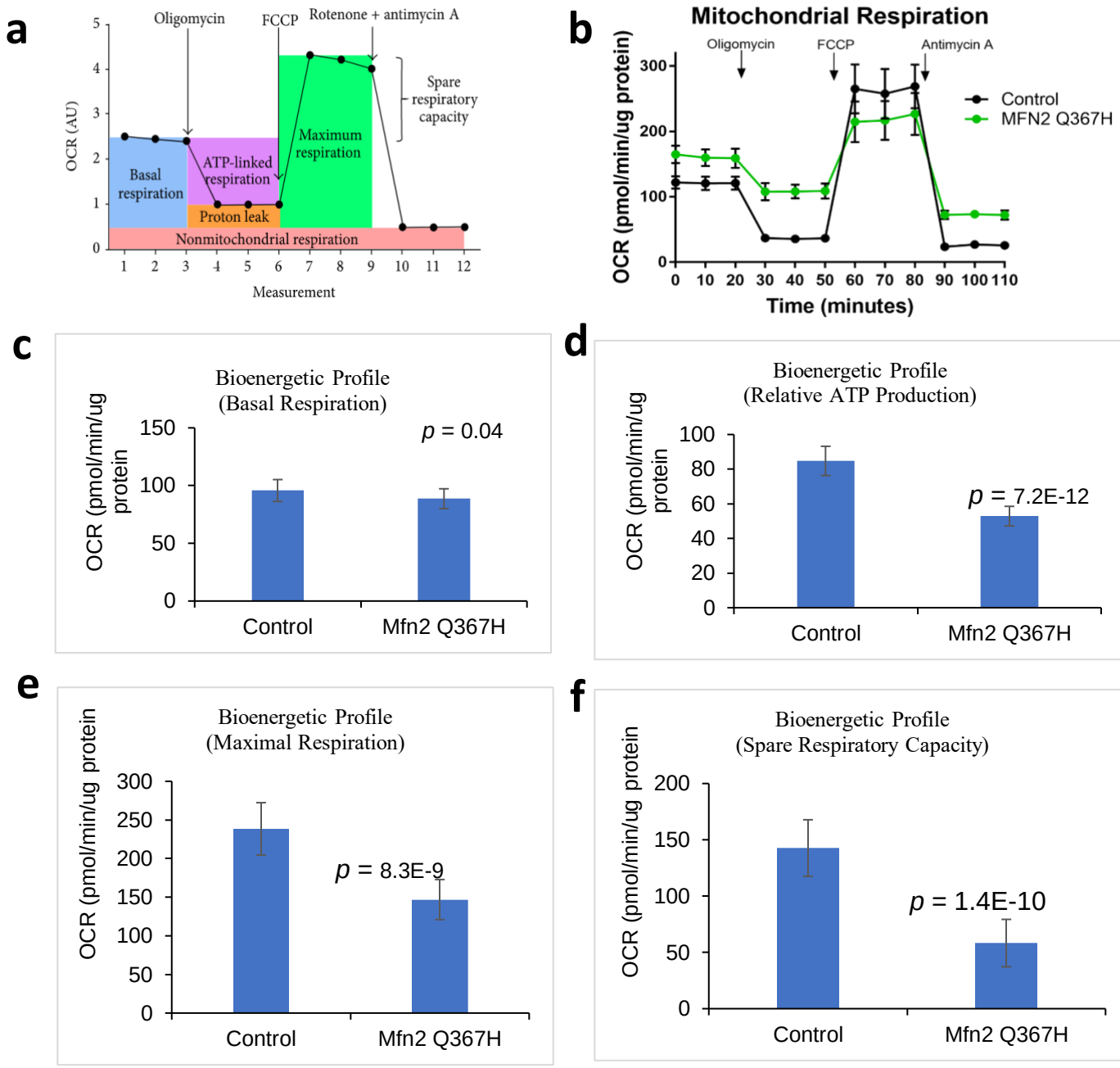

Figure 4.10 Respiratory flux profiles of Mfn2 Q367H and control fibroblasts.
(a) Respiratory flux profiles of Mfn-2 Q367H and control fibroblasts Determined by a Seahorse Extracellular Flux Analyzer with measurements of oxygen consumption rate (OCR) – Mitochondrial profile measurement test. Results are expressed as mean ± SEM. Addition of ATP synthase inhibitor oligomycin, electron transport chain uncoupler FCCP and complex I and III inhibitors rotenone and antimycin A are indicated. (b) Illustrative respiratory flux profile indicating various parameters of respiratory control. These include; (c)OCR due to non-mitochondrial respiration (rotenone/antimycin A response) and basal mitochondrial OCR (basal measurement minus rotenone/antimycin A response); (d)ATP-linked OCR (basal measurement minus oligomycin response); OCR due to proton leak (oligomycin response minus rotenone/antimycin A response); ATP coupling efficiency (basal mitochondrial OCR divided by ATP-linked OCR); (e) maximum OCR (FCCP response minus rotenone/antimycin A response), and (f)spare respiratory capacity (maximum OCR divided by basal mitochondrial OCR). Experiment was done in at least two biological replicates and three technical replicates.

4.3 Discussion

Mfn2 is responsible for mitochondrial fusion and mitochondria-ER tethering (de Brito & Scorrano, 2008). The deletion of *MFN2* in mice is lethal, causing severe impairments in the cerebellum during development (Chen et al., 2003). In *MFN2* knockout cells, mitochondria showed excessively fragmented mitochondria with “variable sizes and diameters” (Chen et al., 2003; Filadi et al., 2015). Overexpression of Mfn1 in *MFN2* knockout or Mfn2 in *MFN1* knocked out cells, rescued mitochondrial fragmentation partially (Chen et al., 2003). The overexpression of either *MFN1* or *MFN2* in the wildtype cells induced mitochondrial aggregation and accumulation of mitochondria at the perinuclear area (Filadi et al., 2015; Rojo, Legros, Chateau, & Lombes, 2002). In fact, mutations in the *MFN2* gene are classically linked to neurological disorders that cause neuropathies involving legs, arms, and sensory loss, known clinically as CMT diseases. There are more than 100 dominant mutations in the *MFN2* gene that have been reported in CMT patients (Pareyson et al., 2015). However, it is unclear how mutations in *MFN2* lead to peripheral neuropathy. In regards to mitochondrial network, some *MFN2* mutations cause mitochondrial aggregation and are considered as "gain of function" mutations, while other MFN2 mutations cause mitochondrial fusion defects and are considered as "loss of function" (Calvo et al., 2009; Verhoeven et al., 2006). Also, few studies reported abnormal mitochondrial accumulation at distal sites of neurons, abnormal mitochondrial motility, and other altered aspects like cristae architecture and mitochondrial respiration (Calvo et al., 2009; Loiseau et al., 2007; Sole et al., 2009; Verhoeven et al., 2006). Thus, given this array of different phenotypes impacted by *MFN2*, it is unclear exactly how Mfn2 dysfunction leads to peripheral neuropathy phenotypes. Here we describe a novel mutation in Mfn2, Q367H, which is not associated with a CMT disease phenotype. Our characterization of fibroblasts from the

patient harboring the Mfn2 Q367H mutation, described below, provides novel insight regarding various Mfn2 functions and their correlation to peripheral neuropathies.

4.3.1 Mitochondrial Morphology in Mfn2 Q367 Fibroblasts

Fibroblasts harboring the Mfn2 Q367H mutation showed a fused mitochondrial network, which is similar to mitochondrial morphology, the wildtype fibroblasts. However, when Mfn2 Q367H cells were pushed to rely on oxidative phosphorylation, mitochondria in these cells remained fused compared to the fragmented mitochondrial in control fibroblasts. The hyper-fused mitochondria in the Mfn2 Q367H cells imply that this variant may be a "gain of function" mutation. These findings are also consistent with reports showing mitochondrial fusion can still occur despite the presence of certain Mfn2 mutants (Amiott et al., 2008; Larrea et al., 2019; Misko, Sasaki, Tuck, Milbrandt, & Baloh, 2012; Pera et al., 2017). Significantly, a report by Detmer and Chan suggested that Mfn1 can rescue the fusion function of mutant Mfn2 mutants via forming hetero-oligomeric complexes between Mfn1 and mutant Mfn2 (Detmer & Chan, 2007a). This report also indicated that the Mfn2-Mfn2 mutants "homo-oligomeric" complexes are "non-functional" for mitochondrial fusion (Detmer & Chan, 2007a). In support of this observation, Larrea et al. documented higher expression of Mfn1 transcripts in fibroblasts harboring the R364W mutation, fortifying the compensatory role of Mfn1 for Mfn2 mutants. Although we have not done further experiments to investigate whether Mfn1 compensates the Mfn2 Q367H mutant, this is a possibility.

It is also worth mentioning that the higher levels of fragmentation for control fibroblasts in glucose-free media compared to standard media are inconsistent with the behavior of control fibroblasts tested at the same conditions in the Beresewicz et al. 2018 study. In the Beresewicz et al. study, control cells showed a lower fragmentation percentage in glucose-free media (30% less

fragmentation). This difference might be attributed to the age difference of utilized control lines. A match in age and gender fibroblasts from a healthy donor was utilized (e.g., fibroblasts from 68 years, old, and healthy male donor). It is expected that Beresewicz et al. used a control fibroblast cell that also matches the age of their patient (10-23-year-old). Currently, there are no studies in humans that show how aging can affect mitochondrial morphology. Only one report showed the age link to mitochondrial morphology in *the C.elegans* model (Regmi, Rolland, & Conradt, 2014). In *C. elegans,* an increased fragmentation in the mitochondrial network with aging was observed.

Finally, based on observations from experiments in this study, the fusion phenotype, the Mfn2 Q367H mutation, appears to behave as a gain of function. However, more experiments need to be done to derive a conclusion. Future experiments could examine the ability of Mfn2 Q367H to rescue fusion in *MFN1*/*MFN2* null cells.

4.3.2 Mitochondria-ER Morphology in Mfn2 Q367 Fibroblasts

In addition to its localization at MOMs, Mfn2 is also proposed to regulate mitochondria-ER interactions. However, the exact function of Mfn2 in this interaction is still debatable. Unlike Mfn1, Mfn2 is located at the ER (de Brito & Scorrano, 2008). Earlier studies suggested that Mfn2 facilitates mitochondria-ER tethering, and the absence of Mfn2 leads to ER network alterations and reduced mitochondria-ER interactions (de Brito & Scorrano, 2008; Naon et al., 2016). In contrast, recent studies challenged the previous observations and showed an increase in mitochondria-ER juxtaposition in Mfn2 deficient or *MFN2* null cells (Cosson, Marchetti, Ravazzola, & Orci, 2012; Filadi et al., 2015; Leal et al., 2016).

The effect of *MFN2* mutations on MAMs and their involvement in CMT pathogenicity is still not fully understood. A recent study suggested that alterations to mitochondria-ER contacts

may underlie the CMT phenotype associated with *MFN2* mutations (Larrea et al., 2019). A higher inter-organellar distance was observed in mitochondria- ER connectivity in fibroblasts harboring *MFN2* mutations (Larrea et al., 2019), suggesting that the functional crosstalk between ER and mitochondria might be contributing to peripheral neuropathy phenotype.

There were no observed changes in mitochondrial-ER architecture or morphology in our screen of the ER-mitochondria contact in fibroblasts carrying the Mfn2 Q367H mutation. However, the method utilized in this study is considered to be very basic (Chakkarapani, Zhang, & Kang, 2018). Also, due to time constraints, no quantification was done for mitochondria-ER morphology. Currently, there is no consensus on the accuracy and validity of techniques used to confirm organelles vicinity in documented studies. With the current controversy in the field about the exact role of Mfn2 in mitochondria-ER, it is hard to conclude whether Mfn2 Q367H is affecting the MAMs in a "loss of function" or "gain of function" manner. More advanced and optimized techniques need to be utilized to conclude the effect of Mfn2 Q367H on mitochondria-ER architecture or morphology.

4.3.3 Lipid Droplet Alteration

Lipid droplets are often located in proximity to several organelles, particularly, ER (Ozeki et al., 2005; Turro et al., 2006) and mitochondria (Shaw, Jones, & Wagenmakers, 2008; Sturmey, ’'Toole’'Toole, & Leese, 2006; Tarnopolsky et al., 2007). While the formation of lipid droplets is suggested to be initiated at ER membranes (Londos et al., 1995; Ohsaki, Cheng, Suzuki, Fujita, & Fujimoto, 2008; Wilfling et al., 2013), mitochondria are also involved in the regulation of lipid droplet (Murphy, Martin, & Parton, 2009). Notably, lipid droplets in *MFN2* knockout MEFs showed a significant increase in their size, but not the number, (McFie, Ambilwade, Vu, &

Stone, 2016) as well as impaired mitochondria; highlighting the link between Mfn2 and lipid droplets (Boutant et al., 2017).

The effects of *MFN2* mutations on lipid droplet morphology have been studied very minimally. Currently, only a couple of reports have shown that a few CMT-*MFN2* mutations caused alterations to lipid droplets (Boutant et al., 2017; Pera et al., 2017). Because the full spectrum of Mfn2 functions is/are not fully recognized, the mechanisms by which *MFN2* mutations are causing lipid droplet changes and its correlation to CMT pathogenicity cannot be explained. In our study, microscopy images reflected a noticeable alteration in lipid droplet abundance (reflected by a significantly higher intensity) in cells harboring the Mfn2 Q367H mutation compared to control fibroblasts. Due to the current lack of *MFN2* knockdown studies, it is hard to interpret how the Mfn2 Q367H mutation affects lipid droplets. Our findings, along with findings from previous reports, support the role of Mfn2 in lipid droplet homeostasis.

4.3.4 Altered Bioenergetics and mtDNA Content Associated with the Mfn2 Q367H Variant

The involvement of Mfn2 in cell bioenergetics was described previously (Zorzano, Liesa, Sebastian, Segales, & Palacin, 2010). Mfn2 suppression caused a significant decrease in glucose oxidation, membrane potential, and proton leak (Bach et al., 2003). On the other hand, Mfn2 overexpression caused an increase in cellular respiration even when expressed as a truncated protein lacking the transmembrane domain (Pich et al., 2005). Our observation supports the work showing *MFN2* mutations, and Mfn2 deficiency is associated with mitochondrial-coupling defects and diminished mitochondrial respiration (Bach et al., 2003; Pich et al., 2005). Thus, our finding suggests that the Mfn2 Q367H mutation behaves as a loss of function for mitochondrial respiration.

Mitochondrial fusion is necessary to maintain mtDNA stability (Chen, McCaffery, & Chan, 2007; Rouzier et al., 2012). The mtDNA replisome is maintained by mitochondrial fusion (Silva Ramos et al., 2019). Loss of MOMs fusion leads to nucleoid clustering (Silva Ramos et al., 2019). Also, severe impairment of mitochondrial fusion drastically affects mtDNA copy number. In MEFs, lacking either *MFN1/ MFN2* or both, a significant reduction of mtDNA copy number was observed (Chen et al., 2007; Kawalec et al., 2015). Notably, mutations in other proteins that mediate mitochondrial fusion also lead to depletion of the mtDNA genome (e.g., Opa1, Msto1, Fbxl4) (Donkervoort et al., 2019; Sabouny et al., 2019; Zhang et al., 2017), confirming the importance of mitochondrial fusion in maintaining mitochondrial DNA stability. In this study, relative mtDNA levels were not significantly different in Mfn2 Q367H from control fibroblasts in glucose media. However, the replacement of glucose by glucose-free media was associated with a significant drop in the mtDNA/nDNA ratio to more than 50 % compared to the wild type control cells. This observation seems to be in line with previous reports (Beresewicz, Charzewski, Krzysko, Kochanski, & Zablocka, 2018; Chen et al., 2007; Kawalec et al., 2015). Because mtDNA encodes 13 proteins of the respiratory chain complex, it is reasonable that mtDNA depletion may impair oxidative phosphorylation. Our observation of the reduced overall OXPHOS respiration and depleted mtDNA strengthens the previously proposed link between mtDNA and oxidative phosphorylation.

4.3.5 Mfn Q367H: A comparison to other nearby mutations

Earlier studies reported many mutations in *MFN2*, most of which are missense mutations located in critical protein domains, particularly close to or within the GTPase domain, or within the two HR domains, reviewed in (Bergamin et al., 2014; Cartoni & Martinou, 2009; Pareyson et al., 2015). Nonetheless, it is not yet clear how the different Mfn2 domains mediate mitochondrial

fusion. The two HR domains, which are coiled-coil domains, are thought to be important for *trans* Mfn2 molecules interactions [Figure 4.10] (Koshiba et al., 2004). The GTPase domain facilitates the GTP hydrolysis required for mitochondrial fusion activity (Santel & Fuller, 2001). The GTPase domain's critical role was reported earlier in the rescue experiments to Mfn2-deficient cells (Cao et al., 2017; Chen et al., 2003). In these experiments, constructs carrying fusion-deficient mutants in the GTPase motif could not restore the tubular structure in *MFN2* knockout cells (Cao et al., 2017; Chen et al., 2003).

The most frequently mutated amino acid in Mfn2 is arginine in position 94, located upstream of the GTPase domain. Mutations in this codon have been reported multiple times in independent CMT cases (Chung et al., 2006; Kijima et al., 2005; Neusch et al., 2007; Verhoeven et al., 2006; Wolf et al., 2019; Zuchner et al., 2006; Zuchner et al., 2004). Importantly, this amino acid is highly conserved from *C.elegans* to humans (Zuchner et al., 2004). R94Q mutant causes a fragmented mitochondrial phenotype (Wolf et al., 2019). Interestingly, re-expression the R94Q mutant in *MFN2* null cells rescued the mitochondrial network of but not the ER morphology (de Brito & Scorrano, 2008).

The novel Q367H Mfn2 mutation in this study occurs in the alpha-helical domain of Mfn2 near the borderline between the GTPase domain and HR1 [Figure 4.11]. Hypothetically, the alpha-helical domain functions as a structural hinge allowing for a degree of movement. Such a structure may facilitate conformational changes induced by binding of GTPase domains or facilitate GTP hydrolysis (Beresewicz, Charzewski, Krzysko, Kochanski, & Zablocka, 2018; Shy, 2004). In trying to determine how mutations in the alpha-helical domain may affect mitochondrial fusion or other mitochondrial linked functions, I searched the literature for the closest other mutations in this region.

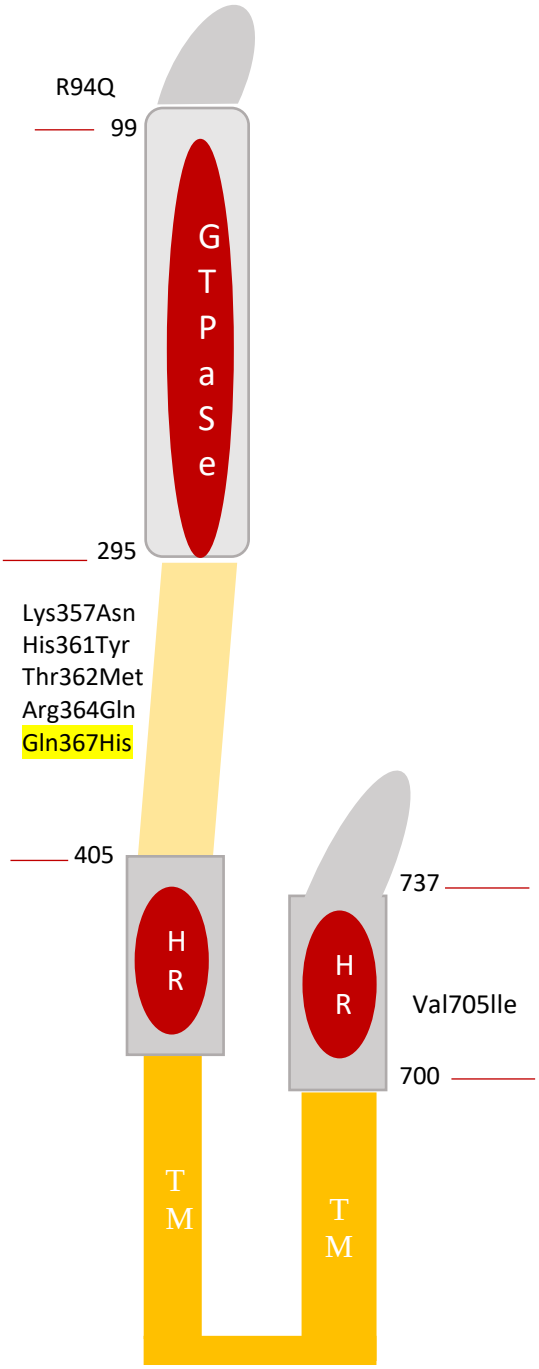

Figure 4.11 Schematic diagram of the human Mfn-2 proteins and other mutated variants. Mutations are indicated with their corresponding frequency. Abbreviations: HR, heptad repeated region, TM; Transmembrane domain. Adapted from (Cartoni & Martinou, 2009). Detected mutation in this study (MFN-2Q367) is highlighted.

Other nearby mutations in this region were found at codons 357 (p.Lys357Asn), 361 (p.His361Tyr), 362 (p.Thr362Met), and 364 (p.Arg364Trp), which all associate CMT disease (Chung et al., 2006; Kijima et al., 2005; Loiseau et al., 2002; Nicholson et al., 2008; Polke et al., 2011; Zuchner et al., 2005). Unfortunately, except for R364W, these mutations were not examined closely for mitochondrial morphology or other Mfn2 linked functions. In fibroblasts harboring the R364W mutation, changes in mitochondrial morphology were not observed; however, an increased distance between mitochondria and ER was detected (Larrea et al., 2019). Moreover, lipid droplet abundance was significantly higher in R364W fibroblasts (Larrea et al., 2019). Our observations with the Mfn2 Q367H mutant are in line with R364W mutation observations; fusion still occurs efficiently, and lipid droplet intensity (immunofluorescence signals) is considerably higher. Regarding the mitochondria-ER contacts, though my method is basic, I did not see evident changes in cells harboring the Mfn2 Q367H mutation. Given that the main difference between the Mfn2 Q367H and R364W mutations appears to be the ER-mitochondrial contacts, this suggests that impairments to the ER-mitochondrial contacts cause the peripheral neuropathy phenotype.

In conclusion, while Mfn2 is a mitochondrial fusion protein that localizes to both mitochondria and ER membranes, it is involved in multiple cellular functions. Mutations in *MFN2* are known to cause CMT disease. However, it is not clear what underlying cellular dysfunction is causing the pathology. An intriguing finding in this study showed for the first time that Mfn2 Q367H is a pathogenic variant that is not associated with CMT. Although some aspects of the Mfn2 function are disrupted, the Mfn2 Q367 mutant can promote mitochondrial fusion. This finding raises the possibility that impaired mitochondrial fusion *per se* is not the cause of CMT neuropathies. Our study also supports the notion that the underlying mechanism

causing peripheral neuropathies in patients with *MFN2* mutations could involve mechanisms other than fusion, such as defective mitochondria- ER contacts. In Mfn2 Q367H, the mitochondria juxtaposition was not altered, possibly explaining why our patient does not have a CMT phenotype. Taken together, our observations could have implications for further work investigating the mechanism of pathogenesis in CMT disease or other neuropathies. Given these differences in patient phenotypes and cellular characteristics, it is tempting to speculate that the CMT phenotype may involve impaired ER-mitochondria biology, structure, or communication, rather than loss of mitochondrial fusion.

Chapter Five

Discussion and Future Directions

5.1 Peripheral neuropathies: insights from NMIIC study and future directions

Mitochondria are highly dynamic and essential organelles for cellular survival. Within the cell, the mitochondrial network is constantly remodeled via a balanced interplay between fusion and fission events. Recently, the ER has come into light as a significant organelle in mediating mitochondrial dynamics. PNs are significant manifestations associated with mitochondrial disorders or with mutations involving genes regulating mitochondrial dynamics. CMT is the most common form of hereditary PN affecting mainly peripheral nerves. CMT has been linked to mutations in several genes, including two genes studied at this work: *MYH14* and *MFN2*. Multiple mechanisms underlying PNs have been proposed in earlier reports and reviewed in section 1.5.3- Chapter one. Recent studies suggested that impairment of mitophagy, which requires mitochondrial fission, and which functions in neuronal axons (Ashrafi et al., 2014; Maday et al., 2012), can also cause PNs (Rizzo et al., 2016). In my NMIIC study, hyper-fused mitochondrial networks were documented mostly at the cell periphery. This phenomenon is consistent with the expression patterns of NMIIC as filaments at the periphery of the cell (Smith, 2016). Therefore, it is tempting to speculate that the impaired mitochondrial fission at the cell periphery in R941L fibroblasts may impair mitophagy machinery at the cell periphery as well. Globally, mitochondrial quality control is accomplished by mitophagy and requires fission events to turnover organelles and degrade protein aggregates (Chen & Chan, 2009). Currently, mechanisms for removing damaged mitochondria by mitophagy in neurons are still not clear, and studies in this field are limited. With these observations and speculations, I am

adding a possible new mechanism underlying peripheral neuropathies: inhibition of fission at the cellular periphery may impede the regular housekeeping machinery for maintaining mitochondrial quality control, illustrated in [Figure 5.1].

It is well known that NMIIA and NMIIB play important roles during development and that loss of function mutations in these genes cause lethality (Conti, Even-Ram, Liu, Yamada, & Adelstein, 2004; Tullio et al., 1997). On the contrary, mice lacking NMIIC can still survive with no defects but need NMIIB expression later in adulthood (Ma et al., 2010). In addition to their role in mitochondrial fission, NMII proteins modulate other functions like cell migration (Vicente-Manzanares, Zareno, Whitmore, Choi, & Horwitz, 2007), cell adhesion (Vicente-Manzanares et al., 2009), and cytokinesis (Ma et al., 2012). Currently, the full array of cellular functions mediated by the three NMII isoforms is unknown. Just as the cell-type expression of the NMII isoforms varies, the different NMIIs protein isoforms' roles may also vary. Earlier reports demonstrated the complementary role of NMIIA and NMIIB in the assembly of actomyosin fibers during fibroblast polarization (M. Shutova, Yang, Vasiliev, & Svitkina, 2012; Vicente-Manzanares, Newell-Litwa, Bachir, Whitmore, & Horwitz, 2011). While NMIIA is a more dynamic protein and assembles into short actomyosin structures during the early polarization step (Sandquist & Means, 2008), NMIIB stabilizes the actomyosin structures at a later time during this process (Vicente-Manzanares et al., 2008 (Vicente-Manzanares, Koach, Whitmore, Lamers, & Horwitz, 2008). Recently, mice studies suggested that NMIIA can replace some functions of NMIIB (M. S. Shutova & Svitkina, 2018; Wang et al., 2003). This function compensation might not be applicable in neurons as neurons only express NMIIB and NMIIC. Because we do not know all cellular specific functions of NMIIC, a limitation of this study is that we cannot say with certainty that peripheral neuropathies are caused specifically by impaired

mitochondrial fission, and not some other functions of NMIIC. Future work using a peripheral neuron model expressing the R941L mutant would strengthen the observed connection in this study. Other mitochondrial linked functions like motility, communication with ER, respiratory functions, and other involvements in neuronal function involvement can be further investigated. We also do not know how the NMIIB and NMIIC proteins interact in mitochondrial fission in neurons under normal circumstances, and whether endogenous or exogenous NMIIB can rescue the functions of R941L or other NMIIC mutations. Worth mentioning is that all NMII isoforms can form homo- or heterodimers (Beach et al., 2014). In our study, structural modeling suggests that the R941L mutation may affect dimerization. Yet, the effects of R941L variant on homo-dimerization versus hetero-dimerization, and on fission functions are still needed to be investigated.

In summary, there is a strong correlation between mitochondrial dysfunction and CMT. Our finding that the R941L variant of *MYH14* causes CMT with a possible mitochondrial pathology contributes to the growing body of literature connecting mitochondrial dysfunction to health and diseases. While there are currently no effective pharmacological treatments for CMT or mitochondrial disease (Patzko & Shy, 2011; Pfeffer, Majamaa, Turnbull, Thorburn, & Chinnery, 2012), identifying the molecular pathogenesis of CMT may allow the future development of CMT treatments.

5.2 The Mfn2 Q367H Variant as a Pathogenic Allele: What is Next ?

Mfn2 is ubiquitously expressed in human tissues and involved mainly in mitochondrial fusion and other functions. *MFN2* mutations have been associated only with neurological dysfunction, and particularly to peripheral neuropathies. Today more than 100 *MFN2* pathogenic variants are known (Pareyson et al., 2015), most of which are located in critical Mfn2's regions.

Thus, it was puzzling to detect the Mfn2 Q367H mutation associated with myopathy, but without the typical CMT2A-*MFN2* phenotype, peripheral neuropathy. Therefore, a question emerged as to whether the novel Mfn2 Q367H mutation affects mitochondrial morphology and/or other mitochondrial-linked functions, and whether this study would help us gain insights about possible underlying mechanisms of PNs associated with *MFN2* mutations. Currently, it is unclear how *MFN2* mutations mechanistically lead to CMT or other patient phenotypes. It is notable that many *MFN2* mutations causing CMT2A are linked to impaired mitochondrial fusion, which is one of the major proposed mechanisms underlaying PNs (Chen & Chan, 2009). In this model, reduced fusion due to *MFN2* mutations leads to abnormal transport of mitochondria, which causes distal axonal degeneration, and is proposed to explain the pathophysiological mechanism for peripheral neuropathies. *In-vitro* transfection studies showed that several *MFN2* mutations affect the fusion process. However, some *MFN2* mutations do not impair mitochondrial fusion, yet still associated with PN phenotype (Detmer & Chan, 2007a; Misko, Sasaki, Tuck, Milbrandt, & Baloh, 2012). Moreover, other *MFN2* mutants seem to promote mitochondrial fusion (Detmer & Chan, 2007b). These latter observations challenged the earlier model proposing impaired fusion, due to mutations in *MFN2*, causes PNs. Also, these observations suggest the involvement of other mechanisms underlying PNs.

Significantly, MAMs dictate materials exchange, including lipid transfer, between mitochondria and ER (Rizzuto et al., 1992, 1993, 1998). Mfn2 facilitates the mitochondria-ER tethering at MAMs (de Brito & Scorrano, 2008; Naon et al., 2016). A recent report showed CMT2A-*MFN2* mutations altered ER-mitochondrial connectivity and MAMs function, suggesting MAMs alteration might be correlated with CMT- severity and possibly NPs (Larrea et al., 2019).

Our preliminary screen of ER and mitochondrial distribution (by immunofluorescence) in fibroblasts harboring the Mfn2 Q367H mutant showed no overt changes compared to control fibroblasts. This lack of MAMs impairment may explain the atypical manifestation in our patients. Admittedly, the methods used in this study were basic. In-depth advanced methods need to be utilized to conclude the effect of Mfn2 Q367 mutation on the biology or functions of MAMs (Larrea et al., 2019). Herein, I am are proposing that MAM impairments might be significant to PN development [Figure 5.1]. Currently, there is no solid agreement in literature on how MAMs defects affect mitochondria-ER functions, but the imbalance of juxta-positioning between the ER and mitochondria is suggested to be significant to CMT diseases (Cosson, Marchetti, Ravazzola, & Orci, 2012; Filadi et al., 2015; Larrea et al., 2019; Leal et al., 2016).

Another significant observation of this study is the changes in lipid droplet morphology found in Mfn2 Q367H fibroblasts. It is now appreciated that Mfn2 is involved in the interaction between mitochondria and lipid droplets (Boutant et al., 2017; McFie, Ambilwade, Vu, & Stone, 2016). Interestingly, increased numbers of lipid droplets and lipid metabolism changes were reported in neurodegenerative diseases like Parkinson's and Alzheimer's diseases (Cole et al., 2002; Lane & Farlow, 2005). However, the relevance of lipid droplet changes due to *MFN2* mutations to PNs is not clear. Along with our novel finding of lipid droplet alterations in the absence of PNs phenotype, it is reasonable to suggest that Mfn2 impairments might also alter lipid metabolism, and *MFN2* mutations are not necessarily causative for PNs. However, due to the gaps in our knowledge about lipid droplet biology and its correlation to Mfn2 functions, we cannot explain why alterations in lipid droplet morphology occurred. It is also worth mentioning that various cellular and animal models to study CMT showed a discrepancy in the consequences of *MFN2* mutations.

These models included gene knockouts, gene silencing, and gene overexpression. Importantly, earlier animal model indicated heterozygous mutant allele may not specifically manifest neurological phenotype (Detmer & Chan, 2007a), or showed phenotypes that do not mimic full CMT phenotypes. Some NPs phenotype only manifested following expressing significant level of mutant transgene (Detmer, Vande Velde, Cleveland, & Chan, 2008). The reason for these discrepancies might be because both WT and mutant alleles need to be in equilibrium, which is difficult to be accurately accomplished when mimicking the diseases in various models. The pathological effects of CMT-*MFN2* alleles would be ideally studied in patients-obtained neurons. However, it is not feasible to obtain neuronal tissues from patients. Therefore, primary patient fibroblast was used in our studies. Future studies may utilize patient induced pluripotent stem cells (iPSCs) differentiated to neurons to answer further questions.

Despite the knowledge obtained from these studies, several important questions remain: Which Mfn2 functions/defects are relevant to CMT diseases? by which mechanisms dose Mfn2 modulate mitochondria-ER tethering? Dose lipid droplet dysfunction contribute to pathogenesis CMT or any other disorders? Does Mfn1 compensate for Mfn2 Q367H in the context of mitochondrial fusion? By which mechanism dose the *MFN2* Q367H allele alter lipid droplet morphology? What is the mitochondrial phenotype in the affected tissues (muscles), and are other Mfn2 linked functions also affected? Answers to these questions would be informational for understanding the molecular pathogenesis of CMT, and the mechanisms of other disorders associated with *MFN2* mutations.

Many mitochondrial functions are known to be dependent on mitochondrial fusion and are associated with loss of Mfn2 functions, including oxidative phosphorylation, mitochondrial DNA integrity, and mitochondrial transport. Abnormal mitochondrial transport may partly explain

peripheral neuropathies caused by *MFN2* mutations. However, accumulating evidence suggests that the *MFN2*- linked PNs may be attributed to changes in other Mfn2 functions such as mitochondria-ER tethering.

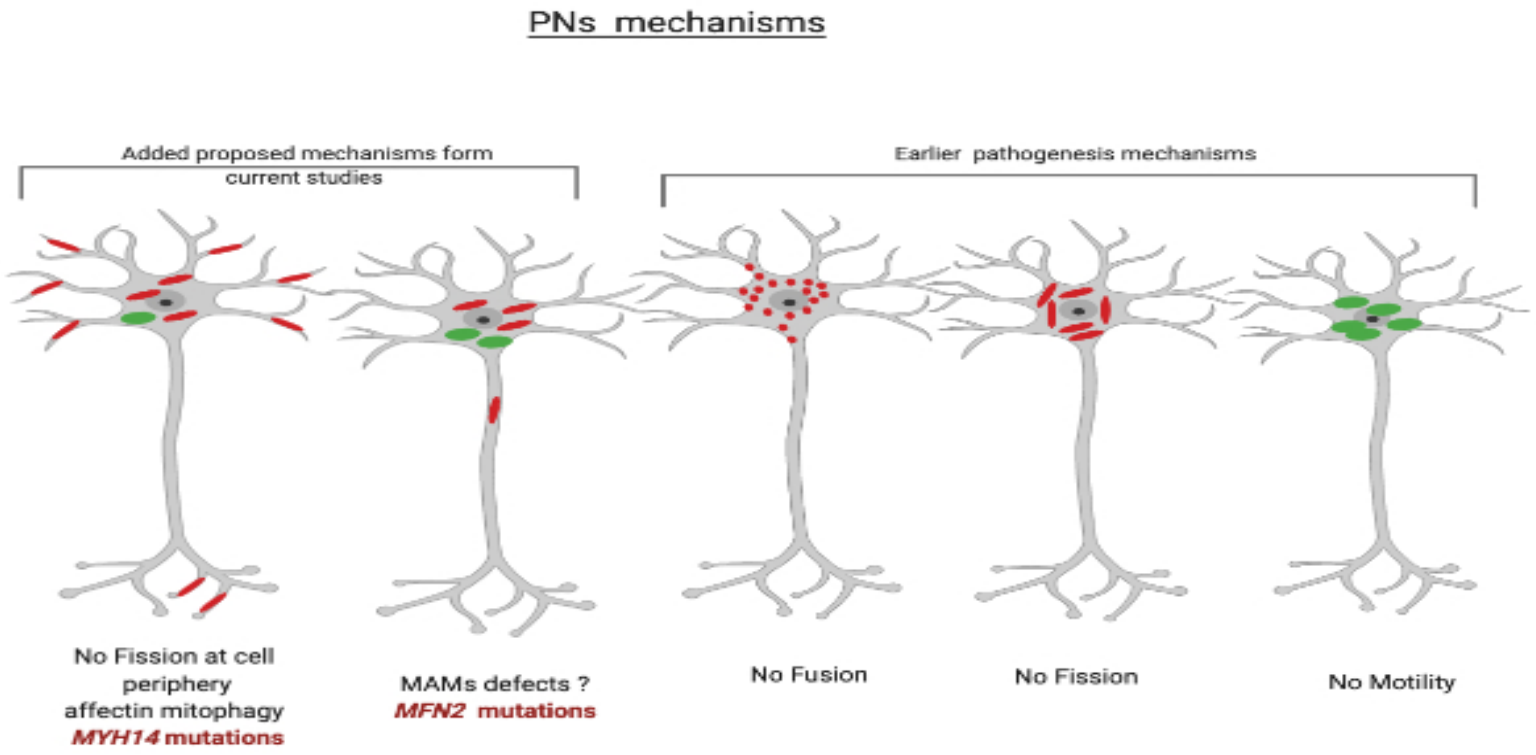

Figure 5.1 Impaired Mitochondrial Dynamics involvement in PNs Pathogenesis
Early proposed mechanisms for PNs pathogenesis involving mitochondrial dynamics in earlier literature and new proposed mechanisms from the current studies

Bibliography

Andres, D., Keyser, B. M., Petrali, J., Benton, B., Hubbard, K. S., McNutt, P. M., & Ray, R. (2013). Morphological and functional differentiation in BE(2)-M17 human neuroblastoma cells by treatment with Trans-retinoic acid. *BMC Neurosci, 14*, 49. doi:10.1186/1471-2202-14-49

Ashrafi, G., Schlehe, J. S., LaVoie, M. J., & Schwarz, T. L. (2014). Mitophagy of damaged mitochondria occurs locally in distal neuronal axons and requires PINK1 and Parkin. *J Cell Biol, 206*(5), 655-670. doi:10.1083/jcb.201401070

Ban-Ishihara, R., Ishihara, T., Sasaki, N., Mihara, K., & Ishihara, N. (2013). Dynamics of nucleoid structure regulated by mitochondrial fission contributes to cristae reformation and release of cytochrome c. *Proc Natl Acad Sci U S A, 110*(29), 11863-11868. doi:10.1073/pnas.1301951110

Beach, J. R., Shao, L., Remmert, K., Li, D., Betzig, E., & Hammer, J. A., 3rd. (2014). Nonmuscle myosin II isoforms coassemble in living cells. *Curr Biol, 24*(10), 1160-1166. doi:10.1016/j.cub.2014.03.071

Benador, I. Y., Veliova, M., Liesa, M., & Shirihai, O. S. (2019). Mitochondria Bound to Lipid Droplets: Where Mitochondrial Dynamics Regulate Lipid Storage and Utilization. *Cell Metab, 29*(4), 827-835. doi:10.1016/j.cmet.2019.02.011

Betapudi, V. (2014). Life without double-headed non-muscle myosin II motor proteins. *Front Chem, 2*, 45. doi:10.3389/fchem.2014.00045

Bobylev, I., Joshi, A. R., Barham, M., Neiss, W. F., & Lehmann, H. C. (2018). Depletion of Mitofusin-2 Causes Mitochondrial Damage in Cisplatin-Induced Neuropathy. *Mol Neurobiol, 55*(2), 1227-1235. doi:10.1007/s12035-016-0364-7

Boyer, O., Nevo, F., Plaisier, E., Funalot, B., Gribouval, O., Benoit, G., . . . Mollet, G. (2011). INF2 mutations in Charcot-Marie-Tooth disease with glomerulopathy. *N Engl J Med, 365*(25), 2377-2388. doi:10.1056/NEJMoa1109122

Canta, A., Pozzi, E., & Carozzi, V. A. (2015). Mitochondrial Dysfunction in Chemotherapy-Induced Peripheral Neuropathy (CIPN). *Toxics, 3*(2), 198-223. doi:10.3390/toxics3020198

Cartoni, R., & Martinou, J. C. (2009). Role of mitofusin 2 mutations in the physiopathology of Charcot-Marie-Tooth disease type 2A. *Exp Neurol, 218*(2), 268-273. doi:10.1016/j.expneurol.2009.05.003

Cassereau, J., Chevrollier, A., Gueguen, N., Desquiret, V., Verny, C., Nicolas, G., . . . Procaccio, V. (2011). Mitochondrial dysfunction and pathophysiology of Charcot-Marie-Tooth disease involving GDAP1 mutations. *Exp Neurol, 227*(1), 31-41. doi:10.1016/j.expneurol.2010.09.006

Chen, H., & Chan, D. C. (2009). Mitochondrial dynamics--fusion, fission, movement, and mitophagy--in neurodegenerative diseases. *Hum Mol Genet, 18*(R2), R169-176. doi:10.1093/hmg/ddp326

Choi, B. O., Kang, S. H., Hyun, Y. S., Kanwal, S., Park, S. W., Koo, H., . . . Chung, K. W. (2011). A complex phenotype of peripheral neuropathy, myopathy, hoarseness, and hearing loss is linked to an autosomal dominant mutation in MYH14. *Hum Mutat, 32*(6), 669-677. doi:10.1002/humu.21488

Cocetta, V., Ragazzi, E., & Montopoli, M. (2019). Mitochondrial Involvement in Cisplatin Resistance. *Int J Mol Sci, 20*(14). doi:10.3390/ijms20143384

Detmer, S. A., & Chan, D. C. (2007). Functions and dysfunctions of mitochondrial dynamics. *Nat Rev Mol Cell Biol, 8*(11), 870-879. doi:10.1038/nrm2275

Donaudy, F., Snoeckx, R., Pfister, M., Zenner, H. P., Blin, N., Di Stazio, M., . . . Savoia, A. (2004). Nonmuscle myosin heavy-chain gene MYH14 is expressed in cochlea and mutated in patients affected by autosomal dominant hearing impairment (DFNA4). *Am J Hum Genet, 74*(4), 770-776. doi:10.1086/383285

Fortsch, J., Hummel, E., Krist, M., & Westermann, B. (2011). The myosin-related motor protein Myo2 is an essential mediator of bud-directed mitochondrial movement in yeast. *J Cell Biol, 194*(3), 473-488. doi:10.1083/jcb.201012088

Friedman, J. R., Lackner, L. L., West, M., DiBenedetto, J. R., Nunnari, J., & Voeltz, G. K. (2011). ER tubules mark sites of mitochondrial division. *Science, 334*(6054), 358-362. doi:10.1126/science.1207385

Fu, X., Zhang, L., Jin, Y., Sun, X., Zhang, A., Wen, Z., . . . Gao, J. (2016). Loss of Myh14 Increases Susceptibility to Noise-Induced Hearing Loss in CBA/CaJ Mice. *Neural Plast, 2016*, 6720420. doi:10.1155/2016/6720420

Fukuoh, A., Cannino, G., Gerards, M., Buckley, S., Kazancioglu, S., Scialo, F., . . . Jacobs, H. T. (2014). Screen for mitochondrial DNA copy number maintenance genes reveals essential role for ATP synthase. *Mol Syst Biol, 10*, 734. doi:10.15252/msb.20145117

Garrido, N., Griparic, L., Jokitalo, E., Wartiovaara, J., van der Bliek, A. M., & Spelbrink, J. N. (2003). Composition and dynamics of human mitochondrial nucleoids. *Mol Biol Cell, 14*(4), 1583-1596. doi:10.1091/mbc.e02-07-0399

Golomb, E., Ma, X., Jana, S. S., Preston, Y. A., Kawamoto, S., Shoham, N. G., . . . Adelstein, R. S. (2004). Identification and characterization of nonmuscle myosin II-C, a new member of the myosin II family. *J Biol Chem, 279*(4), 2800-2808. doi:10.1074/jbc.M309981200

Gonzaga-Jauregui, C., Harel, T., Gambin, T., Kousi, M., Griffin, L. B., Francescatto, L., . . . Lupski, J. R. (2015). Exome Sequence Analysis Suggests that Genetic Burden Contributes to Phenotypic Variability and Complex Neuropathy. *Cell Rep, 12*(7), 1169-1183. doi:10.1016/j.celrep.2015.07.023

Hatch, A. L., Gurel, P. S., & Higgs, H. N. (2014). Novel roles for actin in mitochondrial fission. *J Cell Sci, 127*(Pt 21), 4549-4560. doi:10.1242/jcs.153791

Hatch, A. L., Ji, W. K., Merrill, R. A., Strack, S., & Higgs, H. N. (2016). Actin filaments as dynamic reservoirs for Drp1 recruitment. *Mol Biol Cell, 27*(20), 3109-3121. doi:10.1091/mbc.E16-03-0193

He, J., Mao, C. C., Reyes, A., Sembongi, H., Di Re, M., Granycome, C., . . . Holt, I. J. (2007). The AAA+ protein ATAD3 has displacement loop binding properties and is involved in mitochondrial nucleoid organization. *J Cell Biol, 176*(2), 141-146. doi:10.1083/jcb.200609158

Hirama, M., Isonishi, S., Yasuda, M., & Ishikawa, H. (2006). Characterization of mitochondria in cisplatin-resistant human ovarian carcinoma cells. *Oncol Rep, 16*(5), 997-1002.

Hong, J. Y., Kim, G. H., Kim, J. W., Kwon, S. S., Sato, E. F., Cho, K. H., & Shim, E. B. (2012). Computational modeling of apoptotic signaling pathways induced by cisplatin. *BMC Syst Biol, 6*, 122. doi:10.1186/1752-0509-6-122

Iborra, F. J., Kimura, H., & Cook, P. R. (2004). The functional organization of mitochondrial genomes in human cells. *BMC Biol, 2*, 9. doi:10.1186/1741-7007-2-9

Iyadurai, S., Arnold, W. D., Kissel, J. T., Ruhno, C., McGovern, V. L., Snyder, P. J., . . . Kolb, S. J. (2017). Variable phenotypic expression and onset in MYH14 distal hereditary motor

neuropathy phenotype in a large, multigenerational North American family. *Muscle Nerve, 56*(2), 341-345. doi:10.1002/mus.25491
Ji, W. K., Hatch, A. L., Merrill, R. A., Strack, S., & Higgs, H. N. (2015). Actin filaments target the oligomeric maturation of the dynamin GTPase Drp1 to mitochondrial fission sites. *Elife, 4*, e11553. doi:10.7554/eLife.11553
Kent, W. J., Sugnet, C. W., Furey, T. S., Roskin, K. M., Pringle, T. H., Zahler, A. M., & Haussler, D. (2002). The human genome browser at UCSC. *Genome Res, 12*(6), 996-1006. doi:10.1101/gr.229102
Kim, B. J., Kim, A. R., Han, J. H., Lee, C., Oh, D. Y., & Choi, B. Y. (2017). Discovery of MYH14 as an important and unique deafness gene causing prelingually severe autosomal dominant nonsyndromic hearing loss. *J Gene Med, 19*(4). doi:10.1002/jgm.2950
Kim, K. Y., Kovacs, M., Kawamoto, S., Sellers, J. R., & Adelstein, R. S. (2005). Disease-associated mutations and alternative splicing alter the enzymatic and motile activity of nonmuscle myosins II-B and II-C. *J Biol Chem, 280*(24), 22769-22775. doi:10.1074/jbc.M503488200
Kim, S. J., Lee, S., Park, H. J., Kang, T. H., Sagong, B., Baek, J. I., . . . Kim, U. K. (2016). Genetic association of MYH genes with hereditary hearing loss in Korea. *Gene, 591*(1), 177-182. doi:10.1016/j.gene.2016.07.011
Kneussel, M., & Wagner, W. (2013). Myosin motors at neuronal synapses: drivers of membrane transport and actin dynamics. *Nat Rev Neurosci, 14*(4), 233-247. doi:10.1038/nrn3445
Koch, J., Feichtinger, R. G., Freisinger, P., Pies, M., Schrodl, F., Iuso, A., . . . Haack, T. B. (2016). Disturbed mitochondrial and peroxisomal dynamics due to loss of MFF causes Leigh-like encephalopathy, optic atrophy and peripheral neuropathy. *J Med Genet, 53*(4), 270-278. doi:10.1136/jmedgenet-2015-103500
Korobova, F., Gauvin, T. J., & Higgs, H. N. (2014). A role for myosin II in mammalian mitochondrial fission. *Curr Biol, 24*(4), 409-414. doi:10.1016/j.cub.2013.12.032
Kraus, F., & Ryan, M. T. (2017). The constriction and scission machineries involved in mitochondrial fission. *J Cell Sci, 130*(18), 2953-2960. doi:10.1242/jcs.199562
Lee, J. E., Westrate, L. M., Wu, H., Page, C., & Voeltz, G. K. (2016). Multiple dynamin family members collaborate to drive mitochondrial division. *Nature, 540*(7631), 139-143. doi:10.1038/nature20555
Lee-Glover, L. (2018). The Regulation of Mitochondrial Morphology by AKAP12.
Lek, M., Karczewski, K. J., Minikel, E. V., Samocha, K. E., Banks, E., Fennell, T., . . . Exome Aggregation, C. (2016). Analysis of protein-coding genetic variation in 60,706 humans. *Nature, 536*(7616), 285-291. doi:10.1038/nature19057
Lewis, S. C., Uchiyama, L. F., & Nunnari, J. (2016). ER-mitochondria contacts couple mtDNA synthesis with mitochondrial division in human cells. *Science, 353*(6296), aaf5549. doi:10.1126/science.aaf5549
Macias, M. P., Gonzales, A. M., Siniard, A. L., Walker, A. W., Corneveaux, J. J., Huentelman, M. J., . . . Decourt, B. (2014). A cellular model of amyloid precursor protein processing and amyloid-beta peptide production. *J Neurosci Methods, 223*, 114-122. doi:10.1016/j.jneumeth.2013.11.024
Maday, S., Wallace, K. E., & Holzbaur, E. L. (2012). Autophagosomes initiate distally and mature during transport toward the cell soma in primary neurons. *J Cell Biol, 196*(4), 407-417. doi:10.1083/jcb.201106120

Marchi, S., Patergnani, S., & Pinton, P. (2014). The endoplasmic reticulum-mitochondria connection: one touch, multiple functions. *Biochim Biophys Acta, 1837*(4), 461-469. doi:10.1016/j.bbabio.2013.10.015

Maunakea, A. K., Nagarajan, R. P., Bilenky, M., Ballinger, T. J., D'Souza, C., Fouse, S. D., . . . Costello, J. F. (2010). Conserved role of intragenic DNA methylation in regulating alternative promoters. *Nature, 466*(7303), 253-257. doi:10.1038/nature09165

Mishra, P., & Chan, D. C. (2014). Mitochondrial dynamics and inheritance during cell division, development and disease. *Nat Rev Mol Cell Biol, 15*(10), 634-646. doi:10.1038/nrm3877

Pareyson, D., Saveri, P., Sagnelli, A., & Piscosquito, G. (2015). Mitochondrial dynamics and inherited peripheral nerve diseases. *Neurosci Lett, 596*, 66-77. doi:10.1016/j.neulet.2015.04.001

Piekny, A. J., Johnson, J. L., Cham, G. D., & Mains, P. E. (2003). The Caenorhabditis elegans nonmuscle myosin genes nmy-1 and nmy-2 function as redundant components of the let-502/Rho-binding kinase and mel-11/myosin phosphatase pathway during embryonic morphogenesis. *Development, 130*(23), 5695-5704. doi:10.1242/dev.00807

Prudent, J., & McBride, H. M. (2016). Mitochondrial Dynamics: ER Actin Tightens the Drp1 Noose. *Curr Biol, 26*(5), R207-209. doi:10.1016/j.cub.2016.01.009

Reyes, A., He, J., Mao, C. C., Bailey, L. J., Di Re, M., Sembongi, H., . . . Holt, I. J. (2011). Actin and myosin contribute to mammalian mitochondrial DNA maintenance. *Nucleic Acids Res, 39*(12), 5098-5108. doi:10.1093/nar/gkr052

Tilokani, L., Nagashima, S., Paupe, V., & Prudent, J. (2018). Mitochondrial dynamics: overview of molecular mechanisms. *Essays Biochem, 62*(3), 341-360. doi:10.1042/ebc20170104

Twig, G., Elorza, A., Molina, A. J., Mohamed, H., Wikstrom, J. D., Walzer, G., . . . Shirihai, O. S. (2008). Fission and selective fusion govern mitochondrial segregation and elimination by autophagy. *Embo j, 27*(2), 433-446. doi:10.1038/sj.emboj.7601963

van Meerloo, J., Kaspers, G. J., & Cloos, J. (2011). Cell sensitivity assays: the MTT assay. *Methods Mol Biol, 731*, 237-245. doi:10.1007/978-1-61779-080-5_20

Vicente-Manzanares, M., Ma, X., Adelstein, R. S., & Horwitz, A. R. (2009). Non-muscle myosin II takes centre stage in cell adhesion and migration. *Nat Rev Mol Cell Biol, 10*(11), 778-790. doi:10.1038/nrm2786

Yang, T., Pfister, M., Blin, N., Zenner, H. P., Pusch, C. M., & Smith, R. J. (2005). Genetic heterogeneity of deafness phenotypes linked to DFNA4. *Am J Med Genet A, 139*(1), 9-12. doi:10.1002/ajmg.a.30989

APPENDIX -A- Supplementary Data for NMIIC Project

C. elegans work was conducted by Dr. Mains' group at the University of Calgary. *C. elegans* were cultured under standard conditions at the indicated temperatures. (Brenner, 1974). Whole broods of at least four hermaphrodites were determined, with a total of 450-1300 progeny scored. The following mutations were used: the temperature-sensitive allele *mel-11(it26)*, the null allele *nmy-1(sb113)* as described previously in [Piekny et al, 2003], and the R915L CRISPR allele *nmy-1(sb139)* described here. To introduce the R915L mutation into *nmy-1*, *eft-3: Cas9*, pJA58[*dpy-10(cn64)* gRNA], and a *dpy-10(cn64)* repair single-stranded oligonucleotide (University of Calgary Core DNA Services) were used as described for "Co-CRISPR (Arribere et al., 2014).CRISPR targeting sequence and primers used in the generation of the mutant *nmy-1(sb113)* allele are provided in the additional methods (Table 1). Two *nmy-1* gRNA PCR products were created using PCR "stitching." PCR's on pJW1285 (*pha-1* gRNA(F_+_E), a gift from Jordan Ward, Addgene) using oJW1787 + nmy1sgRNA1rev and oJW1790 + nmy1sgRNA1fwd were stitched together, substituting *nmy-1* sequences for those of *pha-1* and gel-purified to make *nmy-1* gRNA-1 (oligonucleotides and *nmy-1* gRNA target sequence are listed below). Similarly, PCR using oJW1787 + nmy1sgRNA2rev and oJW1790 + nmy1sgRNA2fwd were stitched together and gel purified to make *nmy-1* gRNA-2. The single-stranded repair oligonucleotide nmy-1-R915L-rescue-oligo (IDT), was designed to have 60 base pair homology arms, a (GC >TT) mutation resulting in R915L and two silent mutations in R911 (G> A) and N916 (C > T) to disrupt *nmy-1* gRNA targeting of the new allele and to introduce *Sal*I/*Mse*I restriction enzyme sites respectively. Gravid wild-type hermaphrodites were injected with 50 ng/µL *eft-3::Cas9*, 25 ng/µL pJA58(*dpy-10(cn64)* gRNA),500 nM *dpy-10(cn64)* oligonucleotide (Arribere et al. 2014), 25 ng/µL *nmy-1* gRNA-1, 25 ng/µL *nmy-*

1 gRNA-2, and 500 nM nmy-1-R915L-rescueoligo. PCR and restriction enzyme digestion screened dpy and Rol F1 progeny for insertions. One allele was identified, *nmy-1(sb139)*, and confirmed by sequencing.

Table.1 DNA Oligos used for CRISPER Editing of nmy-1 gene in *C.elegans*

Original (WT):
CTTCAACAAGAATCGGAGAACAGTGCTGAACTGGACGATATCCGTGGTCGGCTTCA
GACTCGCAACCAAGAGCTCGAGTATATTGTCAACGATATGAGAGACCGTCTTTCCGA
GGAAGAACAG

Template (sb139):
CTTCAACAAGAATCGGAGAACAGTGCTGAACTGGACGATATCCGTGGTCGaCTTCAG
ACTCttAAtCAAGAGCTCGAGTATATTGTCAACGATATGAGAGACCGTCTTTCCGAGG
AAGAACAG

gRNA-1: ACTGGACGATATCCGTGGT CGG

gRNA-2: GACAATATACTCGAGCTCT TGG

>nmy1sgRNA1fwd gACTGGACGATATCCGTGGTgtttaagagctatgctgg >nmy1sgRNA1rev
ACCACGGATATCGTCCAGTcaagacatctcgcaataggagg >nmy1sgRNA2fwd
gGACAATATACTCGAGCTCTgtttaagagctatgctgg >nmy1sgRNA2rev
AGAGCTCGAGTATATTGTCcaagacatctcgcaataggagg >oJW1787
ATTGTGTTCGTTGAGTGACCC >oJW1790 AAAAATAGGCGTATCACGAGG

---

*gRNA targeting sequences are underlined and mutations highlighted. Courtesy of ©Paul Mains

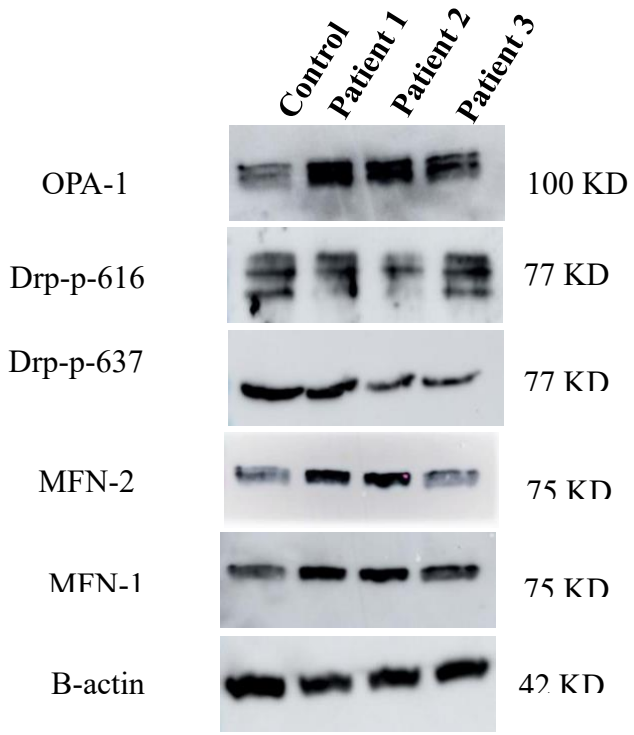

Fig. 1. Major Fusion and Fission Protein Expression in R941L Patients' Fibroblast. NMIIC does not promote mitochondrial fission in differentiated M17 neuronal cells. (a) Imunoblots of OPA-1 (100 kDa), Drp-1-p-616 (77 kDa), Drp-1-p-637(77kDa), MFN-2 (77 KDa), MFN-1 (75 KDa) and the internal control, β-actin (42 kDa).
b) representative histogram for probed proteins) in R941L patients' Fibroblast. Optical density (OD) values were normalized against β-actin. Lanes 1–4: Control, Patient 1, Patient 2, Patient 3. (n = 1), for percentage values of OD ratios. *$p < 0.05$ *versus* control.

APPENDIX-B-

AKAP12: A Possible Player in Mitochondrial Dynamics

1. Introduction

Mitochondria are vital to cell function and survival, as they are fundamental in cell regulation and hemostasis. Post-translational modifications, including phosphorylation, are recognized to regulate mitochondrial functions. In this context, one of the key regulatory molecules responsible for governing this organelle is the A-kinase anchoring proteins (AKAPs). AKAPs are members of a large family of scaffolding proteins that play a crucial role in modulating intracellular signaling. The central role of AKAPs is to bring protein kinases to a specific intracellular compartment via protein-membrane or protein-protein interactions. Each anchoring AKAP is associated with a unique subset of effectors compromising protein kinases, small GTPases, transmembrane receptors, and ion channels (Dodge-Kafka et al., 2005). In mitochondrial function, several AKAPs were reported to recruit PKA and other kinases to the mitochondrial outer membrane, modulating aspects of mitochondrial dynamics associated with several cell signaling pathways. Of note, AKAP1 has been guiding the field of AKAPs and has been clearly identified as a critical protein responsible for the regulation of mitochondrial dynamics via post-translation modifications (H. Kim et al., 2011; Livigni et al., 2006)). AKAP1 also functions as an intermediary in the oxidative synthesis of ATP, regulation of membrane potential, Ca2+ maintenance, and most importantly, mediating mitochondrial fission to protect cells against apoptosis (H. Kim et al., 2011; Livigni et al., 2006; Scorziello et al., 2013).
One of the critical regulators of fission event is the abundant GTPase protein, Drp1, which forms an oligomeric ring around mitochondrial tubules that mediates mitochondrial division.

The activity of Drp1 can be modulated by many post modifications, including sumoylation, ubiquitination, and phosphorylation. Phosphorylation of DRP-1 on the residue serine-616 (S616) activates Drp1 and promotes mitochondrial fission, whereas phosphorylation on serine-637 (S637) deactivates Drp1's GTPase activity, inhibiting fission. Phosphorylation of either site on Drp1 can be mediated by several protein kinases, which can be regulated by AKAPs. For example, the protein kinase C (PKC) activates DRP-1 via phosphorylation at the serine-616 (Qi, Disatnik, Shen, Sobel, & Mochly-Rosen, 2011). Meanwhile, protein kinase A (PKA) deactivates DRP-1 via phosphorylation at the serine-637 (Pidoux & Tasken, 2015). AKAP1 recruits PKA and PKC to the outer mitochondrial membrane. Also, many other AKAPs have been proposed through literature to be involved in the recruitment of such kinases to mitochondria. Several findings in the literature are consistent with a potential role for AKAP12. The initial intention of this project was to recapitulate some of the AKAP1 models published in the literature and examine if the AKAP12 is involved in similar fashion of AKAP1 in regulating mitochondrial dynamic.

1.1 AKAP12: A Brief Overview

The A-kinase Anchoring protein12 (AKAP12), also known as Gravin/AKP250 in humans, and Src-suppressed C kinase substrate (SSeCKS) in rodents, is localized to the cytosol and at the plasma membrane. The AKAP12 gene encodes three different protein isoforms (designated α, β, γ), which share around 95 % amino acid sequence but differ in their N-terminus and subcellular localization (Streb, Kitchen, Gelman, & Miano, 2004) [Figure 1]. AKAP12 functions as a scaffolding protein that controls mitogenic signaling and cytoskeletal re-modeling by binding key signaling mediators, including but not limited to PKA and PKC (Gelman, 2010).

A) **B)**

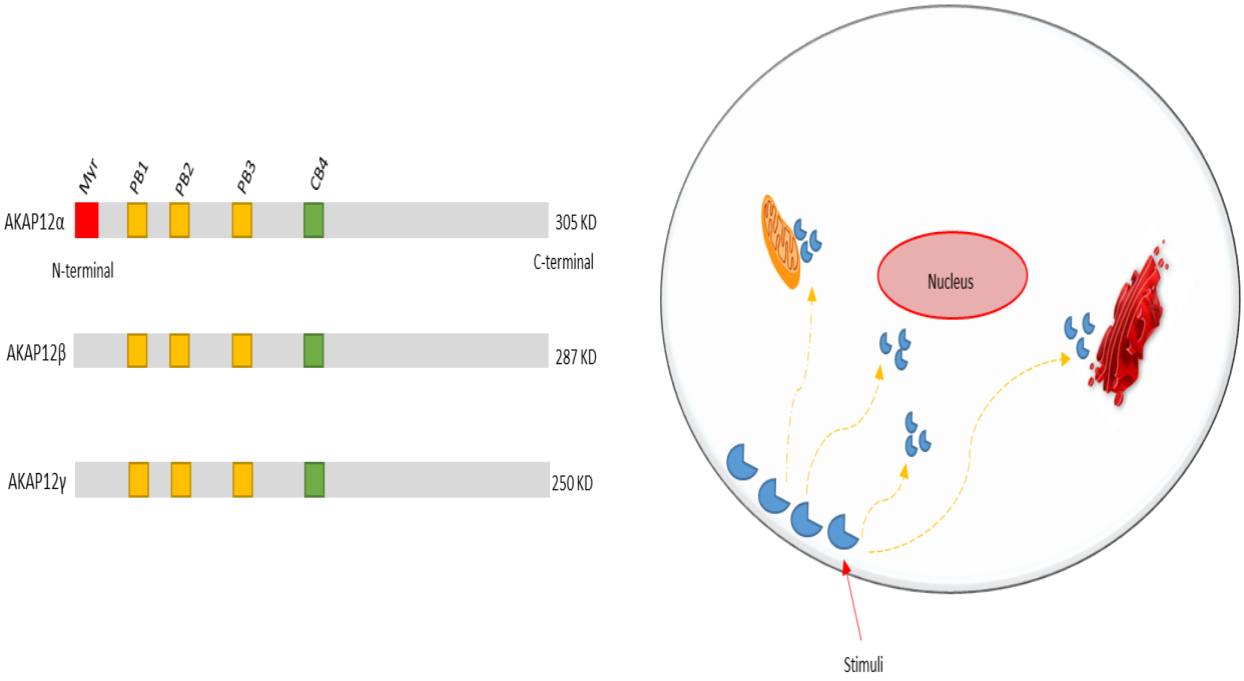

Figure 1. AKAP12 proteins and its localization in the cell.
A) AKAP12 isoforms. Most cells express the AKAP12 proteins. The 305 kDa isoforms is the myristylated AKAP12α whereas the 287 kDa isoforms is AKAP1β, and the 250 kDa is AKAP12γ. All AKAP 12 proteins include 3 polybasic domains (PB1, PB2, PB3) followed by calmodulin binding domain in their N terminus. B) AKAP12 translocation from cell periphery to cytosol, peri-nuclear space and vesicles in response to stimuli.

The N-terminal myristoylation motif differentiates the two major isoforms, being present in α and absent from β AKAP12 (Streb et al., 2004). The function of this domain is not clear. While some reports indicate that the N-terminal myristoylation motif is required for retaining AKAP12 at the cell periphery and its re-localization to the ER (Finger et al., 2015), other reports show that the N-terminal myristoylation motif has no impact on AKAP12 localization (Tao, Wang, & Malbon, 2010). Currently, the role of AKAP12 in the regulation of mitochondrial dynamic is not yet explored. Some reports in the literature documented mitochondrial morphology changes in response to stimuli associated with AKAP12 relocation [Figure.1). Moreover, AKAP12 has been found upregulated in some cancer cell lines (discussed in the next section).

1.2 AKAP12 in The Human Cancer Context

Differential regulation of AKAP12 is involved in a variety of human cancers. Mounting evidence suggests that AKAP12 acts as a tumor suppressor protein and is involved in cell cycle regulation (Hirama, Isonishi, Yasuda, & Ishikawa, 2006). Downregulation of the AKAP12 was noticed in several tumors, reviewed in (X. Wu et al., 2018). The re-expression of AKAP12 in some cancer types was observed to suppress tumorigenesis and inhibit metastasis (Gelman, 2012; Liu, Guan, Hu, Gu, & Lu, 2011). In contrast to these observations, some reports documented a moderate AKAP12 induction in other cancer types (Carinci et al., 2005; Bateman et al., 2015), indicating an ambiguous role of AKAP12 in carcinogenesis.

Cisplatin is one of the most potent Platinum based-chemotherapy agents used in the treatment of various cancers. Cisplatin activates mitochondrial death pathway, reviewed in (Cocetta, Ragazzi, & Montopoli, 2019; Hong et al., 2012). Cisplatin causes cellular cytotoxicity due to its ability to form inter- and intra-strand nuclear DNA crosslink (adducts). In turn, DNA adducts cause impairments in nuclear DNA, leading to disturbed cell replication, inhibited RNA

transcription, and leads to cellular apoptosis. Many nuclear genes govern and are involved in the synthesis of many encoding proteins essential for mitochondrial dynamics and morphology. Notably, Cisplatin-resistance in some *in-vitro* models was associated with a hyper-fused mitochondrial network. Intriguingly, a recent study documented higher expression levels of AKAP12 in mitochondrial fractions of Cisplatin-resistant ovarian carcinoma cells associated with hyper-fused tubules compared to Cisplatin-sensitive cells (Chappell et al., 2012). The precise molecular mechanism of Cisplatin resistance is not fully understood but might involve changes in protein expression related to the mitochondrial-apoptotic pathway. Currently, there is a considerable gap in our understanding of how AKAP12 might be involved in regulating mitochondria dynamics in cancer context and how it could be linked to cellular resistance to chemotherapeutics.

2. Rational

Mitochondrial dysfunction plays a role in many diseases. Modulating mitochondrial may restore mitochondrial function. Evidence of higher AKAP 12 expression in mitochondrial fractions in ovarian cancer cells and is targeted to ER under specific conditions is of most interest to this study. However, unlike AKAP1, which is tethered to the MOMs, AKP12 is located at the cell periphery, raising the question about which stimuli activates AKAP12 re-localization. In relevance to this idea, AKAPs compartmentalization reported to regulates the specificity of recruited kinases (Alto, Carlisle Michel, Dodge, Langeberg, & Scott, 2002; Pidoux & Tasken, 2010). This factor has been considered carefully through my initial plans.

I am proposing that the specificity of the recruited protein kinase by AKAP12 depends on AKAP12 translocation, and possibly, as a result, modulates mitochondrial morphology to either inhibited-fission or enhanced-fusion. In this study, I planned to focus on PKA and PKC, which

perform different intercellular functions, as they are the most identified kinases in literature in connection to mitochondria. I hypothesized that AKAP12 localizes to the MOM, leading to changes in mitochondrial dynamics. Also, Given the role of ER in mediating mitochondrial fission through the actin-myosin cytoskeleton, it is also possible that localization of AKAP12 to ER alter fission events. Since activation of myosin can be inhibited via either PKC or PKA, AKAP12 could play a significant role in the cessation of the constriction generated by the actin-myosin assembly over mitochondrial tubules and inhibit fission. Thus, this alternative hypothesis can be tested, as well.

3.Hypothesis, Research Questions, and Proposed Models

3.1 Hypothesis

"AKAP12 alters mitochondrial dynamic via protein kinase(s)".

3.2 Outstanding Questions

Considering the gap in our knowledge about the role of AKAP12 in mitochondrial regulation and the above-discussed observations from the literature, the following questions arose:

- Does AKAP12 regulate mitochondrial fission if it is recruited to the MOMs? If yes, what effect does it have on mitochondrial morphology? Is this effect facilitated by the established AKAP/PKA-mediated Drp1 S637 or AKAP/PKC Drp1 S616 phosphorylation? What happens to mitochondrial morphology if AKAP12 phosphorylates Drp1 at both sites?
- Does AKAP12 regulate mitochondrial fission once it is recruited to the ER? If so, which downstream signaling pathway is activated/involved?

- Based on observations in Cisplatin-resistant ovarian carcinoma cells, can DNA damage stimulate AKAP12/PKA/PKC redistribution from the cell periphery to either mitochondria or ER?
- How the hyper-fused mitochondrial phenotype is linked to Cisplatin resistance in OSCC lines (*in-vitro* model)? Is this a cause-effect phenomenon mediated by PKA or PKC? If yes, would PKA/ PKC inhibition prevent Cisplatin-resistance in these cancer cells? Can we implicate PKA/PKC as a target to rebalance fission in these cancer cells?

3.3 Proposed Models

Based on the previously established AKAP1-PKA/PKC mediated Drp1 S616/S637 phosphorylation, and the recent reports proposing endoplasmic reticulum-mitochondria involvement in facilitating fission events (Fortsch, Hummel, Krist, & Westermann, 2011; Hatch, Gurel, & Higgs, 2014; Marchi, Patergnani, & Pinton, 2014), I hypothesis that AKAP12 affect mitochondrial dynamic via one of the following models [Figure.2];

- Model A: PKC is recruited to the MOMs via AKAP12 to phosphorylate Drp1 at S616 to inhibit fission leading to a fused mitochondrial phenotype
- Model B- PKA is recruited to the MOMs via AKAP12 to phosphorylate Drp1 S637 to activate fission resulting in fragmented mitochondria
- Model C- PKA is recruited via AKAP12 to ER-mitochondria contact sites to phosphorylate (RhoA kinase (ROCK) signaling, inhibiting the actin-myosin cytoskeleton formation and consequently suppressing fission.

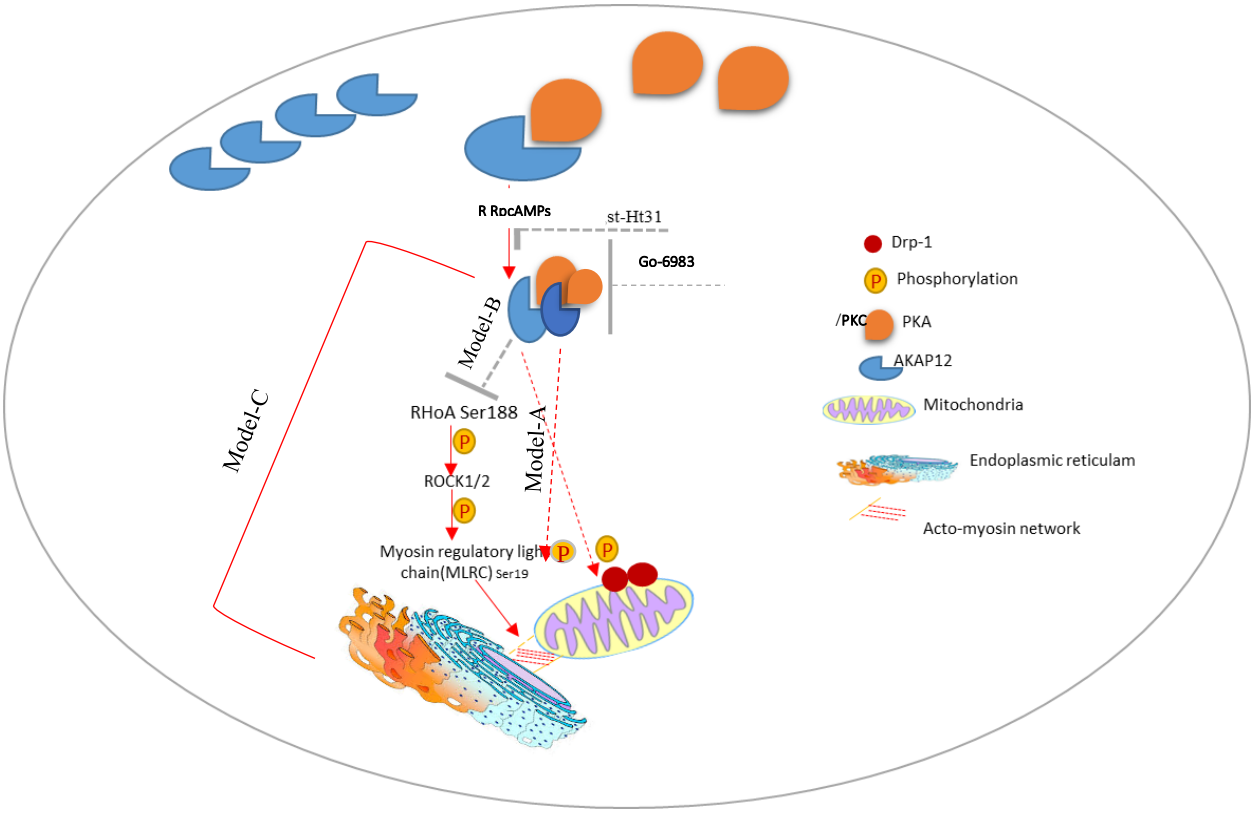

Figure 2. Proposed Models for Cisplatin/or Stress-induced Hyperfused Mitochondrial Morphology Model-A: Induced- mitochondrial Fragmentation occurs via AKP12/PKC recruitment to the MOM and subsequent phosphorylation of Drp-1$_{\text{Ser 616}}$. Model-B: Induced mitochondrial hyperfusion via AKAP12/PKA recruitment at the MOM and subsequent phosphorylation of Drp-1$_{\text{Ser 637}}$. Model-C: suppressed mitochondrial fragmentation via PKA recruitment to ER-mitochondrial contact sites followed by inhibition of the RhoA pathway. PKA inhibitor RpcAMPs, PKC inhibitor; Go-6983.

4. Material and Method

Herein, I am presenting material and method that was utilized in this project, by myself or by Laurie Glover, or that can be used for future experiments for whom wishes to continue this project.

4.1 Cloning

Cloning to produce the final plasmids encoding m-Ruby-tagged human αAKAP12, βAKAP12, and Laurie Glover did empty vectors through a series of modifications to the original human αAKAP12 plasmid, a gift from Michael Davidson (Addgene #55913). For details, kindly refer to Luria's BSc Honour's Thesis. Briefly, a mitochondrial-targeting signal was taken from the rat TOM2041 and an ER targeting signal from rabbit CYP2C142 followed by a ten amino acid flexible linker. m-Ruby was PCR amplified from pmRuby2-TOMM20-N-10, a gift from Michael Davidson (Addgene #55913). Gene fragments and PCR primers were designed and then generated using In-Fusion Cloning (TaKaRa). PCR was performed using Phusion® DNA polymerase (NEB) according to the manufacturer's protocol. Following identifying the correct size PCR products on an agarose gel, gel extraction for the DNA was performed using QIAquick Gel Extraction Kit (Qiagen), followed by In-Fusion Cloning (TaKaRa) reactions to the desired PCR products according to the manufacturer's protocol. Colonies transformation was done via Stellar Competent Cells (TaKaRa) plated on 50ug/mL kanamycin agar. Selected colonies were grown overnight in 5mL LB at 50 ug /ml kanamycin. DNA plasmids were prepped using Qiaprep Spin Mini-kit (Qiagen). Confirmation of plasmids was done by restriction enzyme digest and agarose gel electrophoresis. The sequences were also confirmed by Sanger sequencing. Final DNA plasmids were transformed into DH5alpha (Thermo Fisher) cells, grown overnight in 200mL kanamycin LB, and prepped using EZNA Plasmid Midi Prep Kit.

4.2 Cell Culture

The Oral Squamous Carcinoma Cells (OSCC) were a gift from Dr. Pinaki Boss clinic at the University of Calgary. OSCC cell lines were grown up initially in DMEM media supplemented with 10% FBS and supplemented with Penicillin/Streptomycin (100 IU/ml/100µL/mL). Cells were passaged on pre-coated coverslips coated with poly-D- Lysine diluted in 0.1% gelatin for 24 hrs. The bone carcinoma cell (U2OS) cells were cultured initially in McCoy's 5A medium or DMEM with 10% FBS and supplemented with Penicillin/Streptomycin (100 IU/ml/100µL/mL). Cells were then cultured into coverslip glass in 24-well dish. For transfection experiments, cells were transfected transiently with the following plasmids; GFP-alpha-SSeCKS, αAKAP12-m-Ruby, βAKAP12, mRubyAKAP12 using Lipofectamine 3000 according to the manufacturer's protocol for 24 or 48 hours before analysis. For stress conditions, cells were grown in hypoxia or normoxia conditions. For hypoxic conditions, N2 equilibrated gas of 1% O2 and 5% CO2 was (hypoxia chambers at Dr. Ungrins' lab, UofC). For normoxia conditions, cells were grown in regular 5% CO_2 incubators. For chemical inhibitors, cells were treated with the following chemicals: PKA inhibitor RpcAMPs (SCBT) diluted in water, PKC inhibitor Go-6983 (Abcam) in DMSO, and calcium ionophore calcimycin (Abcam) in DMSO. For cisplatin kill-curve, cells were initially seeded in 10 ml cm dishes then passaged to 96-well plate at concentrations of 2000 cells/well. After 24 hours, cells were treated at the following final concentrations: 5,4,3,2,1, 0.9, 0.8, 0.7, 0.6, 0.5 0.4, 0.3, 0.2, 0.1 Um chosen according to the range used in literature. Cell viability was assayed after 48 hours later using 3-(4,5-Dimethylthiazol-2-yl)-2,5-diphenyltetrazolium bromidefor.
(MTT) assay as described in (van Meerloo, Kaspers, & Cloos, 2011).

4.3 Immunofluorescence

Cells were fixed in pre-warmed 4% PFA for 10 minutes at 37°C, permeabilized in 0.25% Triton X-100, and quenched with 50 mM ammonium chloride. After blocking with 5% FBS in PBS, cells were incubated overnight with primary antibodies to TOMM20 and AKAP12 (rabbit anti-TOMM20, Santa Cruz Biotechnology, FL-145 and rabbit anti-AKAP12, Thermo Fisher Scientific, PA5-21759) were diluted 1:10 00 in 5% FBS in PBS, and subsequently incubated for 1 hour at room temperature with appropriate Alexafluor secondary antibodies (Thermo Fisher Scientific) diluted 1:1000 in 5% FBS in PBS. Coverslips were then mounted on glass slides with Dako mounting media (Agilent, S3023) and imaged.

4.4 Western Blot

Cells were grown in 10 cm^2. Following reaching 95 -100% confluency, cells were washed three times with cold PBS. Cells were then scraped following the addition of RIPA buffer to each dish. Protease inhibitor was added to each sample. Proteins were resolved by 10 % SDS–PAGE, transferred to PVDF membrane overnight at 22 V at 4°C. Membranes were blocked for an hour at room temperature with 5% skim milk in TBS buffer (50 mM Tris-HCl, 150 mM NaCl, 0.1% Tween-20; pH 8.5) and then probed with antibody to AKAP12 (1:500) incubated overnight at 4°C. Blots were then incubated in 5% skim milk–TBS containing matching horseradish-peroxidase-conjugated second antibody (1: 1:000 dilution in 5 % milk, Santa Cruz Biotech., Santa Cruz, CA, USA) for 2 hours at room temperature. Membranes were stripped and re-probed with antibodies against the housekeeping protein β-actin (1:1000, Millipore Sigma, ABS16), followed by incubation with 1:1000 dilutions of matching horseradish-peroxidase-conjugated secondary antibody. The blots were illuminated with enhanced chemiluminescence

reagents (ClarityÔ, WesternECL substrate# 1705060) for one min and detected by AmershamÔ imager 680.

4.5 Mitochondrial Morphology Quantification

To quantify morphology, a representative image was chosen for a hyper-fused, fused, and fragmented mitochondrial network. These images were used as scoring reference for examined cells. Except where indicated, at least 100 cells were scored per condition.

5. Preliminary Data

5.1 AKAP12 shows cytoplasmic expression and relocates to the nucleus in hypoxia condition

The exact location or pattern of AKAP12 remains under debate in the literature. Herein, I examined the endogenous expression of AKAP12 in OSSC [Figure 3.a]. AKAP12 was observed to be cytoplasmic, with a smaller number of cells showing more peripheral expression. This pattern of AKAP12 expression was confirmed in cells overexpressing rat EGFP-AKAP12 in OSCC [Figure 3.b]. Laurie Glover also observed this pattern with the overexpression of αAKAP12-m-Ruby, βAKAP12-m-Ruby, and m-Ruby (an empty vector control) in U2OS cells- Data are shown in (Lee-Glover, 2018). Mitochondria show fragmented morphology (around 95 % in OSSC) [Figure 4].

Because it is not known whether AKAP12 relocation to discrete compartments occurs in response to external or internal stimuli, I examined if the hypoxic condition could cause AKAP12 relocation to specific sites within our cells, i.e., OSCC. My earlier observation from growing cells under hypoxic conditions reflected that AKAP12 relocate to nuclear space in both cell lines, OSCC, and U2OS.

a)

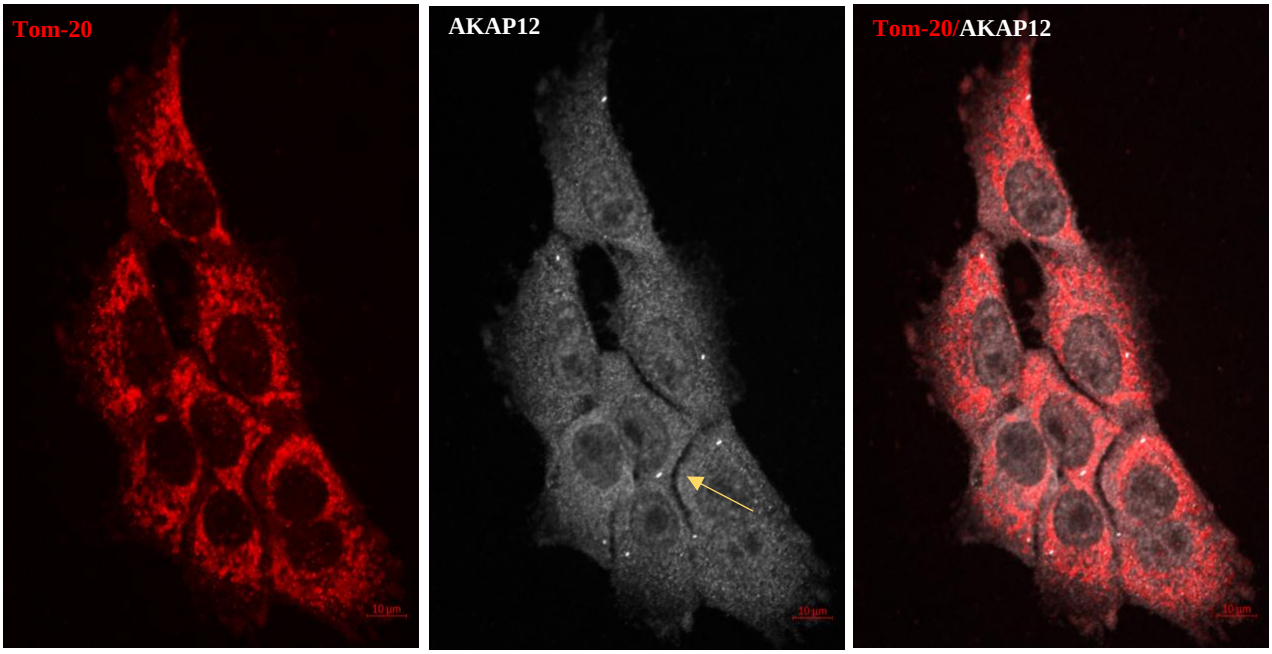

b)

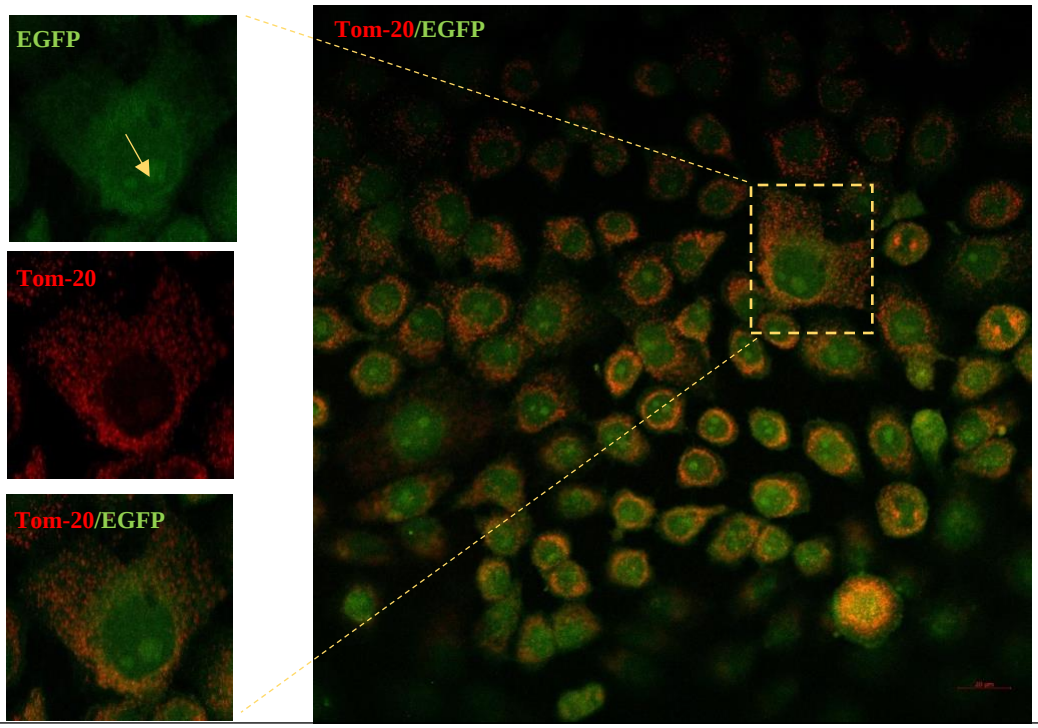

Figure.3 AKAP12 expression pattern in OSSC. a) Endogenous expression of AKAP12 showing cytoplasmic/distribution with some cells expressing peripheral AKAP12. Yellow arrow shows peripheral AKAP12 distribution Scale bar = 10 µm. (mitochondrial Marker TOM20 in red, AKAP12 protein in white .b) Over-expression of the RatEGFP-AKAP12 confirming cytoplasmic distribution of AKAP12 with some cells showing peripheral expression. Mitochondrial Morphology was detected in live cells using mito-tracker red. Yellow arrow shows peripheral AKAP12 distribution. Scale bar =20 µm.

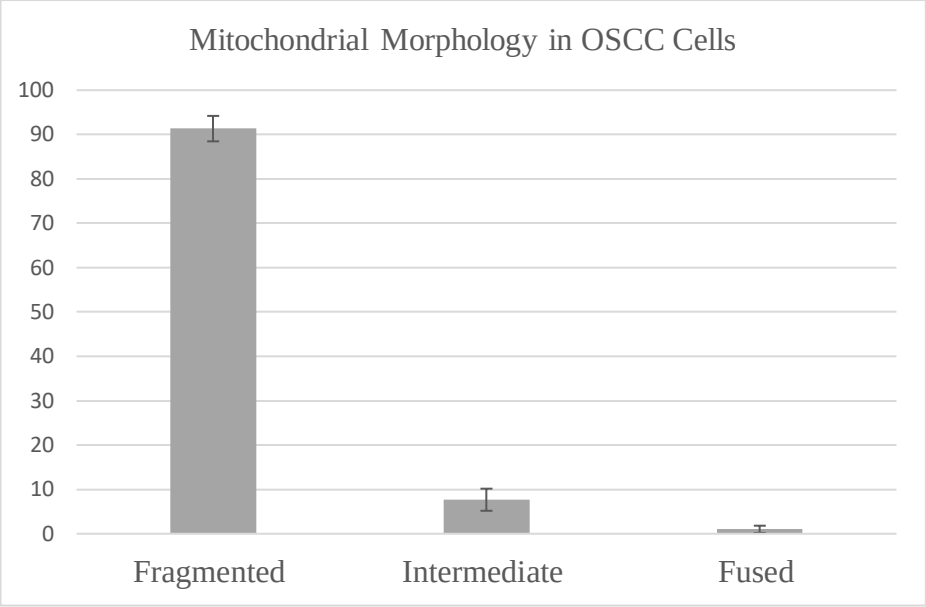

Figure. 4 Quantification of mitochondrial morphology in OSCC cells.

However, with only one replicate, this relocation occurred only in 25% of the cells. Cells that showed the relocated tend to show a more fused mitochondrial network compared to cells that had no relocation and compared to control cells [Figure 5]. Also, preliminary Western blot for cell lysates obtained from hypoxic conditions shows no differential expression for the endogenous AKAP12 expression in hypoxia than in the control condition [Figure 6]. Laurie Glover tested more stress conditions for cells expressing αAKAP12-m-Ruby, βAKAP12-m-Ruby, and m-Ruby AKAP12 (Lee-Glover, 2018). Hence, no relocation was observed neither to the nucleus nor to mitochondria or ER.

5.2 Targeted AKAP12 to the Mitochondria Causes Mitochondrial Fragmentation

This set of experiments was run by Laurie Glover. A summarized interpretation of observed data is presented here. For full report, please refer back to Lee-Glover 'thesis(Lee-Glover, 2018) . U2OS cells were transiently transfected with the mitoβAKAP12-m-Ruby, mitoαAKAP12-m-Ruby, ER-βAKAP12, and proper controls for each plasmid for 24 hours. Cells were labeled with the mitochondrial marker (Tom-20 or Cytochrome C) to visualize mitochondrial morphology. Transfected cells showed a higher fragmentation rate and a significant increased by 10 % compared to the control set. There was no difference between the effect of the α and βAKAP12 at the mitochondria. Also, no significant changes were found with targeted βAKAP12 to the ER.

In efforts to find out which of the proposed models is operating, the phosphorylation activity for Drp-1 S616 and Drp-1 S637 was addressed.

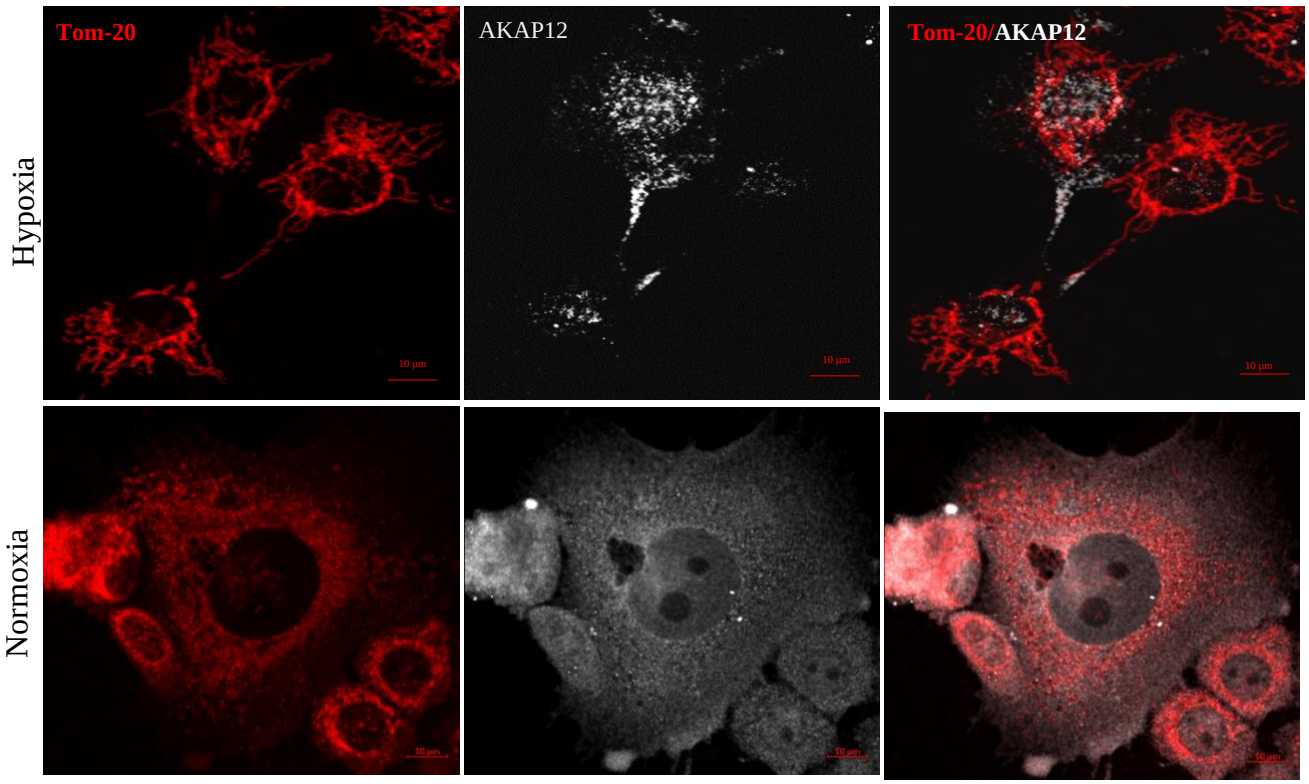

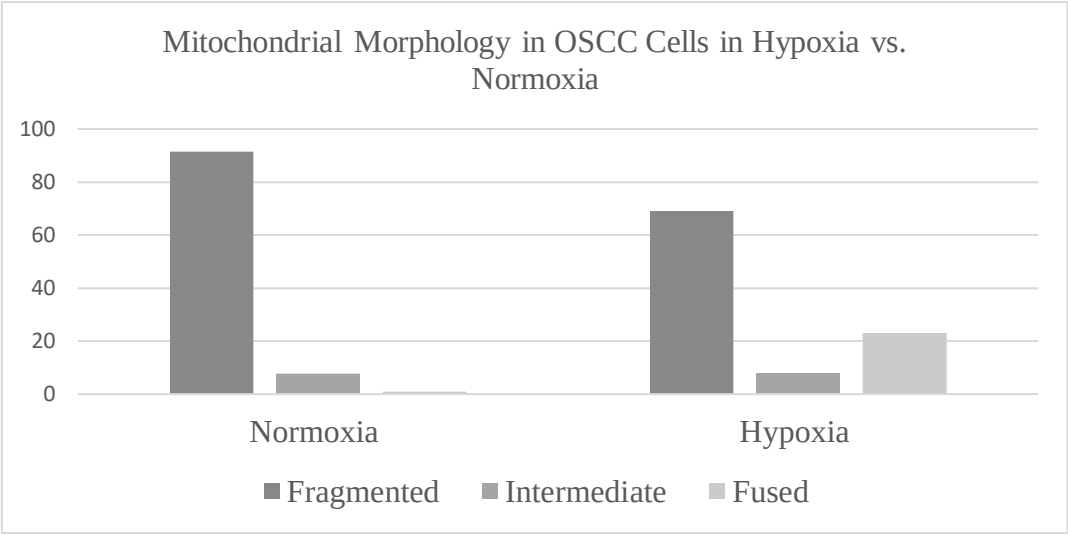

Figure 5. Mitochondrial Morphology in OSCC in hypoxia condtions. a)OSCC cells showing fused mitochondrial morphology in hypoxia condtions and fragmented mitochondria in normoxia condtions. b) quantification of AKAP12 relocation in hypoxia condtiontions. relocation happenes in hypoxia only in 25 % of the OSCC cells, which tend to show fused network compared to normoxia. Scale bar = 10 µm.

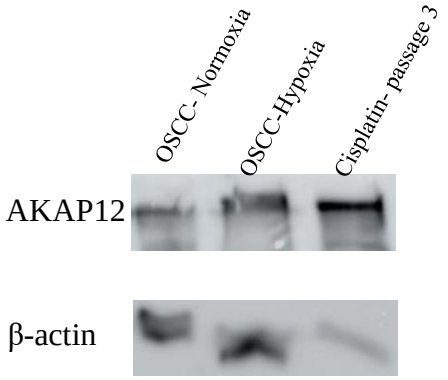

Figure 6. AKAP12 Protien Expression in OSSC Cells Under Different Condtions. AKAP12 expression in OSCC harvested from normoxic, hypoxia, treated with cipltain fro 3 passages.AKAP12 is 287 kDa and β-actin is 40 kDa.

The phosphorylation of Drp1 S616 showed no clear difference in expression between cells transfected with mitoβAKAP12, βAKAP12, and matching controls.

5.3 Establishment of Kill-Curve for Establishing Cisplatin Resistance in OSCC and Other Drugs Observations

5.3.1 Cisplatin Chemo-Sensitivity Assay

The half-maximal inhibitory concentration (IC50) of Cisplatin was defined as the concentration resulting in a 50 % reduction in growth compared to control cell growth. The experiment was repeated twice only. The Cisplatin dose-response curve was plotted [Figure 7]. Inhibitory concentration was calculated according to the following equation;

$Y = a * X + b$

$IC50 = (0.5 - b)/a.$

The suggested dose range for establishing resistance in OSCC is 6.4-7.00 uM [Figure 7.].

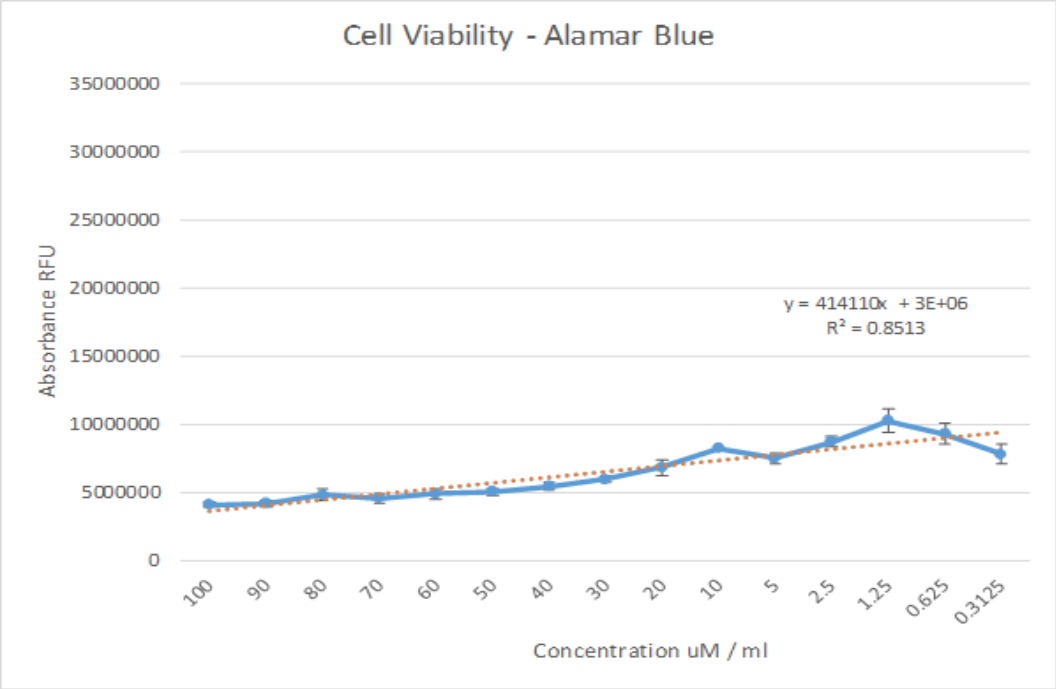

Figure 7. Establishment of Kill Curve. Standred population growth curve in semi-logarithmic normalized representaion for cells treated with Cisplatin. Cells were treated with varible doses of Ciplatin (blue solid line) and IC50 was calculated according to equation mentoned in Section 6.3.1. Logarithms of fluorescence intensity normalized with respect to the initial values.

5.3.2 PKA and PKC Inhibitors

In a trial of elucidating possible mechanisms for the observed fragmentation morphology associated with targeted AKAP12 to mitochondria, Laurie Glover used chemical drugs to inhibit possible suggested downstream protein kinases, i.e., PKA and PKC. Drp1 is a crucial regulator of fission events, and AKAP12 is known to recruit PKA and PKC, which are regulators to DRP1 as PKA and PKC. PKA is known to inhibit Drp1 and, consequently, to turn fission dynamic down. On the other hand, PKC can activate fission by Drp1 phosphorylation at S616, possibly contributing to the fragmentation phenomenon observed in this study. Cells expressing mitoβAKAP12-mRuby along with cells expressing matching control plasmid were treated with either PKA inhibitor or PKC inhibitor, i.e., Rp-cAMPs or Go-6983, at specified concentrations and duration. There was no rescue for mitochondrial fragmentation phenotype following PKA inhibition. Instead, the fragmentation rate increased in a time-dependent manner. Meanwhile, PKC inhibition tended to rescue the fragmentation, but the number of rescued cells was minimal (less than 5 %). Data are documented in Laurie's Thesis (Lee-Glover, 2018).

6. Discussion and Future Directions

In this study, we found that the endogenous expression of AKAP12 shows the cytoplasmic distribution of the protein with a smaller number of cells showing peripheral expression. While not homogenous throughout the cell, cytosolic AKAP12 did not colocalize with the mitochondria or the ER in the high expression cells. Also, Laurie reported the same pattern with cells expressing αAKAP12-m-Ruby, βAKAP12-m-Ruby, and m-Ruby (control). The observed AKAP12 pattern in the cell was in alignment with earlier reports (Gelman, 2010; Streb, Kitchen, Gelman, & Miano, 2004). Since AKAP12 relocation under basal condition is still under debate in the literature, we have tested some stress conditions. I examined if AKAP12

relocates to a specific cell compartment in OSCC cells growing under hypoxic conditions. I noticed that AKAP12 relocate to nuclear space in hypoxic conditions only in 25 % of the growing OSCC cells, which seemed to show a fragmented mitochondrial network. This observation supports the relocation of AKAP12 to perinuclear space following treatment with phorbol esters, which is a chemical drug used to induce stress (Chapline et al., 1998; Gelman, 2012; Nelson & Gelman, 1997; Singer, 1990).

Some earlier reports suggested that induced PKC mediated phosphorylation of AKAP12 may play a role in the PKC-mediated reorganization of the actin cytoskeleton (Akakura & Gelman, 2012; L. W. Guo, Gao, Rothschild, Su, & Gelman, 2011), which in turn plays a pivotal role in the mitochondrial constriction step during fission event (Hatch et al., 2014). This, in turn, might explain the observed fused mitochondria morphology only in cells where AKAP12 relocated to the nucleus. This observation may support the initiation of Model B signaling, where the Rho kinase pathway is proposed to be involved with the AKAP12 in mitochondrial regulation. Hypoxia conditions can be replicated utilizing hypoxia chambers with the same cell line and in cells expressing generated plasmids (αAKAP12-m-Ruby, βAKAP12-m-Ruby, and m-Ruby) and other AKAP12 antibodies that are available in the market can be tested. Hypoxia can also be applied to cells utilizing Cobalt (II) Chloride hexahydrate, a known agent to induce hypoxia in vitro. Confirmation of hypoxia can be done through detecting Hypoxia Responsive Element (HIF-α) at the mRNA level or protein level in cellular harvests (Wu & Yotnda, 2011). Another stress condition was tested, by Laurie Glover, in which cells expressing αAKAP12-m-Ruby, βAKAP12-m-Ruby, and m-Ruby were treated with calcimycin, a calcium ionophore which elevates the levels of intracellular calcium. No re-localization was observed in the tested conditions. However, more optimization for doses and duration is recommended for future

replication of Laurie's experiment. Worth to mention that generated plasmids by Lauri Glover were associated with limitations of fluorescence protein dimerization, thus, causing mitochondrial aggregation. Small peptides tags are recommended for future experiments in this project.

We also sought to identify the role of AKAP12 in mitochondrial dynamics. We proposed three models that may mediate mitochondrial morphology changes. AKAP12 was found to cause mitochondrial fragmentation when forced to the mitochondria. No effect on mitochondrial shape was detected when βAKAP12 was at the ER. However, the other AKAP12 isoform, which ER-αAKAP12, needs to be examined as this isoform was reported to localize to ER once it is overexpressed (Streb et al., 2004). If the targeted αAKAP12-m-Ruby targeted induced mitochondrial hyperfusion, the PKA/RhoA interaction could be confirmed through examining the downstream players of the Rho A pathway. Immunoblots for whole-cell lysates expressing αAKAP12-mRuby in the presence or absence of AKAP12/ PKA inhibitors can be run to confirm the activation of this signaling pathway.

AKAP1 is known to regulate fission via Drp1 deactivating. We were expecting that AKAP12 has a similar effect. AKAP12 recruits both PKA and PKC, which has an opposing impact on Drp1 activity. PKA activates Drp1 for mitochondrial- mediated fission , whereas PKC deactivates Drp1 leading to inhibited fission. Inhibition of PKC reduced the fragmentation caused by targeting AKAP12-m-ruby, whereas PKA inhibition did not have any impact on mitochondrial morphology- Lauri's observations-. In support, the mRNA results presented by Dr. Boss' lab that showed lower PKA transcripts in OSCC cells compared to control cells (data not shown). These observations suggest a more substantial involvement for PKC to the mitochondrial phenomenon. Optimizations for treatment duration are recommended for future

replication for the PKC inhibition experiment. Of note, AKAP12 has also been reported to inhibit the activity of PKC. This may open up the possibility of other protein kinases that can be recruited by AKAP12 and the involvement of different compartment/signaling pathways in mitochondrial regulation in link with AKAP12.

To date, AKAP12 has not been described to regulate mitochondrial dynamics. Our data suggest that AKAP12 can affect mitochondrial dynamics and cause a fragmentation phenomenon once targeted to mitochondria. This observation is contrary to the observed induced AKAP12 expression in mitochondrial fraction of Cisplatin-resistant cancer cells, which showed a hyper-fused mitochondrial network (Kong, Wang, Fung, Xue, & Tsang, 2014; Santin et al., 2013). However, one of the caveats is that the mitochondrial lysate might be contaminated with other cellular organelles. Also, induced Cisplatin resistance can be mediated via many different mechanisms. For instance, the downregulation of apoptotic factors on MOM can desensitize cancer cells to apoptosis even though having a fragmented mitochondrial network. Another explanation could be that our observations might be cell-specific. Therefore, replication of these experiments in other human normal or cancer cell lines is recommended.

7. Conclusion and Significance of The Study

Mitochondrial fission dynamics are fundamental to the regulation of many cellular physiological functions with a central role in modulating cellular response to stress response and signaling. The control of mitochondrial fission dynamics might be achieved at the level of the MOMs and the ER-Mitochondria contact sites. In this study, we identify AKAP12 as novel proteins mediating mitochondrial fission. In trying to be understanding howAKAP12 is regulating mitochondrial fission, we have proposed other pathways as possible effectors/players in promoting /inhibiting mitochondrial fission. Continuing studies in this project may help in

finding novel pathways regulating mitochondrial fission/fusion, which can be significant to translational therapeutic application in Cisplatin-resistance to cancer. Also, it may provide insights to understand the molecular pathogenesis involved in CMT soon. There is still a lot to be investigated in this project. Anyone who finds this preliminary project interesting is welcome to take the lead.

APPENDIX-C- Other Achievements not Reflected in this Thesis

Method Paper:

Expansion of Human Pluripotent Stem Cells in Stirred Suspension Bioreactors. Almutawaa W., Rohani L., Rancourt DE. Springer Method Molecular Biology

Conference Presentations:

1. Stem Cell Network annual meeting conference. Toronto, Canada, 2015, October 26-28th . Walaa Almutawaa, Leili Rohani and Derrick E. Rancourt. Maintenance of Embryonic Stem Cell Pluripotency: The Role of NFκ-B in Response to Shear Stress Mechanotransduction. (Poster presentation)

2. Alberta Children Hospital Research Institute (ACHRI) symposium. Calgary, Canada., 2016. November 10th -11th. Walaa Almutawaa, Christ Smith, Timothy Shutt. The Role of NMIIC in Mediating Mitochondria Fission. (Poster presentation)

3. BMB Advance symposium. Calgary, Canada., 2017, April 26th -27th . Walaa Almutawaa, Christ Smith, Timothy Shutt. The Role of NMIIC in Mediating Mitochondria Fission. (Poster presentation).

4.BMB Advance symposium. Calgary, Canada. 2018. April 24th-25th. The Role of NMIIC in Mediating Mitochondria Fission (poster presentation).

APPENDIX-D-

Approval Page